LBL-20565
UC-34A

# Lawrence Berkeley Laboratory
UNIVERSITY OF CALIFORNIA

## Materials & Molecular Research Division

LAWRENCE
BERKELEY LABORATORY
MAY 19 1986
LIBRARY AND
DOCUMENTS SECTION

A RAMAN SPECTROSCOPIC INVESTIGATION
OF MOLECULAR HYDROGEN

K. Veirs

December 1985

TWO-WEEK LOAN COPY
This is a Library Circulating Copy
which may be borrowed for two weeks.

LBL-20565 c.2

Prepared for the U.S. Department of Energy under Contract DE-AC03-76SF00098

## DISCLAIMER

This document was prepared as an account of work sponsored by the United States Government. While this document is believed to contain correct information, neither the United States Government nor any agency thereof, nor the Regents of the University of California, nor any of their employees, makes any warranty, express or implied, or assumes any legal responsibility for the accuracy, completeness, or usefulness of any information, apparatus, product, or process disclosed, or represents that its use would not infringe privately owned rights. Reference herein to any specific commercial product, process, or service by its trade name, trademark, manufacturer, or otherwise, does not necessarily constitute or imply its endorsement, recommendation, or favoring by the United States Government or any agency thereof, or the Regents of the University of California. The views and opinions of authors expressed herein do not necessarily state or reflect those of the United States Government or any agency thereof or the Regents of the University of California.

LBL-20565
LA-UR-86-276

# A RAMAN SPECTROSCOPIC INVESTIGATION OF MOLECULAR HYDROGEN

Kirk Veirs

Materials & Molecular Research Division
Lawrence Berkeley Laboratory
University of California
Berkeley, California 94720

This work was supported by the Director, Office of Energy Research, U.S. Department of Energy, through the Lawrence Berkeley Laboratory Program Development Funds under contract number DE-AC-03-76SF-00098 and Los Alamos National Laboratory contract number W-7405-ENG-36.

A RAMAN SPECTROSCOPIC INVESTIGATION OF MOLECULAR HYDROGEN


I. Introduction.....1

II. Experimental Apparatus

IIa. Introduction.....3

IIb. External Cavity.....3

IIc. Sample Cell.....8

IId. Detector.....10

IIe. Cooler.....11

IIf. Intensity Calibration.....12

IIg. Polarization.....17

III. Line Positions

IIIa. Introduction.....19

IIIb. Experimental.....22

IIIc. Hydrogen.....24

IIId. Hydrogen Deuteride.....32

IIIe. Hydrogen Tritide.....34

IIIf. Deuterium.....36

IIIg. Deuterium Tritide.....40

IIIh. Tritium.....41

IIIi. Conclusion.....43

IV. Line Intensities

IVa. Introduction.....45

IVb. First-Order Perturbation Theory.....45

IVc. Ab Initio Calculations.....50

IVd. Results.....51

V. Temperature Measurements

Va. Introduction.....56

Vb. J-Dependent Cross Sections.....56

Vc. Temperature Determinations.....57

Vd. Weak Lines.....60

Ve. Results: Pure Rotation.....61

Vf. Results: Q-branch.....62

Vg. Results: First Overtone.....70

Vh. Conclusion.....72

VI. Figures.....74

VII. Bibliography.....101

## I. INTRODUCTION

Molecular hydrogen occupies a unique niche in molecular physics due to it's simple electronic stucture and it's low molecular weight and concomitant large isotope effect. It has been an important model system for many theoretical calculations as well as experimental techniques. Because it is the most abundant molecule in the universe, it has served as an important celestial probe. Molecular hydrogen also is important in the practical sense, being used in major industrial processes, suggested as a storage medium for energy, is a major participant in combustion proceses, and is used in fusion energy experiments as well as fusion weapons.

Among the many applications of the spectroscopy of molecular hydrogen lies accurate temperature determinations at high temperatures using rotational and vibrational Raman intensities. In order for accurate temperatures to be determined more information was needed on the rotational dependence of the Raman cross section. A complete survey of the Raman cross section using all six of the isotopomers of molecular hydrogen was undertaken at Los Alamos National Laboratory because of the ability to handle tritium. A state of the art gas phase Raman spectrometer was assembled taking advantage of recent advances in lasers and microprocessor controlled data acquisition. Survey experiments indicated that line positions as well as Raman cross sections should be investigated. Interest in Raman cross sections and line positions

led to accurate ab initio calculations of these quantities by Carey Schwartz and Robert J. LeRoy at the University of Waterloo for all of the isotopomers of hydrogen[1].

The basic research results, both experimental and theoretical, on Raman cross sections and line positions were applied to the problem of accurate temperature determinations at room temperature. The results of this work indicate that pure rotational Raman intensities are well understood, but have raised questions, still unanswered, about our understanding of vibrational Raman intensities. There appears to be no method that allows one to calculate accurate number densities from Q-branch Raman intensities.

This monograph describes the state of the art Raman spectroscopy apparatus in detail and reports results on Raman line positions, cross sections, and temperature determinations in gas phase hydrogen. In all cases the results indicate that additional research should be considered using the unique capabilities of Los Alamos National Laboratory in both tritium handling and high resolution spectroscopy. The results are extremely encouraging to the application of spontaneous Raman spectroscopy for temperature determinations and gas phase isotopic analysis.

## II. EXPERIMENTAL APPARATUS

### IIa. Introduction

The experimental apparatus consists of a Spectra-Physics 171-18 UV $Ar^+$ laser with an external cavity, collection optics, a Spex 1403 double monochromator of f/7.8 with holographic gratings, a RCA C31034A photomultiplier tube with photon-counting discriminator and a Spex Datamate microprocessor controlled data acquisition system. A description of each component of the experimental apparatus follows, along with calibration procedures and design considerations where appropriate.

### IIb. External Cavity

The external cavity contains two lenses which focus the beam in the scattering region and recollimates the beam for the retroreflecting mirror. The ends of the external cavity are the output coupler of the laser and the retroreflecting mirror. The two lenses are adjusted for maximum power where presumably the wavefront of the retroreflected beam closely matches the wavefront of the beam leaving the laser at the output coupler. The characteristics of the elements in the external cavity are determined by the optical characteristics of the double monochromator and the collection optics. The focal length of the two lenses was chosen to optimize the amount of scattered light reaching the photomultiplier tube. The f/# of the monochromator is determined by the size of the grating (110 mm x 110 mm) and the focal length of the first collimating mirror (f.l. = 850 mm), f/# = f.l. / diameter = 850mm / 110mm = 7.73; which is reasonably close (see

Fig. I). Assuming a 50 mm diameter condensing lens as a reasonably easy lens to attain, the focal length is given by the f/# of the monochromator and the diameter; f.l. = diameter x f/# = 50mm x 7.8 = 390 mm. A shorter focal length lens will overfill the grating whereas a longer focal length lens will underfill the grating. Using the shortest focal length, smallest f/# aspheric lens available commercially (from Melles Griot) for a collection lens, the length of the beam sampled can be calculated. A 50 mm diameter, 35 mm focal length aspheric collection lens from Melles Griot was chosen. The image magnification of the scattering region on the slits of the monochromator is given by the ratio of the collection lens focal length to the condensing lens focal length; magnification = 390 mm / 35 mm = 11. Using a slit height of 20 mm the height of the beam waist imaged on the slits is given by h(beam waist) = h(slit) / mag; h(beam waist) = 20 mm / 11 = 1.8 mm. Taking the optimum condition to be where the height of the beam waist to be imaged on the slits is twice the Rayleigh length of a focused Gaussian wavefront, the beam waist radius, $\omega_0$, can be calculated; $\omega_0 = \frac{2Z_r L}{2\omega}$ where $2Z_r$ = 1.8mm and L = 488.0 nm, $\omega_0$ = 0.0118 mm or 11.8 microns. This gives an image width on the slits of 2 x 11.8 x 11 (beam diameter x magnification) = 260 microns, which is a reasonable slit width to work at. The focal length of the external cavity lenses was calculated from the beam waist, $\omega_0$, and the $Ar^+$ beam diameter given in the specifications by assuming the size of the beam on the lenses is the same as the $1/e^2$ radius (see Fig. II). $\omega_z = \frac{LZ}{\pi\omega_0}$ where $\omega_z$ = 1.58mm (from Spectra-Physics literature). $Z = f.l. = \frac{\omega_z \pi \omega_0}{L} \cdot$ $f.l. = \frac{(0.0118\text{mm} \times \pi \times 1.58\text{mm} / 2)}{488 \times 10^{-6}\text{mm}} = 60\text{mm}$. This last procedure is not strictly correct because of the divergence of the laser, but it is not a bad approximation. The final external cavity/collection optics system is shown in Fig. III. The only change in this system was that the 35 mm asperic did not work as well as the camera lens of unknown focal

length and f/# (nominally f.l. = 50 mm and f/1.5) which is currently being used. The total volume from which light is collected is $(1.8mm) \times \pi \times (0.0118mm)^2 = 7.9 \times 10^{-7} cm^{-3}$. The total number of molecules being interrogated in this volumne at 500 Torr is (500/760 atm) x $2.48 \times 10^{19}$ molecules $atmosphere^{-1}$ $cm^{-3}$ x $7.9 \times 10^{-7}$ $cm^3$ = $1.29 \times 10^{13}$ molecules, at a detection limit of 10 ppm the total number of molecules needed for detection is $1.3 \times 10^8$. The spherical mirror of radius 35mm and diameter 50mm is matched to the original 35mm f.l. lens and is more than is needed for the current collection lens. The increase in collected light was typically x1.8 rather than the expected x2.0 when using the spherical mirror.

To align the external cavity the two lenses are removed from the beam. The two beam directing mirrors are used to align the beam so that it is vertical (parallel to the input slits of the monochromator), in the center of the retroreflecting mirror, and well centered on the line formed from the center of the collimating mirror to the slits of the monochromator. The retroreflecting mirror is then used to redirect the beam back to the output coupler. Fine adjustments are made with the laser turned to a minimum current and maximising the signal on the laser power meter. The first lens (that is the lens closest to the laser in the optical path) is aligned by centering the expanded beam on the retroreflecting mirror. The second lens is then aligned to center the reflected beam on the output coupler. Fine adjustment of the external cavity is done using the double micrometers on the retroreflecting mirror and the micrometers on the lenses (for optimal spacing between the lenses) to maximise the power at the laser power meter. If the sample cell is not present the spacing between the lenses is a few millimeters shorter than when the sample cell is in place, due to the difference in effective path

length between the lenses caused by the sample cell windows. This effect can be rigorously calculated. When the laser is operating at high power the external cavity must be fine tuned again, probably due to changes in the external cavity from heating of the optical elements and mounts by the high power laser beam. The external cavity takes about an hour to stabilize at high power.

The power in the external cavity is monitored using the Spectra-Physics 171 power meter. Because of the high powers in the external cavity a glass neutral density filter was placed between the power meter photodiode and the pickoff. The transmission of the neutral density filter was measured two ways. First the Coherent power meter was used to measure the $Ar^+$ beam without the external cavity while the Spectra-Physics power meter was used to measure the $Ar^+$ beam with the neutral density filter in place. This gave a factor of about 7.8 by which the Spectra-Physics power meter was attenuated. This factor was constant over the range of powers that the $Ar^+$ laser could attain without the external cavity, from less than 0.1 Watt up to 7 Watts. The best power observed with the neutral density filter in place was about 12 Watts or a calculated total power of 12 Watts x 7.8 x 2 = 187 Watts circulating in the external cavity. The factor of two is used because the pickoff is selective to light leaving the output coupler whereas the light at the scattering region is propagating in both directions. The neutral density filter tends to crack due to heating, giving high readings. With the neutral density filter removed the highest possible reading on the Spectra-Physics power meter is 30 Watts. It was difficult to obtain a circulating power of 60 Watts without the neutral density filter in place, so a second calibration was devised. Using the external cavity, the power was measured both with the

neutral density filter in place and removed. The ratio of the two readings gave a constant value of nominally 7.8 up to a power of 10 Watts, at which point the ratio decreased linearly to a factor of 6 at 30 Watts. A relationship was fit to the observed data and the experimental results are shown in Fig. IV:

$$P(\text{actual}) = \frac{9.14\ P(\text{measured,ND})}{1 + 0.106 \times P(\text{measured,ND})} \quad . \tag{1}$$

Thus at 12 Watt(measured,ND), P(actual) = 48 Watts with 96 Watts circulating. Recently the external cavity was always measured without the ND filter. The failure of the ND filter at high powers might be due to saturation. However when using the Spectra-Physics power meter to determine the power in the external cavity, one assumes the proportion of light directed to the power meter from the laser beam is constant. The proportion of light directed to the power meter depends upon the polarization as the pick off is near Brewster's angle for vertically polarized light. The external cavity tends to depolarize the beam which would cause a high reading by the power meter. By using a beam splitter in the external cavity oriented close to perpendicular with just enough horizontal angular offset to provide a beam for a homebuilt, calibrated power meter, the effect of depolarization could be checked. It was found that the Spectra-Physics power meter was giving a correct reading, but this could bear checking again. In summary, the power in the external cavity is best measured directly on the Spectra-Physics power meter without attenuation with a ND filter. This measurement gives a reliable figure as to the power in the external cavity and must be multiplied by 2 to give the circulating power in the scattering region.

## IIc. Sample Cell

The final element of the optical train is the sample cell, which must be designed with both optical and tritium containment considerations. The tritium containment considerations are small volume and no elastomers. The original cell design had Brewster angle windows with indium o-rings. Indium seals to glass quite well, in fact wetting the glass, with a small amount of force. With this cell very intense reflections from the Brewster angle windows were observed. Using a nearly perpendicular beam splitter in the external cavity, the polarization was checked and found to be partially depolarized. The cause of the depolarization was never determined but one possibility is strain induced birefringence in the Brewster angle windows due to the force necessary to seal the metal o-rings. Other metals used as o-rings were gold and a lead/tin allow called Staybright which was obtained from vacuum repair. The gold was not ductile enough and tended to crack the windows. The Staybright seemed to be the best material because it was almost as soft as indium, but did not wet the windows. The indium gripped the windows so tightly that at room temperature the windows would break rather than come out. By heating the cell the windows could be removed intact. The indium on the windows was difficult to remove and inhibited proper cleaning of the windows for re-use. Because of the depolarization of the beam and the presence of the Brewster angles, the maximum power in the external cavity rarely exceeded a factor of 2 above the normal output of the laser. A new cell was designed with windows normal to the beam and AR coated. The AR coating is broadband and good for about .1% reflection. The cell was designed for a small volume by using a small bore for the laser beam with observing windows as close to the beam as possible. The cell is shown in Fig. V. Other

possibilities are to use Brewster angle cells with rubber o-rings (to minimize strain induced birefringence) for work with H and D. Or one can use indium and discard the entire cell when the windows are too dirty to use; cleaning windows wetted by indium is practically impossible and the added hazard of tritium contamination makes it highly undesirable. The entire cell is black anodized to minimize reflections. The black anodization must be removed where the o-rings seal as it is full of small holes and cracks. The mechanism by which the cell windows get dirty is not entirely understood, however it has to do with the high laser powers at the windows. It results in a rather bluish looking deposit usually (maybe always) on the inside of the cell, possibly due to the laser striking the side of the inside of the cell, and is almost impossible to clean. It is probably responsible for most of the losses within the external cavity. The cell is kinematically mounted to translators which allow the cell to be positioned so that unblemished cell window surfaces transmit the laser beam. The cell, which is currently constructed of aluminum, could be made of stainless steel. It is rumored that there are black surface coatings for stainless steel which are less reflective and not as porous as aluminum black anodization. All of the cell windows were ordered from Melles Griot with Hebbar coatings. The cell windows, as well as the external cavity lenses, tend to fluoresce orange. Using quartz does not seem to alleviate this problem. When tritium is used special precautions are instituted. The cell filled with tritium is always stored overnight in the tritium facility. To carry the cell from the tritium facility to the lab a special carrying container with two valved ports and a tie-down for the cell is used. The cell is never filled to or above local atmospheric pressure with tritium. The valved ports on the carrying container are used to sweep air through the container and into a tritium monitor. Every cell "leaks" tritium

to some extent, possibly due to permeation through the cell body, o-rings, and windows. By leaving the cell in the closed container overnight and checking the amount of tritium leaked into the container or by flowing the exhaust of a tritium monitor back into the container the leak rate of the cell can be determined. For one cell on which both measurements were made the leak rate was about 2 microCuries per hour. If the cell is left in the carrying container overnight the outside of the cell is permanently contaminated. The carrying container is typically pumped out through a tritium monitor each morning. The exhaust for the tritium monitor is terminated in a tritium hood. The tritium level will decrease rapidly at first, following a kind of exponential decay. It takes about 0.5 hour to get to about 30 microCuries per meter$^3$ at which point it is considered to be not leaking and quite safe for transport and use in the Raman lab. A tritium monitor on the exhaust tube from the laser table to the hood constantly monitors the cell for catastrophic failure. Rubber gloves are always used to handle the tritium containing cell. There has never been any problems with the tritium cells.

IId. Detector

The detector is a RCA C31034A photomultiplier tube specially selected by RCA for low dark count. The Spex Datamate collects the signal using a Spex discriminator and counter. The count rate was kept below $10^6$ as the response at higher count rates is non-linear and there is a possibility of damage to the photomultiplier tube at higher count rates. The tube was run at 1440 V, which was the voltage on the original specifications card from RCA. No attempt to optimise the voltage was made. The discriminator setting was optimised in the following manner. A strong signal from one of the Oriel

spectral lamps was incident upon the photomultiplier tube. For each 1/4 turn on the discriminator a signal count and a dark count (taken by closing the shutter into the double monochromator) was taken and ratioed. The S/N ratio was graphed versus the discriminator setting. The results are given in Fig. VI. The rapid rise is due to stable large signals with a decreasing large noise. The small plateau region is where the discriminator was set. Recently the signal has been decreasing and it was found that the discriminator level was no longer optimum. The reason could be a lower amplification by the PMT indicating that it is starting to wear out. The best Raman signals are typically $2 \times 10^5$ cps with a background of about 10. The dark count should be about 2-4 cps. Occasionally the PMT housing should be warmed up and the water that is condensed on the PMT and the window should be cleaned up. The window has a lens built in with two possible orientations as shown in Fig. VII. The original position was as in (a), but it is not obvious that either position is better. It is currently positioned as in (b). When the PMT is cooling back down the cooler power supply tends to blow fuses and should be periodically checked. The PMT housing is usually operated at -50 °C on the cooler power supply. The dark count versus temperature is as expected from RCA and PRA brochures. There is no reason to believe that the temperature is not -50 °C although this has not been specifically measured.

## IIe. Cooler

The laser is cooled using a Neslab recirculating cooler which keeps the input water temperature constant at about 20°C, adjustable on the control unit above the laser power supply. This unit uses deionized water and dumps heat

into the building's cooling water loop. The deionized water reservoir is open to the atmosphere and is subject to evaporation. Deionized water needs to periodically be added. The unit is in the basement below the lab. A water pressure of 70 psi is maintained at the laser, read off the meter near the control box. This pressure can be adjusted with a valve on the cooling unit. When the unit is shut off all of the water drains downstairs and it takes about a minute to flush the air out when it is turned on again.

## IIf. Intensity Calibration

The intensity calibration uses a NBS traceable calibration lamp from Optronics Laboratories. The lamp is calibrated in absolute photon flux when placed at 50 cm from the detector and operated with a fixed 6.50 amp current. The lamp filament is a coiled-coil tungsten filament, currently considered more accurate then the flat ribbon tungsten filaments used previously[2]. Two methods were used to insure the proper current was applied to the lamp. First a series of precision resistors were calibrated relative to one another to check consistency of their calibration. This was done by applying a constant voltage across them in series and measuring the voltage drop across each of them using an HP autoranging voltmeter. The voltage measurement is quite accurate. The ratio of the voltage drops across the precision resistors were compared to the ratio of the resistances and were found to be quite accurate. A high current nominally 1 ohm precision resistor was used in series with the lamp to measure the lamp current. A high-current stable- voltage power supply was used to supply the current. The power supply had a feedback loop to stabilize the voltage. The circuit is shown in Fig. VIII. As the lamp heats up its resistance changes so the power supply was

continually adjusted to keep the voltage across the precision resistor constant. The second method was based upon a new HP constant-current/constant-voltage power supply. The unit was operated in constant-current mode at 6.50 amps. This power supply was checked using the precision resistor and was found to be accurate within specifications. There are two sets of terminals on the precision resistor; one set for the voltage input and one set for voltage measurement. The lamp has a limited lifetime before recalibration needs to be considered, both in operating time and actual time. The lamp output has oscillations in intensity as a function of frequency for small changes in frequency, shown in Fig. IX. The oscillations apparantly are due to interference on the photomultiplier's photocathode between rays of light originating from the filament and passing into the spectrometer either immediately or after being reflected by the outside quartz envelope of the lamp. The magnitude of the oscillations are about 1% of the total intensity and therefore are important for accurate intensity calibration. The period is independent of other optical elements within the light's path such as lenses, windows, and filters. Reducing the overall intensity by a factor of 10 with an ND1 filter does not affect the period or the relative intensity which remains at 1% of the total intensity. A bandpass filter of a few nanometers does not affect the oscillations within the pass band. Shifting the relative orientation of the calibration lamp significantly shifts the period of the oscillations but not the relative intensity, indicating that the rays entering the spectrometer are now coming from a different part of the lamp's envelope. The periods observed ranged from 1.3 $cm^{-1}$ to 2.2 $cm^{-1}$ depending upon lamp orientation. Using $\delta\nu = 1/2d$, the free spectral range for an etalon, the separation between filament and envelope would range from 2.3 mm to 3.8 mm, the measured distance being about 3 mm. This etaloning effect was

a surprize to the manufacturers of the lamp and to my knowledge has not been reported previously. Most applications of this lamp have bandpasses large enough to average out the oscillations, i.e. any spectrometer with a resolution greater than 2 $cm^{-1}$ (0.05 nm) will be insensitive to these oscillations. The noise imposed upon the oscillations was about .1% which is within the needed tolerances. For actual calibration purposes the slit width was increased to a resolution greater than 2 $cm^{-1}$.

The calibration that comes with the lamp has intensities (W $cm^{-2}$ $nm^{-1}$) spaced far apart in wavelength and are not useful as is for calibration of two close wavelengths. Rather than extrapolating or fitting the points to some arbitrary polynomial for interpolation, the known blackbody radiation equation was used with a single parameter, T. The calibrated intensities were compared to intensities using this equation and the temperature with the best fit was selected. Intensities for any wavelength, aperture, and bandpass could then be calculated using the blackbody radiation equation:

$$I(\nu,T) = 2\,\pi\,h\,c^2\,\nu^5\left(\frac{1}{\exp(hc\nu/\,kT) - 1}\right) \times \text{Emissivity}\,(\nu)\ . \qquad (2)$$

The emissivity data of De Vos[2], accepted as the most accurate determination[3,4,5], was fit to a polynomial in wavenumber for a temperature of 2800°K:

$$\text{Emissivity}(\nu) = .51803 - \frac{1.9085 \times 10^3}{\nu} + \frac{1.8355 \times 10^7}{\nu^2} - \frac{1.6162 \times 10^{11}}{\nu^3}\ . \qquad (3)$$

The procedure used found the absolute intensities at the wavelengths for which the lamp was calibrated for a series of temperatures differing by 1 °K. The temperature for which the relative deviations over the set of wavelengths was smallest was chosen as the temperature of the lamp filament. The present lamp, L-310, had a best temperature of T=2923 °K. This temperature was used

along with the emissivity of De Vos[3] to calculate the photon flux within a bandwidth determined by the spectrometer for calibration of the spectrometer:

$$I(\nu) = 2\,\pi\,h\,c^2\,\nu^3\,\delta\nu\,\left(\frac{\text{Emissivity}\,(\nu)}{\exp\,(hc\nu\,/\,kT) - 1}\right) \quad . \qquad (4)$$

where $I(\nu)$ is in Watts $cm^{-2}$ and T=2923°K. The spectrometer bandwidth, $\delta\nu$, is a function of slit width and was determined from measuring the FWHM of spectral lines across a wide frequency range, for slit widths of 300-400-400-300 microns. The measured set of FWHM was fit to a polynomial:

$$\delta\nu = A\,\nu^2 + B\,\nu \quad . \qquad (5)$$

where $A = 1.257 \times 10^{-8}$ cm and $B = -5.5198 \times 10^{-5}$. The calibration of the spectrometer will only be good if the slits are at the same settings. For relative intensities other slit widths can be used as the bandwidth is linear with regard to the slitwidth and the linear multiplier will cancel out. The response function of the optical system and spectrometer is given by:

$$R(\nu) = I_o(\nu)\,\frac{\exp(hc\nu\,/\,kT) - 1}{2\pi\,c\,\nu^2\,\delta\nu\,\text{Emissivity}\,(\nu)} \quad . \qquad (6)$$

where $I_o(\nu)$ is in photons $sec^{-1}$ and is the measured quantity. There are two convenient ways to measure intensities using the digital data collection of the Datamate, first to integrate the peak and secondly to measure the peak intensity. In both methods the background must be subtracted by either subtracting an integrated background or by subtracting an average background. The two methods are illustrated in Fig. X.

Method I is easy to implement digitally and has the advantage of having more total counts. The drawback is that for two different frequencies the linewidth of the spectrometer must be accurately taken into account a second

time. Method II, also easy to implement digitally, has the advantage that the linewidth is not needed a second time.

Method I was used for the first data that was taken on relative line intensities. The scatter in the data was poor, and at that time the polarization was not properly accounted for. All of the initial data on $H_2$, $D_2$ and $T_2$ was disregarded because of these difficulties.

Method II was adopted for the final data on $H_2$ intensities and for use in all analytical determinations. Because it is sensitive to peak heights, two adjacent peaks which overlap slightly, which makes it difficult to obtain accurate numbers using method I, can be readily compared using method II. $R(\nu)$ as calculated above can be applied directly to the measured intensity, $I_{meas}(\nu)$, to give the corrected intensity:

$$I_{corr}(\nu) = I_{meas}(\nu) \ / \ R(\nu) \ . \qquad (7)$$

The time dependence of the spectrometer response function was checked by ratioing two sets of calibration response functions, $R(\nu)$, taken at different times. Because the absolute response function is very dependent on the exact placement of the lamp, the ratio was not one, but rather about 0.98. For a frequency range of greater than 1000 $cm^{-1}$ the ratio varied by about 1%. Within any small frequency range the RMS value would be around 0.25%.

Because of the etaloning of the calibration lamp, the spectrometer response function at a particular wavelength was found by fitting to a straight line 20 individual measurements, 10 at higher frequency and 10 at lower frequency, and calculating $R(\nu)$ from the parameters of that straight line. This procedure was checked using a graphical technique to determine

R(ν) and was found to be quite good. The differences between the linear regression and the graphical technique were less than 0.06% for all pairs of lines for $H_2$. The wavelength error, or the slope, was found to be 0.007% / 50 $cm^{-1}$, that is going 50 $cm^{-1}$ from the line R(ν) changed by 0.007% at the slope minimum and 0.2% at the slope maximum.

## IIg. Polarization

All previous publications concerning Raman intensities in $H_2$ have neglected the effect of polarization. The scattered Raman light is highly polarized, which has been widely recognized of course, but the investigations concerning the effect of centrifugal distortion on the Raman cross section have used unpolarized light for the spectrometer response function and have made no attempt to de-polarize the Raman scattered light, or have used the Raman light itself for calibration. The effect of polarization on the throughput of the spectrometer can be approximated by looking at the efficiencies of the gratings for light polarized perpendicular and parrallel to the grooves on the grating as a function of wavelength. The effect is quite dramatic, the ratio of intensities for perpendicular to parrallel polarization can range from greater than 50 to less then 0.001 depending on the wavelength, a range of greater than four orders of magnitude. The measured and calculated spectrometer efficiencies are shown in Fig. XI and the ratio of perpendicular to parrallel response calculated from measured efficiencies are shown in Fig. XII. The accepted method to deal with polarized light is to use a de-polarizer purchased from Spex. The device is a piece of wedged quartz cut so that the optical axis is perpendicular to the light path (i.e. parrallel to the face). The polarization of the light is rotated as it traverses the crystal, and rotated different amounts depending

upon the thickness of the crystal the light traverses. A simple drawing of a typical de-polarizer is shown in Fig. XIII. Using a polarized HeNe in the experimental arrangement shown in Fig. XIV it was found that the polarization rotated by 180° about 4 times over the height of the depolarizer.

Four rotations of the polarization is not enough to adequately de-polarize Raman light for intensity measurements accurate to 1%. Using a good Glan-Thompson prism polarizer, extinction ratio $< 10^{-5}$, the intensity as a function of the angular position of the polarizer was determined for a Raman line. The de-polarizer was then placed before the polarizer and the intensity versus angle was redetermined. With the de-polarizer, if it worked as it should, the result would be a flat line. The results are shown in Fig. XV. The de-polarizer helps but it is far from adequate. I could find no other device that de-polarized light without a large drop in throughput. Because the Raman light is mostly polarized in the direction for maximum throughput, it was decided that a good Glan-Thompson prism polarizer would be used both to collect data and to calibrate the spectrometer. The spectrometer response function in this case can still be directly applied to the measured intensity as before.

## III. LINE POSITIONS

### IIIa. Introduction

The study of line positions yields a wealth of information concerning a molecule. Accurate transition frequencies are used to identify a molecule from it's spectra, the reduction of transition frequencies to a set of molecular constants provides a shorthand method for the spectroscopist to tabulate transition frequencies, the set of molecular constants are related to the potential energy well of the molecule and can be used to calculate the potential energy well, theoretical calculations of energy levels can be compared to experimental transition frequencies to test theoretical models, and isotopic shifts can be examined to further test the theoretical models. For the hydrogen molecule all of these uses of line positions acquire additional importance because molecular hydrogen is the simplest molecule, amenable to extremely accurate ab initio calculations, and possesses the largest isotope shift of any molecule.

There exists an immense literature concerning line positions of the hydrogen molecule, both theoretical and experimental. Recent advances in spectroscopic instrumentation have resulted in extremely accurate line positions for many transitions in $H_2$ and some transitions in HD and $D_2$. The experimental results for the tritium containing isotopomers however is sparse and has not reflected the advances in instrumentation, with line positions being less accurate by two to three orders of magnitude. Coupled with the advances in experiment there have been advances in theoretical

calculations which yield energy levels from which line positions can be calculated and compared to experiment. Theoretical line positions are in excellant agreement with the recent experimental results for the non-tritium containing molecules. There is no way as yet to accurately test the ab initio results for the tritium containing molecules. I shall try to summarize the advances and results in both areas and show where these results support both recent experiments and theory.

Molecular constants are used to calculate rotational and vibrational energies of a molecule, and there are a number of different formulations. Rotational energies are given by an expansion in J(J+1):

$$E_v(J) = B_v\, J(J+1) - D_v\, [J(J+1)]^2 + H_v\, [J(J+1)]^3 + L_v\, [J(J+1)]^4 \ldots . (8)$$

where v is the vibrational quantum number of the vibrational level that the rotational state occupies. Each vibrational level has it's own set of B, D, H, L.... . The B, D, H, L.... can be expanded in v + 1/2 about the equilibrium internuclear distance value:

$$B_v = B_e - \alpha_e(v + \tfrac{1}{2}) + \gamma_e(v + \tfrac{1}{2})^2 - \ldots\ldots \qquad (9)$$

$$D_v = D_e + \beta_e\,(v + \tfrac{1}{2}) + \delta_e\,(v + \tfrac{1}{2})^2 + \ldots\ldots \qquad (10)$$

$$H_v = H_e + \ldots\ldots \qquad (11)$$

When only the ground vibrational state (v=0) is observed $B_o$, $D_o$, $H_o$ .... are usually reported. When Q-branch spectra are observed as well then either $B_o$, $B_1$, $D_o$, $D_1$, $H_0$, $H_1$ .... and/or $B_e$, $\alpha_e$, $\gamma_e$, $D_e$, $\beta_e$, $\delta_e$, .... are reported, the latter especially when the observations include many vibrational levels. From $B_e$ the equilibrium internuclear distance, $r_e$, can be determined.

The vibrational seperation observed in $Q_1(0)$ can be reported as $\nu_{01}$ or, if more than one vibrational level is observed, the vibrational energies can be expanded around $v + \frac{1}{2}$:

$$G(v) = \omega_e (v + \frac{1}{2}) - \omega_e x_e (v + \frac{1}{2})^2 + \omega_e y_e (v + \frac{1}{2})^3 \ldots\ldots \quad (12)$$

G(v) represents the vibrational energy above the bottom of the potential energy well. For v=0 this energy is called the zero point energy and is given by:

$$G(0) = \frac{1}{2}\omega_e - \frac{1}{4}\omega_e x_e \ldots. \quad (13)$$

All of these constants are contained in Dunham's formulation which represents the total energy of any rotational-vibrational level above the bottom of the potential energy well as:

$$E(v,J) = \sum_{\ell,k} Y_{\ell,k} (v + \frac{1}{2})^{\ell} [J(J+1)]^k \quad . \quad (14)$$

Note that $B_e \sim Y_{0,1}$, $D_e \sim Y_{0,2}$, $\omega_e \sim Y_{1,0}$ etc. Within the literature one encounters all of these formulations of molecular constants.

For molecular hydrogen it is particularly difficult to develop a reliable set of molecular constants for a variety of reasons. First of all the light weight of hydrogen requires that the rotational and vibrational constants, which are inversely proportional to powers of the reduced mass $(m_1 m_2/\{m_1+m_2\})$ and the square root of the reduced mass respectively, are quite large relative to other diatomic molecules. This means that more constants are needed for accurate calculations. For instance the rotational constant, $B_e$, for $H_2$ (60.853) is 42 times larger than the rotational constant of $O_2$ (1.44563). Secondly, the large rotational constant means that very few rotational levels

are observed, up to J=6 for room temperature $H_2$ versus up to J=100 for room temperature $I_2$. Finally the potential well of molecular hydrogen is extremely anharmonic requiring many molecular constants for accurate results. All of these factors, along with the unsatisfying mathematical formulation for molecular constants, make extrapolation to rotational levels beyond the observed rotational levels dangerous at best. For instance in one paper where J=0 to 5 were observed for pure rotation to 0.001 $cm^{-1}$ accuracy, two sets of molecular constants were derived. One set contained $B_0$, $D_0$, $H_0$, and $L_0$, 4 constants for 6 transitions, and reproduced all of the observed lines to less than .001 $cm^{-1}$. A second set containing $B_0$, $D_0$, $H_0$, $L_0$, and $M_0$, based on an intelligent guess for $M_0$, were derived, 5 constants from 6 transitions. These constants also reproduced the observed lines to less than 0.001 $cm^{-1}$. Although the two sets seemed to be virtually identical up to J=5 ($\Delta\nu$ = 0.0001 $cm^{-1}$), at J=15 they disagreed by 62 $cm^{-1}$, an increase in difference by almost 6 orders of magnitude. One cannot tell which is more correct from the experimental data. The reason why one would want to know the transition frequency at J=15 is that it is believed to have been seen in astronomical observations and may be populated and observed in rocket exhaust and combustion processes. Astronomical observations especially could benefit from exact transition frequencies in calculating accurate Doppler shifts.

## IIIb. Experimental

The external cavity laser and double monochromator Raman apparatus has been described previously. The laser was run with 50 Watts circulating in the external cavity. Gas pressures of 550 Torr were used and corrections due to pressure shifts were not needed. Uranium lines from a hollow cathode lamp

were used for calibration of each of the $H_2$ Raman transitions[7]. The hollow cathode lamp was focused within the scattering volume and then proceeded through the same optical train as the Raman scattered light. The uranium hollow cathode lamp has many transitions as well as contributing scattered background radiation so a shutter was incorporated that would block the lamp when Raman scattering data was being collected.

For hydrogen, a typical run consisted of scanning a 30 $cm^{-1}$ region containing the Raman line of interest and several uranium lines. The scan rate was 0.005 $cm^{-1}$ per step with an integration time of 10 seconds per step. The slits were set at 10 microns entrance and exit and 50 microns intermediate when acquiring uranium calibration lines. As the scan approached the known position of a Raman line the shutter was closed and the slits were increased up to an additional 150 microns depending upon the intensity of the Raman transition.

Computer data reduction consisted in finding the centers of lines using a code patterned after Hurlock and Hanratty[8], fitting 5 or more calibration lines to a 3rd order polynomial, and using the polynomial to calculate the position of the Raman line as well as a few uranium lines not included in the fit for a check. The polynomial generally reproduced the fitted lines to better than ±0.01 $cm^{-1}$ and the known uranium lines to less than ±0.02 $cm^{-1}$. Some uranium lines yielded much worse fits due to overlaps. The measured Raman lines are estimated to be accurate to ±0.03 $cm^{-1}$. A measurement of the Argon laser line yielded 20486.638 $cm^{-1}$, in error by -0.017 $cm^{-1}$ from the accepted value of 20486.655 $cm^{-1}$. A typical spectrum is given in Fig. XVI.

For the remaining 5 isotopomers, Raman spectra were collected without uranium calibration. Known Raman lines from the literature were compared to measured lines yielding a calibration value for the spectrometer. This value was added to the remaining lines. The accuracy of lines measured in this manner is estimated to be ±0.1 $cm^{-1}$.

IIIc. Hydrogen

The quintessential Raman experiment in the ground vibrational state of molecular hydrogen was published by B. P. Stoicheff in 1957[9]. He reported pure rotational frequencies up to J=3 for $H_2$ and J=4 for HD and $D_2$ and Q-branch vibrational frequencies up to J=3 for $H_2$ and HD and J=4 for $D_2$. The reported accuracy of ±0.02 $cm^{-1}$ for the pure rotational spectra and ±0.05 $cm^{-1}$ for the Q-branch transitions have been verified by recent, more accurate experimental results. The set of molecular constants reported in Stoicheff's paper yield accurate line positions up to the last observed rotational level but rapidly diverge at higher J. At J=6 the Q-branch line is off by 1.5 $cm^{-1}$. Regardless, this paper is the most often quoted for molecular constants.

In 1965 the quadrupole spectrum of $H_2$ was reported by Rank's group at Penn State[10]. Although the quadrupole spectrum appears due to a different mechanism than the Raman spectrum (absorption due to the quadrupole moment, there is no dipole moment) the selection rules are basically similar. They measured absolute frequency and the pressure shift with hydrogen as the backing gas and extrapolated to zero pressure. Their zero pressure frequencies were used to derive molecular constants up to v=3 and these remain among the

most accurate reported. They relied upon Stoicheff's data for v=0 and their calculated pure rotational line frequencies at J=5 are in error by 0.2 $cm^{-1}$. Their experimental results represent an order of magnitude increase in accuracy over the measurements of Stoicheff. Other authors have investigated pressure shifts[11,12,13]. The values reported are of the order of 0.001 $cm^{-1}$/amagat, which means that pressure shifts can be ignored in the current work, but must be taken into account for higher accuracy work.

The electric field induced spectra of $H_2$, HD, and $D_2$ was reported in 1968[14]. This paper also determined pressure shift coefficients and from the zero pressure frequencies determined molecular constants. Their observed frequencies are reported to ±0.02 $cm^{-1}$ and their molecular constants are not nearly as accurate as the Penn State's values. They did extend the measurements to the deuterium containing molecules however.

Recently the Fourier transform spectrometer at Kitt Peak National Observatory has been used to obtain extremely accurate line positions for molecular hydrogen. This group has been inspired by the observation of many transitions in molecular hydrogen at high J in the Orion molecular cloud[15,16,17]. Their first paper[18] measured the line positions of two S-branch lines to ±0.0001 $cm^{-1}$ accuracy, an increase in accuracy by two orders of magnitude. They next measured the line positions and pressure shifts for the 1-0 through 4-0 bands[19]. From these measurements, accurate to ±0.00005 $cm^{-1}$ in some cases, they derived a new set of molecular constants. Unfortunately these constants could not be extrapolated in the vibrational ground state beyond J=5. The pure rotational S-branch up to J=5 was measured to an accuracy of ±0.0005 $cm^{-1}$[20] and a new set of molecular constants

were determined. They included for the first time $L_0$ and $M_0$, but still did not agree with the Orion measurements at high J. In order to account for the high J values new molecular constants were determined using the Orion measurements as part of the data base[21]. They determined transition frequencies based on these constants up to J=17. In order to test these new molecular constants a laboratory measurement of $S_0(9)$ was made with an accuracy of ±0.004 $cm^{-1}$. It was found that the Orion measurements were undoubtedly in error by about 1 $cm^{-1}$, and new constants were determined using corrected Orion frequencies[22].

Finally there have been very accurate measurements of individual lines for $H_2$. The $S_0(1)$ line was measured to ±0.00021 $cm^{-1}$[23] and the $S_0(3)$ line was measured to ±0.0007 $cm^{-1}$[24].

On the theoretical side, the principal figure has been L. Wolniewicz of the Institute of Physics, Nicolas Copernicus University, Torun, Poland. In a series of papers Kolos and Wolniewicz developed an accurate adiabatic potential energy function for the hydrogen molecule which they used to calculate expectation values of several operators[25,26,27,28,29]. Robert LeRoy used the potential energy function of Kolos and Wolniewicz with relativistic and adiabatic corrections to calculate all of the bound levels for $H_2$, $D_2$, and HD[30]. Tables of the results are given in University of Wisconsin Theoretical Chemistry Institute Report WIS-TCI-387 and are available from the National Auxiliary Publications Service of the A.S.I.S. CCM Information Corp., 909 Third Ave., New York as Document Number 01374. Nonadiabatic effects were calculated for rovibronic energy levels by Dave Bishop[31]. <u>Ab initio</u> nonadiabatic energy corrections to all vibrational

levels in the ground electronic state of molecular hydrogen were calculated for $H_2$, HD and $D_2$ in 1983[32]. These levels produced exact agreement with our experimental results for the first time. Because we needed energy levels for the tritium containing molecules as well we asked Bob LeRoy to take Wolniewicz's results and extrapolate to HT, DT and $T_2$. LeRoy calculated for us the energy levels for all bound states and all isotopic molecules to 0.0001 $cm^{-1}$ [1]. Comparing these values to the recent experiments by the Kitt Peak group show agreement to within experimental error for all pure rotational spectra. The situation for the higher vibrational levels is more complicated. LeRoy also calculated the transition matrix elements. In 1984 the energy levels for all the isotopic molecules were published by Wolniewicz without the non-adiabatic corrections, making the literature somewhat confusing as they are less accurate than previous work[33]. I shall use LeRoy's theoretical results in all of the following as they are the most accurate and well tabulated (i.e. all bound rovibrational energies are tabulated in contrast to Wolniewicz's results).

The results for hydrogen are given in Table I. The measured lines are pure rotational Stokes lines $S_0(0)$ through $S_0(5)$ and rotation-vibration lines O-branch $O_1(2)$ through $O_1(5)$, Q-branch $Q_1(0)$ through $Q_1(6)$ and $Q_2(0)$ through $Q_2(3)$, and S-branch $S_1(0)$ through $S_1(5)$.

Table I

MEASURED $H_2$ RAMAN TRANSITIONS

| J | STOKES | O-BRANCH | Q-BRANCH | S-BRANCH | OVERTONE Q-BRANCH |
|---|---|---|---|---|---|
| 0 | 354.365 | -------- | 4161.200 | 4497.848 | 8087.030 |
| 1 | 587.087 | -------- | 4155.281 | 4712.938 | 8075.283 |
| 2 | 814.456 | 3806.859 | 4143.493 | 4917.032 | 8051.964 |
| 3 | 1034.698 | 3568.239 | 4125.903 | 5108.415 | 8017.168 |
| 4 | 1246.082 | 3329.144 | 4102.592 | 5285.632 | -------- |
| 5 | 1447.247 | 3091.141 | 4073.698 | 5448.037 | -------- |
| 6 | -------- | -------- | 4039.451 | -------- | -------- |

In Table II the results are compared to the most accurate experimental values and to line positions calculated from LeRoy's theoretical energy levels. I have chosen LeRoy's values as a standard; the entries in the table are differences between LeRoy and experiment. I include Stoicheff's data because it remains the most often cited. The average deviation from LeRoy without $S_1(5)$ and the O-branch is 0.028 $cm^{-1}$, which is nearly equal to the estimated accuracy of ±0.03 $cm^{-1}$. The $S_1(5)$ line was extremely weak and difficult to measure accurately because, in order to see it, the slits had to be opened to a linewidth of several wavenumbers. The good agreement with the more precise experimental measurements gives one confidence in the accuracy of the stronger lines that have not been measured previously. In particular this technique can be used with confidence for accurate measurements of line positions of the tritium containing isotopomers. The first overtone has been observed for the first time in spontaneous Raman spectroscopy and an additional line observed, the $Q_2(0)$. Quadrupole spectroscopy is not sensitive to a Qv(0) transition. Two additional lines have been added to the known transitions of $H_2$, the $S_1(4)$ and the $Q_1(6)$. The $S_1(5)$ has been seen but not to the accuracy necessary for good spectroscopic data. The $Q_1(0)$ has been measured more accurately than Stoicheff's original observations. The O-branch data add nothing new as they can be calculated from previously observed pure rotational and Q-branch data.

Table II

COMPARISON OF AB INITIO CALCULATIONS TO BEST EXPERIMENTS FOR $H_2$

| J | Schwartz and LeRoy | Veirs and Rosenblatt | Jennings and Brault | Bragg, Brault, and Smith | Fink, Wiggins, and Rank | Stoicheff |
|---|---|---|---|---|---|---|
| **STOKES** | | | | | | |
| 0 | 354.3732 | 0.008 | -0.0003(4) | -------- | -------- | -0.008 |
| 1 | 587.0320 | -0.055 | -0.0001(2) | -------- | -------- | -0.023 |
| 2 | 814.4243 | -0.032 | -0.0004(1) | -------- | -------- | 0.018 |
| 3 | 1034.6706 | -0.027 | 0.0004(1) | -------- | -------- | 0.020 |
| 4 | 1246.0992 | 0.017 | 0.0011(2) | -------- | -------- | -------- |
| 5 | 1447.2803 | -0.033 | 0.0015(4) | -------- | -------- | -------- |
| **O-BRANCH** | | | | | | |
| 2 | 3806.8009 | -0.058 | -------- | -------- | -------- | -------- |
| 3 | 3568.2291 | -0.010 | -------- | -------- | -------- | -------- |
| 4 | 3329.0471 | -0.097 | -------- | -------- | -------- | -------- |
| 5 | 3091.2063 | -0.065 | -------- | -------- | -------- | -------- |
| **Q-BRANCH** | | | | | | |
| 0 | 4161.1741 | -0.026 | -------- | -------- | -------- | 0.040 |
| 1 | 4155.2611 | -0.020 | -------- | 0.0064(1) | 0.0036 | 0.060 |
| 2 | 4143.4714 | -0.022 | -------- | 0.0054(3) | 0.0046 | 0.084 |
| 3 | 4125.8769 | -0.026 | -------- | 0.0030(4) | 0.0051 | 0.045 |
| 4 | 4102.5836 | -0.008 | -------- | 0.0016(40) | -------- | -------- |
| 5 | 4073.7304 | 0.032 | -------- | -0.0086(250) | -------- | -------- |
| 6 | 4039.4856 | 0.035 | -------- | -------- | -------- | -------- |
| **S-BRANCH** | | | | | | |
| 0 | 4497.8446 | -0.003 | -------- | 0.0055(2) | 0.0061 | -------- |
| 1 | 4712.9089 | -0.029 | -------- | 0.0035(2) | 0.0001 | -------- |
| 2 | 4917.0079 | -0.024 | -------- | 0.0010(3) | -0.0039 | -------- |
| 3 | 5108.4010 | -0.014 | -------- | -0.0030(6) | -0.0056 | -------- |
| 4 | 5285.5848 | -0.047 | -------- | -------- | -------- | -------- |
| 5 | 5447.3240 | -0.774 | -------- | -------- | -------- | -------- |
| **OVERTONE Q-BRANCH** | | | | | | |
| 0 | 8087.0203 | -0.010 | -------- | -------- | -------- | -------- |
| 1 | 8075.3237 | 0.041 | -------- | 0.0123(6) | 0.0132 | -------- |
| 2 | 8052.0013 | 0.037 | -------- | 0.0103(70) | -------- | -------- |
| 3 | 8017.1929 | 0.025 | -------- | 0.0029(100) | -------- | -------- |

There are three points which should be emphasized in regards to the existing data and the calculations by Schwartz and LeRoy. The non-adiabatic corrections to the energy take two forms, the J-dependent corrections and the vibrational level corrections. First, the energy levels as calculated by Schwartz and LeRoy improve the accuracy by at least two orders of magnitude. For example, in pure rotation the $S_0(3)$ line agrees with experiment to within 0.0004 $cm^{-1}$ whereas the line from the previous theoretical work agrees to 0.0700 $cm^{-1}$, an increase in accuracy by a factor of 200. For the vibrational energies if one compares the $Q_1(1)$ line then most of the rotational uncertainty will be removed. The $Q_1(0)$ line is not measured as accurately as the $Q_1(1)$ or all of the rotational uncertainty could be removed. For LeRoy one gets agreement to within 0.006 $cm^{-1}$, whereas the previous calculations show agreement to within 0.869 $cm^{-1}$, improvement by slightly more than 100. Nevertheless there still seems to be disagreement between the best experiments and theory. In pure rotation the disagreement seems to increase with J from around 0.0002 $cm^{-1}$ to above 0.001 $cm^{-1}$, outside of the assigned experimental errors. The difference between the theoretical line positions and the experimental values of Jennings and Brault (in units of $10^{-3}$ $cm^{-1}$) are given in Fig. XVII. The error bars represent the stated experimental uncertainty. For vibration one sees a trend in going to higher vibrational levels. Using the quadrupole transition frequencies of Bragg, Brault, and Smith and a hydrogen pressure shift coefficient of 0.002 $cm^{-1}$/amagat with a linear vibrational dependence[34], one can compare zero pressure transition frequencies to those calculated from theoretical energy levels up to v=4. The differences (in units of $10^{-3}$ $cm^{-1}$) are given for the S-branch transitions in Table III and plotted in Fig. XVIII. The trends

show a strong vibrational effect and a weaker rotational effect similar to that seen in Jennings and Brault's data. The data for v=1 and v=2 of Fink, Wiggins, and Rank show the same trend.

Table III

DIFFERENCES (IN $10^{-3}$ $cm^{-1}$) BETWEEN AB INITIO CALCULATIONS AND THE BEST EXPERIMENTAL TRANSITION FREQUENCIES: VIBRATIONAL AND ROTATIONAL EFFECTS IN $H_2$

| | v=1 | v=2 | v=3 | v=4 |
|---|---|---|---|---|
| S(0) | 4.7 | 10.3 | 69.4 | 130 |
| S(1) | 2.8 | 6.1 | 63.3 | 129 |
| S(2) | -1.0 | 0.1 | 48.5 | 108 |
| S(3) | -3.4 | -5.7 | 35.2 | 85 |

A final note on higher J pure rotational transitions in $H_2$. The calculated transition frequencies of Jennings, Bragg, and Brault and the values obtained from the improved constants of Jennings, Rahn, and Owyoung are compared to the theoretical values in Table IV. As can be seen the improved version agrees better with the theoretical values at very high J. The fact that the measured value of $S_0(9)$ is within experimental error, 0.004 $cm^{-1}$, of the theoretical value seems to indicate that experiment has yet to match the accuracy of the theoretical energy levels. This indicates that the best source of transition frequencies at high J is still the threoretical values.

Table IV

COMPARISON OF FRQUENCIES CALCULATED FROM AB INITIO ENERGIES AND EXPERIMENTAL MOLECULAR CONSTRANTS: DIFFERENCES AT HIGH J FOR $H_2$

| J | LeRoy and Schwartz | Jennings, Bragg, and Brault | | Jennings, Rahn, and Owyoung | |
|---|---|---|---|---|---|
| 6 | 1637.0450 | 1637.05 | 0.00 | 1637.0456 | -0.0006 |
| 7 | 1814.4909 | 1814.5 | 0.0 | 1814.4961 | -0.0052 |
| 8 | 1978.9754 | 1979.0 | 0.0 | 1978.9844 | -0.0090 |
| 9 | 2130.0983 | 2130.1 | 0.0 | 2130.1011 | -0.0028 |
| 10 | 2267.6782 | 2267.7 | 0.0 | 2267.6478 | 0.0304 |
| 11 | 2391.7245 | 2391.8 | -0.1 | 2391.6124 | 0.1121 |
| 12 | 2502.4063 | 2502.4 | 0.0 | 2502.1529 | 0.2534 |
| 13 | 2600.0222 | 2600.1 | -0.1 | 2599.5948 | 0.4274 |
| 14 | 2684.9714 | 2685.3 | -0.3 | 2684.4537 | 0.5177 |
| 15 | 2757.7263 | 2759.0 | -1.3 | 2757.4928 | 0.2335 |
| 16 | 2818.8092 | 2822 | -3.2 | 2819.8224 | -1.0132 |
| 17 | 2868.7708 | 2877 | -8.2 | 2873.0558 | -4.2850 |

IIId. Hydrogen Deuteride

The current experimental results for HD at this time consist of the Q-branch at low resolution. Measurements of the Q-branch lines of all six isotopomers were made at the same time with a sample used for muon catalysed fusion experiments in Switzerland. From known line positions, an instrument correction factor was determined for calibration purposes. The experimental results are compared to theoretical line positions in Table V.

Table V

Q-BRANCH LINE POSITIONS OF HD

| J | EXPERIMENT | THEORETICAL | DIFFERENCE |
|---|---|---|---|
| 0 | 3632.2 | 3632.1624 | -0.04 |
| 1 | 3628.4 | 3628.3062 | -0.09 |
| 2 | 3620.6 | 3620.6118 | 0.01 |
| 3 | 3609.2 | 3609.1143 | -0.09 |
| 4 | 3593.1 | 3593.8665 | 0.77 |
| 5 | 3574.9 | 3574.9372 | 0.04 |

In many respects there is more experimental data available on HD than for $H_2$. This is because of the small permanent dipole of HD, due to nuclear vibrations about the center of mass which is displaced from the geometric center of the molecule, gives rise to an allowed infrared absorption band system. The intensity of infrared absorption due to the permanent dipole moment and the abundance of the molecule in the atmospheres of the large planets makes HD an interesting molecule to observe both astronomically and in the laboratory. The work by Stoicheff and Brannon, Church, and Peters applies to HD as well as $H_2$. The 1-0, 2-0, 3-0, and 4-0 rotation-vibration spectra were seen by Herzberg[34] and remeasured and extended to the 5-0 and 6-0 bands by McKellar[35,36]. A single well calibrated 5-0 line was measured using the sensitive photoacoustic detection method[37]. The pure rotational spectra has been studied using a diode laser spectrometer[38]. The experimental line positions are compared to the theoretical line positions in Table VI. The experimental line positions do not need to be corrected for pressure shifts because the largest pressure shift is an order of magnitude below the difference between experiment and theory. The vibrational trend seen in $H_2$ continues in HD. There also seems to be a rotational dependence that is amplified at higher vibrational levels. The vibrational trend in differences between experiment and theory are given in Fig. XIX for HD and illustrates the accuracy of the first few vibrational energy levels. Because the transitions are directly to the higher vibrational level, the differences represent the sum of all of the errors between individual vibrational levels.

Table VI

DIFFERENCES BETWEEN THEORY AND OBSERVED LINE POSITIONS FOR THE R-BRANCH OF HD

| J | V = 1 | V = 2 | V = 3 | V = 4 | V = 5 | V = 6 |
|---|---|---|---|---|---|---|
| 0 | 0.001 | 0.035 | 0.061 | 0.120 | 0.150 | 0.176 |
| 1 | -0.002 | 0.023 | 0.057 | 0.117 | 0.137 | 0.162 |
| 2 | -0.003 | -0.069 | 0.045 | 0.103 | 0.125 | 0.147 |
| 3 | -0.001 | -0.022 | 0.040 | 0.097 | 0.071 | 0.108 |
| 4 | -0.003 | | 0.021 | 0.092 | | |
| 5 | -0.008 | | | | | |

The molecular constants derived from the previous experiments undergo modification each time new data are obtained. As is often the case, the new data do not always encompass the same vibrational levels, so the new molecular constants are derived for the vibrational levels observed only. When using these new molecular constants with the old constants for the other vibrational levels, errors are generated. It is best to use molecular constants only for the levels observed and not to mix molecular constants for different vibrational levels from seperate experiments.

## IIIe. Hydrogen Tritide

The only experimental work that I am aware of for HT that is published comes from England[39]. Their results are compared to theory along with my initial results in Table VII.

Table VII

COMPARISON OF EXPERIMENTAL TRANSITION FREQUENCIES
TO AB INITIO CALCULATIONS FOR HT

| | Schwartz and LeRoy | | Edwards et al. | | Veirs et al. |
|---|---|---|---|---|---|
| J | $S_0$-Branch | $Q_1$-Branch | $S_0$-Branch | $Q_1$-branch | $Q_1$-Branch |
| 0 | 237.8830 | 3434.8957 | -0.044 | 6.526 | 0.0 |
| 1 | 394.8595 | 3431.6577 | -0.093 | 6.525 | 0.1 |
| 2 | 549.4532 | 3425.1951 | -0.217 | 6.524 | 0.1 |
| 3 | | 3415.5342 | | 6.487 | -0.1 |
| 4 | | 3402.7144 | | 6.317 | -0.1 |

Edwards et al. claim that their calibration is good to ±0.005 $cm^{-1}$, however the large discrepancy between their reported Q-branch lines and both the theoretical line positions and this work indicates that something is drastically wrong. Their frequency differences within the Q-branch are excellant as shown by the reproducibility of the line position differences. Since they use a fifth order polynomial to fit their calibration lines, it is possible that with a small number of calibration lines they could fit an arbitrary set of lines with high reproducibility. With this set of data I would conclude that there is no evidence for the theoretical energy levels showing an isotope dependent error from the true energy levels.

Zare's group[41] at Stanford is using the permanent dipole of HT for laser diode measurements of the 4th and 5th vibrational levels to high accuracy. Their preliminary results indicate that by v=4 the theoretical vibrational band is in error by 0.3 $cm^{-1}$. Although this error is much larger than the error seen in HD or $H_2$, it is reasonable in that the vibrational spacing error seems to have an isotopic dependence, growing from $H_2$ to HD. Their results are compared to theoretical line positions in Table VIII. More exact experimental work needs to be done on HT. The Raman

apparatus is probably not accurate enough for answering these questions. An experiment using the new Los Alamos Fourier Transform instrument and infrared to visible absorption seems approbriate.

Table VIII

COMPARISON OF THEORY TO EXPERIMENT: DIFFERENCES AT HIGH v FOR HT

| J | LeRoy et al. P-Branch | LeRoy et al. R-Branch | Zare et al. P-Branch | Zare et al. R-Branch |
|---|---|---|---|---|
| v=4 | | | | |
| 0 | | 12869.1543 | | 0.368 |
| 1 | 12722.8785 | 12922.8991 | 0.363 | 0.365 |
| 2 | 12631.2713 | 12963.1917 | | 0.366 |
| 3 | 12528.0396 | 12989.7220 | | 0.353 |
| 4 | 12413.7385 | 13002.2549 | | 0.337 |

| | LeRoy et al. P-Branch | LeRoy et al. R-Branch | Zare et al. P-Branch | Zare et al. R-Branch |
|---|---|---|---|---|
| v=5 | | | | |
| 0 | | 15683.4532 | | 0.469 |
| 1 | 15540.2578 | 15731.0478 | 0.461 | 0.458 |
| 2 | 15445.5702 | 15762.1418 | 0.452 | 0.450 |
| 3 | 15336.1883 | 15776.4568 | | 0.447 |

IIIf. Deuterium

Deuterium, a homonuclear molecule, exhibits both Raman and quadrupole spectra. Since deuterium does not have a permanent dipole moment it's higher vibrational levels have not been as intensively studied as HD or HT. It is amenable to electric field induced infrared studies. Both Stoicheff (Raman) and Brannon, Church, and Peters (Electric Field Induced Infrared Spectra) included $D_2$ in their studies. Accurate cw coherent anti-Stokes spectroscopy (CARS) was used to determine the $Q_1(2)$ line positon[42]. Zero density

Q-branch Raman frequencies were determined with an accuracy of 0.02 $cm^{-1}$[43]. The quadrupole spectra yielded frequencies with an uncertainty of ±0.004 $cm^{-1}$[12]. The results for this experiment are accurate to only 0.1 $cm^{-1}$, but extend to higher J. There is one current result accurate to 0.03 $cm^{-1}$. The experimental results are compared to Schwartz and LeRoy's theoretical values in Table IX.

Table IX

COMPARISON OF EXPERIMENT TO THEORY: $D_2$

Pure Rotation

| J | LeRoy et al. | Veirs et al. | Stoicheff |
|---|---|---|---|
| 0 | 179.0670 | -0.041 | 0.011 |
| 1 | 297.5336 | 0.02 | 0.013 |
| 2 | 414.6484 | 0.04 | -0.007 |
| 3 | 529.9001 | 0.09 | -0.007 |
| 4 | 642.8063 | 0.10 | -0.001 |
| 5 | 752.9195 | 0.01 | |
| 6 | 859.8319 | 0.07 | |
| 7 | 963.1795 | 0.02 | |
| 8 | 1062.6447 | 0.07 | |

O-Branch

| J | LeRoy et al. | Veirs et al. | McKellar et al. | Brannon et al. |
|---|---|---|---|---|
| 2 | 2814.5474 | -0.02 | 0.0015 | 0.017 |
| 3 | 2693.9710 | -0.14 | -0.0013 | -0.079 |
| 4 | 2572.6434 | 0.14 | 0.0006 | |
| 5 | 2451.0885 | 0.04 | | |
| 6 | 2329.8082 | | | |
| 7 | 2209.2757 | 0.05 | | |

Q-Branch

| J | LeRoy | Veirs et al. | McKellar et al. | Brannon et al. | Stoicheff | Henesian et al. | Looi et al. |
|---|---|---|---|---|---|---|---|
| 0 | 2993.6144 | 0.0 | | 0.014 | 0.066 | | 0.051 |
| 1 | 2991.5046 | 0.0 | 0.0003 | 0.019 | 0.059 | | 0.040 |
| 2 | 2987.2918 | 0.1 | -0.0037 | 0.006 | 0.062 | 0.0547 | 0.046 |
| 3 | 2980.9886 | 0.0 | 0.0004 | 0.022 | 0.112 | | 0.034 |
| 4 | 2972.6145 | 0.1 | 0.0017 | 0.018 | 0.058 | | 0.047 |
| 5 | 2962.1952 | 0.0 | | 0.019 | | | |
| 6 | 2949.7621 | 0.1 | | 0.077 | | | |
| 7 | 2935.3524 | 0.2 | | | | | |
| 8 | 2919.0086 | 0.2 | | | | | |
| 9 | 2900.7782 | 0.2 | | | | | |

S-Branch

| J | LeRoy | Veirs et al. | McKellar et al. | Brannon et al. |
|---|---|---|---|---|
| 0 | 3166.3588 | | -0.0008 | 0.059 |
| 1 | 3278.5222 | | 0.0000 | 0.088 |
| 2 | 3387.2629 | 0.04 | 0.0023 | 0.043 |
| 3 | 3492.0953 | 0.07 | 0.0040 | 0.031 |
| 4 | 3592.5684 | | | |
| 5 | 3688.2719 | -0.09 | | |
| 6 | 3778.8405 | | | |
| 7 | 3863.9577 | 0.14 | | |

Overtone Q-Branch

| J | LeRoy | Veirs et al. | Brannon et al. |
|---|---|---|---|
| 0 | 5868.0927 | 0.0 | 0.09 |
| 1 | 5863.9093 | 0.0 | 0.07 |
| 2 | 5855.5553 | 0.0 | 0.08 |
| 3 | 5843.0562 | 0.1 | |
| 4 | 5826.4503 | 0.2 | |

Stoicheff's values for pure rotation agree within experimental error. The current Raman instrument can be used to extend the measurements to higher J values, above those seen by Stoicheff. The O-branch measurements of McKellar et al. agree quite well, especially since their uncertainty is given as 0.004 $cm^{-1}$. The $O_1(3)$ line of Brannon is outside their error bars, but because of the measurement of McKellar et al. this discrepancy can be discounted. The Q-branch contains some interesting results. We have extended the observed lines to higher J values and agree with theory as to their

positions. All of McKellar's line positions agree to well within their experimental error of ±0.004 $cm^{-1}$. There seems to be a rotational dependence of the differences in McKellar's results, but because of the large stated uncertainty more work will have to be done. Also the discrepancies are in the regime where pressure shifts will have to be taken account of. All of the results of Brannon et al. are within their stated uncertainty except for J=6 which is about twice the uncertainty. Stoicheff also has lines outside of his uncertainty, presumably because of the low intensity. Henesian et al. have a stated uncertainty of ±0.001 $cm^{-1}$ which disagrees by a factor of 50 with theory as well as with the experimental results of McKellar et al.. Because of the unusual experimental method one must neglect this result. The results of Looi et al. are taken from high density measurements and extrapolated to zero density. The differences are a factor of 10 greater than the reported uncertainties. For the S-branch, we have extended the observations to higher J, again confirming the prediction of where the lines generally lie. McKellar's results confirm the accuracy of the theoretical calculations and Brannon's results indicate that their measurements can be trusted to within a factor of 2 of their reported uncertainties. This is important because their first overtone measurements agree within a factor of 2 of the reported uncertainties.

There is no indication in the experimental results for $D_2$ for any disagreement with the theoretical calculations. The higher rotational and vibrational observed transitions lack the resolution for seeing the small but significant deviations. Because of the lack of resolution there is no additional information on the isotopic dependence of the theoretical

calculations. If the Los Alamos Fourier Transform instrument has the needed sensitivity a quadrupole absorption experiment could be considered, or perhaps a Raman scattering experiment.

## IIIg. Deuterium Tritide

Although DT has an electic dipole moment it has not been studied by any optical absorption technique. DT has been studied by Raman spectroscopy at Los Alamos[44] and in England[40]. The reported uncertainties of Edwards are 0.005 $cm^{-1}$ and Barefield et al. report uncertainties of ±0.1 $cm^{-1}$ for pure rotation and the Q-branch, and 0.5 $cm^{-1}$ for the O and S-branches. The experimental results are tabulated in Table X.

Table X

COMPARISON OF EXPERIMENT TO THEORY FOR DT

Pure Rotation

| J | LeRoy | Edwards et al. | Barefield et al. | Veirs et al. |
|---|---|---|---|---|
| 0 | 149.6121 | 0.008 | 0.2 | |
| 1 | 248.7180 | 0.005 | 0.1 | |
| 2 | 346.8796 | 0.014 | 0.2 | |
| 3 | 443.7367 | -0.014 | 0.1 | |
| 4 | 538.9458 | | 0.0 | |
| 5 | 632.1839 | | 0.2 | |

O-Branch

| J | | | | |
|---|---|---|---|---|
| 2 | 2593.7041 | | 0.1 | |
| 3 | 2492.9889 | | 0.1 | |

Q-Branch

| | | | | |
|---|---|---|---|---|
| 0 | 2743.3162 | -0.120 | -0.1 | |
| 1 | 2741.7069 | -0.106 | -0.1 | |
| 2 | 2738.4926 | -0.086 | -0.2 | 0.1 |
| 3 | 2733.6816 | -0.105 | -0.1 | 0.0 |
| 4 | 2727.2861 | -0.162 | -0.1 | 0.1 |
| 5 | 2719.3224 | | -0.1 | 0.1 |
| 6 | 2709.8108 | | -0.0 | 0.0 |
| 7 | 2698.7752 | | | 0.1 |
| 8 | 2686.2430 | | | -0.1 |

S-Branch

| | | |
|---|---|---|
| 0 | 2888.1047 | 0.1 |
| 1 | 2982.3996 | |
| 2 | 3074.1657 | 0.3 |
| 3 | 3163.0591 | 0.2 |
| 4 | 3248.7566 | 0.1 |

The uncertainty of Edwards et al. indicates that the vibrational fundamental of LeRoy is off by greater than .1 $cm^{-1}$, however their results on HT lead me to use the theoretical calculations for calculating line positions. The data by Barefield et al. and Veirs et al. indicate that the fundamental frequency can not be in error by more than 0.1 $cm^{-1}$ and that the rotational dependence is less than 0.1 $cm^{-1}$ up to the relatively high J value of 8. The fundamental vibrational frequency can be accurately measured using the present Raman apparatus, perhaps reducing the known difference by a factor of 3.

## IIIh. Tritium

The only data reported for $T_2$ has been Raman data[45]. The reported uncertainties are again ±0.005 $cm^{-1}$. The results are compared to theory in Table XI.

Table XI

COMPARISON OF EXPERIMENT TO THEORY: $T_2$

Pure Rotation

| J | LeRoy | Edwards et al. | Veirs et al. |
|---|---|---|---|
| 0 | 120.0659 | 0.017 | 0.015 |
| 1 | 199.7013 | 0.006 | 0.020 |
| 2 | 278.7283 | -0.004 | -0.2 |
| 3 | 356.9128 | -0.041 | -0.1 |
| 4 | 434.0292 | | -0.1 |
| 5 | 509.8627 | | -0.1 |
| 6 | 584.2115 | | -0.1 |
| 7 | 656.8879 | | -0.1 |
| 8 | 727.7197 | | -0.1 |
| 9 | 796.5516 | | -0.1 |
| 10 | 863.2451 | | 0.0 |
| 11 | 927.6790 | | -0.1 |

Q-Branch

| | | | |
|---|---|---|---|
| 0 | 2464.4987 | 0.179 | |
| 1 | 2463.3434 | 0.188 | |
| 2 | 2461.0350 | 0.213 | 0.0 |
| 3 | 2457.5785 | 0.240 | 0.1 |
| 4 | 2452.9810 | 0.256 | 0.0 |
| 5 | 2447.2518 | 0.231 | 0.0 |
| 6 | 2440.4026 | | -0.1 |
| 7 | 2432.4474 | | 0.0 |
| 8 | 2423.4020 | | -0.1 |
| 9 | 2413.2846 | | 0.1 |
| 10 | 2402.1149 | | -0.1 |

Again the values for the fundamental frequency of Edwards et al. seem to indicate a serious failure of the theory. The much lower resolution spectra however indicate that the error is less than 0.1 $cm^{-1}$. These discrepancies can be resolved using the present Raman apparatus. A quadrupole absorption experiment using the Los Alamos Fourier instrument will yield valuable data for testing the isotopic dependence of the theoretical energy levels now that there are excellant values for $H_2$.

## IIIi. Conclusion

The ground vibrational state energy levels are well described by the recent theoretical calculations for all six molecular hydrogen isotopomers. There is some evidence in $H_2$ that the J-dependence of the theoretical calculations is not entirely adequate. The small differences at J=4,5 of 0.001 $cm^{-1}$ between experiment and theory might possibly be due to J dependent pressure shifts or some other weak effect that has not been corrected for. The measurement at J=9 lacks the accuracy to answer this question. For determining line positions at very high J, the evidence suggests that the theoretical predictions remain more reliable than the molecular constants. There is no reason to believe that the theoretical line positions will be off by more than a few hundreths of a wavenumber at J=20, certainly adequate for astronomical observations, while the best molecular constants could be in error by more than 10 $cm^{-1}$. Thus, for the ground vibrational state, there is no evidence for an isotopic dependence in the energy levels that has not been accounted for by the theoretical calculations and there is very little evidence for a J dependence error. There definately needs to be more work on the heavier isotopes such as HT, DT, and $T_2$ at very high resolution, which can only be achieved using instruments such as a Fourier Transform machine or difference frequency lasers, to obtain transition frequencies as accurate as those available for $H_2$ in order to elucidate the isotopic and rotational dependence in the ground vibrational state. It is not clear how to obtain accurate transition frequencies at the very high J's needed to determine the rotational dependence for $H_2$.

The higher vibrational levels exhibit a definate trend for all of the isotopomers, as shown in Fig. XX. There is a vibrational dependence that has not been accounted for in the theoretical calculations. Furthermore the vibrational dependent errors become larger for HD and larger still for HT. There is a question as to whether this is due to an increasing reduced mass or from the anisotropic shift in equilibrium internuclear distance. The results of Edwards et al. indicate that the isotopic dependence goes as the reduced mass as they show an error in v=1 for $T_2$ of 0.18 $cm^{-1}$ while for DT the error is less 0.12 $cm^{-1}$. However the error for $D_2$ is only 0.003 $cm^{-1}$. This fact and the blatant experimental error that Edwards et al. made in the fundamental of HT leads one to distrust their results. Accurate overtone line positions need to be measured for DT and $T_2$ in order to resolve these questions. The observed differences may also have a contribution from pressure shifts or other experimental artifacts, and pressure dependent studies need to be completed to measure the magnitude of these effects. The accuracy required again calls for the use of a Fourier Transform instrument. There are questions about the location of v=1 and v=2 for the tritium containing isotopomers that can be answered with the current Raman instrument.

## IV. LINE INTENSITIES

### IVa. Introduction

The effect of centrifugal distortion and rotation-vibration interaction on the intensity of a Raman line has been studied both theoretically and experimentally since 1959. The first work, which forms the theoretical backbone for much of the subsequent work, was the development of an expression for the intensity with a J dependence using first-order perturbation theory[46]. Further theoretical work extended these expressions to overtones[47]. The first experimental work confirmed the theoretical predictions[48]. This work was almost immediately followed in 1981 by further theoretical work which extended the J dependence another term[49] and experiments which measured the first and second derivatives of the polarizability in $H_2$[50]. The first attempt to calculate the transition matrix elements was published for the O and S-branches for $H_2$ and $D_2$ also in 1981[51]. Our work was begun in 1982 and out of our interest C. Shcwartz and R. J. LeRoy have calculated all of the rotation and rotation-vibration matrix elements for all six of the molecular isotopes, however their work is still unpublished.

### IVb. First-order Perturbation Theory

James and Klemperer[46] used first-order perturbation theory where the polarizability and the polarizability anisotropy are expanded about the equilibrium internuclear distance and the matrix elements are evaluated analytically. They considered two cases, both have the direction of the scattered light perpendicular to the direction of the incident light with the

polarization of the incident light parrallel to the direction of the scattered light in one case, I(obs pl), and perpendicular to the direction of the scattered light in the second case, I(obs pd). The two cases affect the overall intensity somewhat but do not affect the J-dependence of the scattering cross-section. The overall intensity is affected most in the Q-branch where there is a contribution from the polarizability which does not allow scattering in the direction of the polarization. The polarizability anisotropy does allow scattering in the direction of the polarization of the incident beam. The experiments carried out at Los Alamos should have perpendicular polarization so the results for I(obs pd) will only be considered, but I(obs pl) will yield the same results. The equations for all Raman branches are as follows:

Pure Rotation

$\Delta J = -2$

$$I = \frac{64\pi^4 \nu^4}{c^4} I_o N_{v,J} \frac{7\ J(J-1)}{30\ (2J+1)\ (2J-1)} \beta_o^2 \{1 + \frac{\gamma^2}{\chi} (J^2 - J + 1)\}^2 . \qquad (15)$$

$\Delta J = +2$

$$I = \frac{64\pi^4 \nu^4}{c^4} I_o N_{v,J} \frac{7(J+1)(J+2)}{30\ (2J+3)\ (2J+1)} \beta_o^2 \{1 + \frac{\gamma^2}{\chi} (J^2 + 3J + 3)\}^2 . \qquad (16)$$

Vibration-Rotation

Q-branch ($\Delta J$=0)

$$I = \frac{64\pi^4\ \nu^4}{c^4\ 2\alpha} I_o N_{v,J} \{1 - (\frac{3}{4}\gamma^2)\ J(J+1)\}^2 [\kappa_1^2 + \beta_1^2 (\frac{7\ J(J+1)}{45\ (2J+3)\ (2J-1)})] . \qquad (17)$$

O-branch ($\Delta J = -2$)

$$I = \frac{64\pi^4\ \nu^4\ \beta_1^2\ 7\ I_o\ N_{v,J}\ J(J-1)}{c^4\ 2\alpha\ 30\ (2J+1)\ (2J-1)} \{1 - (\frac{3}{4}\gamma^2)\ J(J+1) + 2\ \chi\gamma\ (2J-1)\}^2 . \qquad (18)$$

## IV. LINE INTENSITIES

### IVa. Introduction

The effect of centrifugal distortion and rotation-vibration interaction on the intensity of a Raman line has been studied both theoretically and experimentally since 1959. The first work, which forms the theoretical backbone for much of the subsequent work, was the development of an expression for the intensity with a J dependence using first-order perturbation theory[46]. Further theoretical work extended these expressions to overtones[47]. The first experimental work confirmed the theoretical predictions[48]. This work was almost immediately followed in 1981 by further theoretical work which extended the J dependence another term[49] and experiments which measured the first and second derivatives of the polarizability in $H_2$[50]. The first attempt to calculate the transition matrix elements was published for the O and S-branches for $H_2$ and $D_2$ also in 1981[51]. Our work was begun in 1982 and out of our interest C. Shcwartz and R. J. LeRoy have calculated all of the rotation and rotation-vibration matrix elements for all six of the molecular isotopes, however their work is still unpublished.

### IVb. First-order Perturbation Theory

James and Klemperer[46] used first-order perturbation theory where the polarizability and the polarizability anisotropy are expanded about the equilibrium internuclear distance and the matrix elements are evaluated analytically. They considered two cases, both have the direction of the scattered light perpendicular to the direction of the incident light with the

polarization of the incident light parrallel to the direction of the scattered light in one case, I(obs pl), and perpendicular to the direction of the scattered light in the second case, I(obs pd). The two cases affect the overall intensity somewhat but do not affect the J-dependence of the scattering cross-section. The overall intensity is affected most in the Q-branch where there is a contribution from the polarizability which does not allow scattering in the direction of the polarization. The polarizability anisotropy does allow scattering in the direction of the polarization of the incident beam. The experiments carried out at Los Alamos should have perpendicular polarization so the results for I(obs pd) will only be considered, but I(obs pl) will yield the same results. The equations for all Raman branches are as follows:

<u>Pure Rotation</u>

$\Delta J = -2$

$$I = \frac{64\pi^4 \nu^4}{c^4} I_o N_{v,J} \frac{7\ J(J-1)}{30\ (2J+1)\ (2J-1)} \beta_o^2 \{1 + \frac{\gamma^2}{\chi} (J^2 - J + 1)\}^2 . \qquad (15)$$

$\Delta J = +2$

$$I = \frac{64\pi^4 \nu^4}{c^4} I_o N_{v,J} \frac{7(J+1)(J+2)}{30\ (2J+3)\ (2J+1)} \beta_o^2 \{1 + \frac{\gamma^2}{\chi} (J^2 + 3J + 3)\}^2 . \qquad (16)$$

<u>Vibration-Rotation</u>

Q-branch ($\Delta J=0$)

$$I = \frac{64\pi^4 \nu^4}{c^4\ 2\alpha} I_o N_{v,J} \{1 - (\tfrac{3}{4}\gamma^2)\ J(J+1)\}^2 [\kappa_1^2 + \beta_1^2 (\frac{7\ J(J+1)}{45\ (2J+3)\ (2J-1)})] . \qquad (17)$$

O-branch ($\Delta J = -2$)

$$I = \frac{64\pi^4 \nu^4 \beta_1^2\ 7\ I_o N_{v,J}\ J(J-1)}{c^4\ 2\alpha\ 30\ (2J+1)\ (2J-1)} \{1 - (\tfrac{3}{4}\gamma^2)\ J(J+1) + 2\ \chi\gamma\ (2J-1)\}^2 . \qquad (18)$$

S-branch ($\Delta J=+2$)

$$I = \frac{64\pi^4 \nu^4 \beta_1^2 \; 7 \; I_o \; N_{v,J} \; J(J+1)(J+2)}{c^4 \; 2\alpha \; 30 \; (2J+3)(2J+1)} \{1 - (\tfrac{3}{4}\gamma^2) \; J(J+1) - 2 \; \chi\gamma \; (2J+3)\}^2 . \quad (19)$$

where $\beta_0 = (\alpha|| - \alpha\perp)$, $\beta_1 = (\delta\beta/\delta r)r_e$, $\chi = [\beta_o(r_e)/\beta_1 \; r_e]$, $\alpha = 1/\gamma \; r_e^2$ and $\gamma = 2 \; B_e/\omega_e$. The rest of the symbols should be familiar. The scattering is from unit volume per unit solid angle.

For pure rotation the scattering cross-section always increases with J. When the transition connects the same pair of J-levels the scattering cross-section is the same. For instance the Stokes J=2 → J=4 transition and the anti-Stokes J=4 → J=2 transition both yield $(1 + \gamma^2 \; 13/\chi)^2$. For rotation-vibration transitions the O-branch ($\Delta J=-2$) has an increasing cross-section with increasing J. The term linear in $\gamma$ dominates over the $\gamma^2$ term because $\gamma=0.02766$ for $H_2$. The S-branch ($\Delta J=+2$) has a decreasing cross-section with increasing J. These trends are the same when compared to the transition matrix elements calculated by LeRoy. The Q-branch has a weak dependence on J. The $\gamma^2$ term seen in the O and S-branches is the only term, the term linear in $\gamma$ goes to 0 for the Q-branch. The cross-section decreases with increasing J, only slightly however. This is exactly opposite to the results of Schwartz and LeRoy which show a strong dependence on J with an increasing cross-section. If one examines analogous papers for transitions in the infra-red (the Herman-Wallis effect[52,53]) one finds discussions on higher order perturbation theories yielding terms linear in $\gamma$, which may dominate. I have found no other paper which treats the Q-branch matrix elements, and tend to trust the calculations of Schwartz and LeRoy over first-order perturbation theory. James and Klemperer point out that the effect is

strongest in the O and S-branches and that relative intensity measurements on line pairs originating from the same J will yield a value of $\chi$.

The next paper, by Buckingham and Szabo[47], also was completely theoretical. They used first order perturbation theory and derived approximate expressions for the O and S-branches of the fundamental and the first overtone. Their formulas are cruder than James and Klemperer's, lacking the term in $\gamma^2$. No one has seen the O and S-branches of the overtones as far as I know. I looked but was only able to see the Q-branch of the first overtone for which there is no expression for the intensities available. They point out that first-order perturbation theory may not be adequate to describe the very large effects of vibration-rotation interaction in hydrogen. They reference the original infra-red papers of Oppenheimer and Herman and Wallis but apparantly were unaware of the more complete treatment for Raman transitions by James and Klemperer.

Drake and Rosenblatt[54] describe the use of rotational Raman as a temperature probe in flames in contrast to vibrational bands. They point out that the J-dependence of the cross-section must be taken into account for accurate high-temperature temperature determinations. They give numerous experimental results on temperature determinations assuming a value for $\chi$ of 0.4 for $H_2$ taken from James and Klemperer who used field induced absorption experimental results[55] and purely theoretical calculations[56] to derive a reliable value.

The first experimental determination was by Asawaroengchai and Rosenblatt[48] in 1980. They used the theory of James and Klemperer as follows:

$$\frac{I(O\text{-branch})}{I(S\text{-branch})} = \frac{\dfrac{J(J-1)}{(2J+1)(2J-1)}}{\dfrac{(J+1)(J+2)}{(2J+3)(2J+1)}} \frac{\{1 - (\frac{3}{4})\,\gamma^2 / 4J(J+1) + 2\chi\gamma\,(2J-1)\}^2}{\{1 - (\frac{3}{4})\,\gamma^2 / 4J(J+1) - 2\chi\gamma\,(2J+3)\}^2} \quad . \quad (20)$$

The only unknown quantity is $\chi$ which can now be evaluated from relative intensities. They used an external cavity and report count rates of 600 $s^{-1}$ for $H_2$ which is about what I saw. The entire procedure was quite similar except they did not use a polarizer. They found a value of $\chi$=0.38±0.01 for both $H_2$ and $D_2$ which agrees very well with the theoretical value of 0.0378[57]. They point out that first-order perturbation theory is probably not adequate for $H_2$, and suggest further theoretical work.

The next study was a series of two papers by Buckingham et al.[49,50], the first being entirely theoretical and the second experimental. They used a numerical approach to diagonolize the vibration-rotation matrix. In the first paper they expressed the matrix element as a sum and tabulated the expansion coefficients for $H_2$. They state that with modern computers it is more accurate and less time consuming to calculate the coefficients then to go through a tedious analytical approach. However they give few details as to how the coefficients were calculated so that it is going to be difficult to extend their efforts to pure rotation or Q-branches as well as to the other isotopic molecules. In the second paper they applied their theory to measured line intensities for $H_2$. They used a multi-pass cell and measured line pairs for $H_2$ at four different incident wavelengths. They did their relative calibration of their spectrometer by comparing the intensity ratios at the different wavelengths. They did not use a polarizer. They arrived at a value of $\chi$=0.395±0.02.

## IVc. Ab Initio Calculations

The first theoretical calculations of the matrix elements for both pure rotation (anti-Stokes and Stokes) and the O and S-branches for $H_2$ and $D_2$ appeared in 1981 by Cheung, Bishop, Drapcho and Rosenblatt[51]. They used accurate static polarizabilities of Kolos and Wolniewicz which they modified for a field at 488 nm. They calculated both the matrix elements and the O and S-branch ratio's. They normalized their work to fit first-order perturbation theory using $\chi$=0.372. They did no calculations on the Q-branch line intensities. They note that there is a significant divergence of the theoretical values from the first-order perturbation values at high J, approaching 33% for $H_2$ at J=10. They state that this is not surprizing considering the large contribution of the second derivative to the polarizability anisotropy function which is not taken into account in first-order perturbation theory. They conclude that for highest accuracy their correction factors should be employed rather than those from the perturbation theory expansion.

The most recent theoretical work is that of Schwartz and LeRoy[1]. They used the dynamic polarizability anisotropy developed by Cheung et al.[51]. They calculated the pure rotation, the O, S, and Q-branches for $\Delta v$=1,2 for all of the isotopic species of hydrogen. Their wavefunctions were essentially the same wavefunctions that have been used for hydrogen for years, derived from the potential of Kolos and Wolniewicz. The corrections to the energy that Wolniewicz developed which Schwartz and LeRoy extended did not affect the wavefunctions. Their results for pure rotation are the same as the results of Cheung et al. The real usefulness of their work is that it covers all Raman transitions for all of the isotopes, allowing comparison between isotopes.

## IVd. Results

The only way to compare all of the various experimental and theoretical works is by tabulating the predictions for the ratio of the O and S-branch intensities, $Z^2$, as a function of J, including the measured results of this experiment. For first-order pertubation theory I will include three results, $\chi$=0.38, $\chi$=0.40, and $\chi$=0.42. $\chi$=0.38 is the value determined by Asawaroengchai and Rosenblatt and agrees well with theoretical calculations. $\chi$=0.40 is the value determined by Hamaguchi and Buckingham when the second derivative is taken into account. $\chi$=0.42 is the value which fits my measured values at J=2. For the expressions developed by Hamaguchi and Buckingham there are two entries, one using their results and one using the values of $\beta_1/\beta_0$ and $\beta_2/\beta_0$ determined from my measurements. The measured values are the average and standard deviation of a group of 8 measurements for J=2,3 and 7 measurements

Table XII: Ratio of O-branch to S-branch Intensities

| J | Measured | Schwartz and LeRoy | Cheung et al. | First-Order Pertubation Theory $\chi$=0.38 | $\chi$=0.40 | $\chi$=0.42 | Veirs and Rosenblatt | Hamaguchi and Buckingham |
|---|---|---|---|---|---|---|---|---|
| 2 | 1.636±0.051 | 1.531 | 1.543 | 1.563 | 1.595 | 1.635 | 1.636 | 1.582 |
| 3 | 1.977±0.055 | 1.815 | 1.833 | 1.866 | 1.934 | 2.002 | 1.994 | 1.901 |
| 4 | 2.309±0.118 | 2.150 | 2.178 | 2.249 | 2.353 | 2.467 | 2.427 | 2.282 |
| 5 | 2.969±0.269 | 2.546 | 2.590 | 2.729 | 2.890 | 3.066 | 2.955 | 2.737 |

for J=4,5. Two measurements were rejected as being outside twice the standard deviation of measurements for that J level. The results are tabulated in Table XII.

There are two important facets to these results, one is the relative magnitude and the second is the J-dependence. By looking at the results for J=2 the relative magnitudes can be compared. All of the theoretical results are lower than the values calculated from experimental results, and the experimental results seem to be moving away from the theoretical values. In Table XIII the differences $Z^2$(measured)-$Z^2$(i) are given, where i represents the various results of Table XII. These differences emphasize the J dependence and are also plotted in Fig. XXI.

Table XIII: DIFFERENCES IN INTENSITY RATIOS

| | Schwartz and LeRoy | Cheung et al. | First-Order Perturbation Theory | | | Veirs and Rosenblatt | Hamaguchi and Buckinghal |
|---|---|---|---|---|---|---|---|
| | | | $\chi$=0.38 | $\chi$=0.40 | $\chi$=0.42 | | |
| J | | | | | | | |
| 2 | 0.105 | 0.093 | 0.073 | 0.041 | 0.001 | 0.000 | 0.054 |
| 3 | 0.162 | 0.144 | 0.111 | 0.043 | -0.025 | -0.017 | 0.076 |
| 4 | 0.159 | 0.131 | 0.060 | -0.044 | -0.158 | -0.118 | 0.027 |
| 5 | 0.414 | 0.370 | 0.231 | 0.070 | -0.106 | 0.005 | 0.223 |

From this tabulation a number of points become obvious, first that the measured value for J=4 does not fit the trend in any of the sets of values. Secondly, the purely theoretical calculations show the largest slope. Thirdly, there is no value for $\chi$ in first-order perturbation theory that will have no relative offset and still have the J dependence shown in the data, $\chi$=0.40 has the appropriate J dependence while $\chi$=0.42 has the minimum offset. Finally the best fit, especially if J=4's significance is reduced, is from the equations developed by Hamaguchi and Buckingham and fit to the measured data. It should be noted that the results of Hamaguchi and Buckingham did not go to a J greater than 3 for $H_2$, and their results also included values for $D_2$ for which the leading term, $(\beta_1)^2$, may be different than for $H_2$.

The values of $\beta_1/\beta_0$ and $\beta_2/\beta_0$ from the results given in Table XII are given in Table XIV. The values for Cheung et al. are for a field at 488 nm

Table XIV: RATIO OF THE POLARIZABILITY ANISOTROPY DERIVATIVES

| | $\beta_1/\beta_0$ | $\beta_2/\beta_0$ |
|---|---|---|
| This experiment | 2.38±0.10 | 3.25±0.80 |
| Hamaguchi et al. | 2.53±0.13 | 3.97±1.33 |
| Cheung et al. | 2.658 | |
| Kolos and Wolniewicz | 2.62 | |
| Asawaroengchai et al. | 2.63 | |

while the values of Kolos and Wolniewicz are for a static field. The recent experimental values seem to be moving away from the theoretical values.

Finally one needs to consider what would be the best formulation to use for isotopic analysis. There are only two formulations to consider here, first-order perturbation theory and the theoretical results of Schwartz and LeRoy. The formalism of Hamaguchi et al. does not contain enough information to extend their calculations to the other isotopes. If one contacted them they might be able to provide the set of coefficients needed. The calculations of Cheung et al. do not extend to the other isotopic species and for pure rotation are essentially the same as Schwartz and LeRoy's values. The problem with first-order perturbation theory is that the J dependence is multiplied by $\beta_0$ (for pure rotation) which should be but is not necessarily the same for $H_2$ as it is for $T_2$. For instance the $H_2$ first-order perturbation theory and the theoretical calculations agree to within 0.2% as to the intensity ratio of a line pair originating from J=2. However if one compares the ratio of intensities of Stokes lines originating from J=0 for $H_2$ and $T_2$ one finds an 11% disagreement. For pure Stokes scattering,

$I=\beta_0^2\{1+\gamma^2/\chi[J^2+3J+3]\}^2$ which for J=0 gives $I=\beta_0^2\{1+3\gamma^2/\chi\}^2$. The ratio of intensities for $H_2$ and $T_2$ assumes $\beta_0$ is the same for both yielding $I(H_2)/I(T_2)=\{1+3\gamma(H_2)^2/\chi\}^2/\{1+3\gamma(T_2)^2/\chi\}^2$ where $\chi=0.4$ for both molecules and $\gamma(H_2)=7.65\times10^{-4}$ and $\gamma(T_2)=2.55\times10^{-4}$ which yields $I(H_2)/I(T_2)=1.0076$. The matrix elements from Schwartz and LeRoy combine to give $I(H_2)/I(T_2)=1.1170$. Table XV compares relative intensities predicted by first order perturbation theory to those calculated by Schwartz and LeRoy for all of the isotopic molecules. The factor $\{1+3\gamma^2/\chi\}^2$ for each molecule has been calculated along with the square of the theoretical matrix elements normalized so that the values for $H_2$ agree. The ratios of the first order perturbation theory to the theoretical calculations are given.

Table XV: COMPARISON OF THE ISOTOPIC DEPENDENCE OF INTENSITIES FROM FIRST-ORDER PERTURBATION THEORY AND THEORY FOR J=0

| | $H_2$ | HD | HT | $D_2$ | DT | $T_2$ |
|---|---|---|---|---|---|---|
| Be | 60.8530 | 45.655 | 40.595 | 30.4436 | 25.395 | 20.335 |
| $\omega_e$ | 4401.213 | 3813.15 | 3597.05 | 3115.50 | 2845.52 | 2546.47 |
| $\{1+3\gamma^2/\chi\}^2$ | 1.0115 | 1.0086 | 1.0077 | 1.0057 | 1.0048 | 1.0038 |
| $\langle\psi\|\alpha\|\psi\rangle^2$ | 4.5430 | 4.3863 | 4.3299 | 4.2075 | 4.1403 | 4.0672 |
| normalized | 1.0115 | 0.9766 | 0.9641 | 0.9368 | 0.9218 | 0.9056 |
| Ratio | 1.000 | 1.033 | 1.045 | 1.074 | 1.090 | 1.108 |

The theoretical calculations show a strong isotope dependence of the pure rotational cross-section which is lacking in first-order perturbation theory. Since there is no mechanism in first-order perturbation theory to handle the change in equilibrium internuclear distance as a function of reduced mass, I would not trust it to give adequate results. This is reflected in the results for the analysis of the DOE Round Robin samples, in which the theoretical matrix elements give a better answer. Conversely the work on intensity ratios in hydrogen indicate that the theoretical transition matrix elements are not

especially accurate either. More work definately needs to be done in this area. The relitive Raman cross-sections as a function of reduced mass needs to be investigated if accurate isotopic analysis are to be routine.

One further note on Raman intensities. A recent paper[58] took a look at $N_2$ theoretically. They found $1/\chi=3.15$ as opposed to experimental measurements of Hamaguchi et al. $1/\chi=2.63$ and Asawaroengchai et al. $1/\chi=2.22$, which is the same trend as the discrepancy in $H_2$. They also found an increasing J dependence in the Q-branch as opposed to the prediction of first-order perturbation theory.

## V. TEMPERATURE MEASUREMENTS

### Va. Introduction

Rotational Boltzmann temperatures can be determined from relative intensities of Raman transitions. Accuracy and reproducibility require strong lines with well known corrections for spectrometer response and transition line strengths. Pure rotational Stokes scattering and Q-branch rotational-vibrational scattering are the strongest Raman transitions. For hydrogen and its isotopes the Q-branch rotational lines are separated enough to yield rotational temperatures based on rotational state populations. I have investigated temperature determinations from Stokes pure rotational scattering for $H_2$ and $D_2$ and from Q-branch scattering for all six isotopomers.

### Vb. J-dependent Cross Sections

Accurate temperatures require the J dependence of the transition line strength to be well known, however since the transitions all involve a single molecule the molecular dependence of $\beta_o^2$, as discussed previously, does not need to be known. The J dependence of pure rotational Stokes scattering from both first order perturbation theory and theoretical transition matrix elements are given in Table XVI for $H_2$ and $D_2$, normalized to 1 for J=0.

Table XVI: J DEPENDENT RAMAN CROSS SECTIONS FOR $H_2$ AND $D_2$

| | $H_2$ | | $D_2$ | |
|---|---|---|---|---|
| J | $\{1+\gamma^2/\chi(J^2+3J+3)\}^2$ | $\langle\psi\|\alpha\|\psi\rangle^2$ | $\{1+\gamma^2/X(J^2+3J+3)\}^2$ | $\langle\psi\|\alpha\|\psi\rangle^2$ |
| 0 | 1.0000 | 1.0000 | 1.0000 | 1.0000 |
| 1 | 1.0153 | 1.0153 | 1.0076 | 1.0079 |
| 2 | 1.0384 | 1.0385 | 1.0191 | 1.0197 |
| 3 | 1.0696 | 1.0700 | 1.0346 | 1.0357 |
| 4 | 1.1093 | 1.1102 | 1.0540 | 1.0559 |
| 5 | 1.1578 | 1.1597 | 1.0776 | 1.0804 |
| 6 | 1.2158 | 1.2191 | 1.1055 | 1.1095 |
| 7 | 1.2838 | 1.2892 | 1.1377 | 1.1433 |
| 8 | 1.3625 | 1.3711 | 1.1746 | 1.1821 |
| 9 | 1.4527 | 1.4657 | 1.2162 | 1.2262 |
| 10 | 1.5553 (0.988) | 1.5742 | 1.2629 (0.990) | 1.2759 |

Both methods produce correction factors which agree with one another to within 1% for up to J=10 (the number in parenthesis at J=10 is the ratio of the correction factors for first-order perturbation theory to theoretical transition matrix elements). The discrepancy in absolute cross-sections for $H_2$ as compared to $D_2$ for first-order perturbation theory and theoretical transition matrix elements is illustrated in Table XV and must be kept in mind for isotopic analysis.

## Vc. Temperature Determinations

The intensity of a pure rotational Stokes Raman transition is given by:

$$I(J) = (64\pi^4 \nu^4)\, I_o\, N_{v,J} \left(\frac{7}{30}\right) \frac{(J+1)(J+2)}{(2J+3)(2J+1)} \langle\psi|\alpha|\psi\rangle^2 \tag{21}$$

($\nu$ is in wavenumbers, equivalent to $\nu/c$ in previous equations). The number density, $N_{v,J}$ is given by:

$$N_{v,J} = \sigma\,(2J+1)\,\frac{N_o}{Q}\,\exp(-1.439\,E_{v,J}/T) \tag{22}$$

where $\sigma$ is the nuclear spin degeneracy, $N_o$ is the total number density of the molecular species, $E_{v,J}$ is the energy of the initial rotational-vibrational state, and Q is the partition function. I(J), given in watts, is converted to photons per second by:

$$I(J) = I(J,\text{photons/s})\ hc\nu \quad . \tag{23}$$

The scattered intensity is then:

$$I(J,\text{photons/s}) = \frac{64\pi^4\nu^3}{hc} I_o\ \sigma \frac{N_o}{Q} \frac{7}{30} \frac{(J+1)(J+2)}{(2J+3)} \langle\psi|\alpha|\psi\rangle^2 \exp\{-1.439E_{v,J}/T\} \ . \tag{24}$$

The measured intensity is related to the scattered intensity by the response function of the collection and detection system, $R(\nu)$ by:

$$I(\text{meas},J,\text{p/s}) = I(J,\text{photons/s})\ R(\nu). \tag{25}$$

The measured intensity can be determined from the peak height by measuring the average peak height and the background:

$$I(\text{meas},J,\text{p/s}) = I(\text{peak},J,\text{p/s}) - I(\text{background},\text{p/s}). \tag{26}$$

It must be stressed that both the peak height and the background are composed of two elements, the average intensity and the noise due to counting statistics which is impressed on the average intensity. The counting statistics noise is especially important for weak peaks where a maximum peak height can be more than 50% greater than the average intensity. All measurements I will discuss are made from an average peak height intensity and

an average background. The final relationship is given by:

$$I(p,J) - I(b) = \frac{R(v)\ 64\pi^4\ \nu^3\ I_o\ \sigma\ N_o\ 7\ (J+1)\ (J+2)\ \langle\psi|\alpha|\psi\rangle^2\ \exp\{-1.439E_{v,J}/T\}}{h\ c\ Q\ 30\ (2J+3)} . \quad (27)$$

Rearranging and taking the natural log yields:

$$\ln\left[\frac{I(p,J) - I(b)}{R(v)\ \nu^3\ \sigma\ \langle\psi|\alpha|\psi\rangle^2\ \frac{(J+1)\ (J+2)}{(2J+3)}}\right] + \ln\left[\frac{h\ c\ Q\ 30}{64\pi^4\ N_o\ I_o\ 7}\right] = \frac{-1.439\ E_{v,J}}{T} . \quad (28)$$

From a plot of the left side of this equation versus the energy of the initial state, $E_{v,J}$, a slope can be determined from which the temperature is derived:

$$T=-1.439/\text{slope} . \quad (29)$$

The term $\ln[h\ c\ Q\ 30/(64\pi^4\ N_o\ 7\ I_o)]$ affects the intercept only and can be ignored. A linear least squares of the corrected intensity versus initial state energy yields the temperature directly. The terms $\sigma$ and $(J+1)(J+2)/(2J+3)$ are known exactly and do not contribute any error to the temperature determination. $\nu$ is given by the Rayleigh frequency and the rotational shift by $\nu = \nu(\text{Rayleigh})-\nu(\text{rotational shift})$. $\nu$ is known to 5 parts in a million, contributing negligible error. $R(\nu)$, determined from calibration procedures and known to about 1%, is a major source of error. $\langle\psi|\alpha|\psi\rangle$, given in Table XVI for both first order perturbation theory and theoretical calculations which agree to within 1% up to high J values, is also a source of error. The ability to measure the peak intensities accurately give rise to the major source of error in temperature determinations. One method used to cancel the errors due to $\langle\psi|\alpha|\psi\rangle$ and $R(\nu)$ is to measure the intensities of a gas, assume the rotational temperature of the gas to be that of the sample cell measured with a thermocouple, and determine the product

$R(\nu)\ \langle\psi|\alpha|\psi\rangle$ from the known Boltzmann distribution[58]. Using this method temperatures accurate to 0.5°K were reported at room temperature. However room temperature measurements of rotational temperatures have been reported yielding 329±3°K in which they state that the "effective temperature of the scattering volumne of the gas is some 30°K above that of the cell surface"[59]. In light of this situation I believe it is important to measure $R(\nu)$ and determine $\langle\psi|\alpha|\psi\rangle$ separately.

## Vd. Weak Lines

The importance of incorporating weak lines in temperature determinations can be illustrated by considering the error introduced by small uncertainties in intensity measurements. Consider the example of being able to measure two lines only for a temperature determination in $H_2$. The temperature is given by:

$$\frac{\ln[I(1)] - \ln[I(2)]}{E(2)-E(1)} = \frac{-1.439}{T} \quad . \tag{30}$$

If there is an error in one of the intensities, say I(2), the effect on the temperature is given by:

$$\frac{-d\{I(2)\}}{I(2)\ \{E(2)-E(1)\}} = \frac{1.439\ dT}{T^2} \quad . \tag{31}$$

The error in I(2) can be written as a percentage of I(2), d[I(2)]=I(2) %error:

$$\frac{\%\text{error}\ T^2}{\{E(2)-E(1)\}\ 1.439} = dT \quad . \tag{32}$$

For the specific case of I(2) being either J=1 or J=5 with I(1) belonging to J=0, {E(2)-E(1)} goes from 118 $cm^{-1}$ to 1740 $cm^{-1}$. For the same error on the temperature the %error can increase by a factor of 15 for J=5 over the error

in the intensity for J=1. dT=5°K for a 15% error in J=5, which represents a total intensity of 44 counts if the error is purely statistical. This analysis is simplistic in that a linear least squares tends to average out errors in measuring intensities, but it does emphasis the importance in measuring lines at high J with large energy seperations from J=0.

## Ve. Results: Pure Rotation

The results in Table XVII are temperature determinations from Stokes pure rotational scattering. For $H_2$ the lines included in the determination were J=0-5, and for $D_2$ J=0-8. The room temperature was measured with an uncalibrated thermometer resting on the spectrometer. Determinations 1-4 were

Table XVII: TEMPERATURE DETERMINATIONS FROM PURE ROTATIONAL STOKES SCATTERING

| | Molecule | Temperature (calculated) | Temperature (thermometer) | dT |
|---|---|---|---|---|
| 1. | $H_2$ | 294.0 | 296.0 | -2.0 |
| 2. | $H_2$ | 294.2 | 296.0 | -1.8 |
| 3. | $H_2$ | 294.6 | 296.0 | -1.4 |
| 4. | $H_2$ | 294.4 | 296.0 | -1.6 |
| 5. | $H_2$ | 292.7 | 294.8 | -2.1 |
| 6. | $D_2$ | 294.1 | 296.3 | -2.2 |
| 7. | $D_2$ | 293.6 | 296.3 | -2.7 |
| 8. | $D_2$ | 288.5 | -- | -- |

taken on the same day with the sample essentially in thermal equilibrium with the room. Sample 5 was taken with the same sample on the next day with the room temperature significantly lower. Samples 6 and 7 were two runs on the same sample on the same day. Sample 8 was a tritium containing sample that had been stored in the tritium handling room which is usually colder than the lab.

The average temperature difference between that determined from the Raman spectra and that read from the thermometer is 2.0±0.4°K. However for the repetitive samples 1-4 the temperature is 294.3±0.3°K, indicating that the temperature determination is very reproducible. Because the thermometer was not calibrated and not in thermal contact with the sample cell the accuracy can only be surmised to be within 2°K with the possibility of being equivalent to the reproducibility of ±0.3°K. There is no evidence that the scattering volume is at a higher temperature than the sample cell. The presence of tritium in sample 8 does not disturb the ability to make temperature determinations. Further work needs to be completed with a thermocouple attached to the sample cell to determine the accuracy of the temperature determination. If there is a reproducible difference between sample cell temperatures and Raman temperature determinations, the problem can lie either with the spectrometer calibration or the J dependence of the transition matrix elements. Either of these problems can be corrected for by using intensities from a sample at a known temperature as in Leyendecker et al. At high temperatures when higher J levels are populated the uncertainty in the product of $R(\nu)\ \langle\psi|\alpha|\psi\rangle$ can be boot-strapped by using a temperature determined from the lower J levels.

## Vf. Results: Q-branch

The case of Q-branch temperature determinations is more complex and indicates that there are real problems in understanding the J dependent Raman Q-branch cross-sections. The Q-branch Raman intensity is given by:

$$I(J) = 64\pi^4\ \nu^4\ I_o\ N_{v,J}\ (1/2\alpha)\ \langle\psi|\alpha|\psi\rangle^2 \qquad (33)$$

where

$$\langle\psi|\alpha|\psi\rangle^2 = \quad 1-\frac{3}{4}\gamma^2 \; J(J+1) \qquad K_1^2 + \beta_1^2 \frac{7}{45} \frac{J(J+1)}{(2J+3)(2J-1)} \tag{34}$$

using first order perturbation theory and

$$\langle\psi|\alpha|\psi\rangle^2 = K(J)^2 + \beta(J)^2 \frac{7}{45} \frac{J(J+1)}{(2J+3)(2J-1)} \quad . \tag{35}$$

using the theoretical transition matrix elements, K(J), the polarizability matrix element, and $\beta(J)$, the polarizability anisotropy matrix element. Using the same approach as for pure rotational Stokes scattering the temperature can be determined from a linear least squares fit of the equation:

$$\ln \quad \frac{I(p,J)-I(b)}{R(\nu)\ \nu^3\ \sigma\ (2J+1)\ \langle\psi|\alpha|\psi\rangle^2} = \frac{-1.439E_{v,J}}{T} \tag{36}$$

Reiterating the points covered in the intensity section, first order perturbation theory predicts a decrease in the Q-branch Raman cross section with increasing J while the transition matrix elements increase with increasing J. Also for J=0, K is the only contribution to the cross section while for J>0 $\beta$ also contributes. The cross-sections for $H_2$ and $T_2$ up to J=10 determined form first-order perturbation theory and the theoretical transition matrix elements, normalized to J=0, are plotted in Fig. XXII. The trends are obvious and intuitive with $H_2$ having the stronger J dependence because of it's larger ratio of rotational to vibrational constants. In Table XVIII the cross-sections for all six isotopomers using both formulations are presented.

Table XVIII: J DEPENDENT CROSS-SECTIONS FOR THE HYDROGEN ISOTOPIC MOLECULAR SPECIES USING FIRST ORDER PERTURBATION THEORY (FOPT) AND AB INITIO CALCULATIONS (AIC)

| | $H_2$ | | HD | | HT | | $D_2$ | | DT | | T2 | |
|---|---|---|---|---|---|---|---|---|---|---|---|---|
| J | FOPT | AIC | FOPT | AIC | FOPT | AIC | FOPT | AIC | FOPT | AIC | FOPT | AIC |
| 0 | 1.000 | 1.000 | 1.000 | 1.000 | 1.000 | 1.000 | 1.000 | 1.000 | 1.000 | 1.000 | 1.000 | 1.000 |
| 1 | 1.040 | 1.048 | 1.041 | 1.046 | 1.041 | 1.045 | 1.041 | 1.044 | 1.041 | 1.043 | 1.042 | 1.042 |
| 2 | 1.023 | 1.041 | 1.025 | 1.039 | 1.026 | 1.038 | 1.027 | 1.037 | 1.027 | 1.033 | 1.028 | 1.031 |
| 3 | 1.014 | 1.049 | 1.018 | 1.045 | 1.019 | 1.042 | 1.021 | 1.039 | 1.022 | 1.035 | 1.024 | 1.034 |
| 4 | 1.004 | 1.062 | 1.010 | 1.054 | 1.012 | 1.051 | 1.016 | 1.046 | 1.018 | 1.043 | 1.020 | 1.040 |
| 5 | 0.992 | 1.080 | 1.001 | 1.067 | 1.004 | 1.063 | 1.010 | 1.055 | 1.012 | 1.051 | 1.015 | 1.045 |
| 6 | 0.978 | 1.099 | 0.990 | 1.082 | 0.994 | 1.077 | 1.002 | 1.064 | 1.006 | 1.058 | 1.011 | 1.051 |
| 7 | 0.962 | 1.121 | 0.978 | 1.100 | 0.983 | 1.093 | 0.994 | 1.078 | 1.000 | 1.068 | 1.005 | 1.059 |
| 8 | 0.944 | 1.147 | 0.964 | 1.121 | 0.971 | 1.111 | 0.985 | 1.092 | 0.992 | 1.081 | 0.999 | 1.071 |
| 9 | 0.923 | 1.176 | 0.949 | 1.143 | 0.957 | 1.130 | 0.974 | 1.108 | 0.983 | 1.096 | 0.992 | 1.082 |
| 10 | 0.901 | 1.208 | 0.932 | 1.167 | 0.942 | 1.152 | 0.963 | 1.126 | 0.973 | 1.111 | 0.984 | 1.093 |

I have determined temperatures from Q-branch intensities for all six of the isotopomers. There are 5 samples for $H_2$ and 1 each for the remaining 5 isotopomers. All of the data have the background subtracted, but the peak maximum was used instead of an average peak intensity. This especially affects the data with small count rates. The tables that follow contain the following information: 1) the initial rotational quantum numbers, the average peak intensity, and the background; 2) the initial rotational quantum number, the temperature calculated from the information above assuming a transition matrix element of 1 for all transitions, the temperature using first order perturbation theory, and the temperature using the ab initio transition matrix element. The temperatures are calculated using linear least squares starting with the first J levels and recalculated for each additional J level for which there is data. If there is data for J=0-5, then the first temperature to appear will be for data from J=0 to J=1 and the second temperature incorporates data from J=0 to J=2 and so on.

Tables XIX-XXIII contain the results for $H_2$, and illustrate the problems associated with both Q-branch temperature determinations and intensity measurements in general. In Table XIX and XX the intensity for J=1 is greater than $10^6$ counts per second, within the non-linear regime for the electronics of the photon counting system. As a result the intensity of J=1 is less than it should be and the temperature is significantly lower than

Table XIX: TEMPERATURE FROM $H_2$ Q-BRANCH INTENSITIES

Background=200

| J | INTENSITY | T | T(FOPT) | T(AIC) |
|---|---|---|---|---|
| 0 | 398000 | ------ | ------ | ------ |
| 1 | 1970000 | 284.49 | 267.04 | 264.08 |
| 2 | 377000 | 307.12 | 304.16 | 300.08 |
| 3 | 290000 | 302.65 | 302.60 | 299.55 |
| 4 | 14400 | 303.57 | 304.30 | 301.24 |
| 5 | 3800 | 304.56 | 305.59 | 302.51 |
| 6 | 270 | 308.98 | 309.36 | 306.21 |

Table XX: TEMPERATURE FROM $H_2$ Q-BRANCH INTENSITIES

Background=58

| J | INTENSITY | T | T(FOPT) | T(AIC) |
|---|---|---|---|---|
| 0 | 217010 | ------ | ------ | ------ |
| 1 | 1089000 | 291.07 | 272.83 | 269.74 |
| 2 | 209720 | 310.60 | 307.57 | 304.32 |
| 3 | 157420 | 301.99 | 301.94 | 298.91 |
| 4 | 7457 | 300.76 | 301.47 | 298.47 |
| 5 | 1812 | 300.16 | 301.15 | 298.16 |
| 6 | 91 | 303.58 | 304.74 | 301.68 |

it should be for J=0,1. This effect also shows up to a lesser extent in Table XXI although it should not. The non-linearity of the photon counting system may affect results sooner than previously anticipated. The benefit of

multi-line determinations for temperature is illustrated in all of the results in that the temperatures seem to converge when higher J levels are included. The problem of measuring the peak maximum versus the peak average is illustrated in all of the results in that the last measured line, usually less

Table XXI: TEMPERATURE FROM $H_2$ Q-BRANCH INTENSITIES

Background=30

| J | INTENSITY | T | T(FOPT) | T(AIC) |
|---|---|---|---|---|
| 0 | 124280 | ------ | ------ | ------ |
| 1 | 636670 | 301.69 | 282.14 | 278.84 |
| 2 | 118340 | 306.81 | 303.86 | 300.68 |
| 3 | 91329 | 302.17 | 302.12 | 299.08 |
| 4 | 4362 | 301.66 | 302.38 | 299.36 |
| 5 | 1065 | 301.16 | 302.16 | 299.16 |
| 6 | 54 | 308.63 | 309.82 | 306.65 |

than 100 cps, is overestimated and the temperature jumps significantly. In Table XXII the sudden turn-on of the polarizability anisotropy at J=1 is nicely illustrated in that the temperature assuming $\langle\psi|\alpha|\psi\rangle=1$ is 330°K at J=1 while for both first order perturbation theory and <u>ab initio</u> transition

Table XXII: TEMPERATURE FROM $H_2$ Q-BRANCH INTENSITIES

Background=29

| J | INTENSITY | T | T(FOPT) | T(AIC) |
|---|---|---|---|---|
| 0 | 128820 | ------ | ------ | ------ |
| 1 | 693920 | 331.11 | 307.71 | 303.79 |
| 2 | 119790 | 300.29 | 297.46 | 294.42 |
| 3 | 98358 | 303.37 | 303.32 | 300.26 |
| 4 | 4709 | 303.29 | 304.02 | 300.97 |
| 5 | 1127 | 301.87 | 302.87 | 299.85 |
| 6 | 49 | 304.15 | 305.30 | 302.23 |

matrix elements, which take into account the increased cross section due to the turn-on of the polarizability anisotropy, the temperature is a more reasonable 307 to 303°K. In Table XXIII, where the fraction of $H_2$ in the

Table XXIII: TEMPERATURE FROM $H_2$ Q-BRANCH INTENSITIES

Background=18

| J | INTENSITY | T | T(FOPT) | T(AIC) |
|---|---|---|---|---|
| 0 | 39 | ------ | ------ | ------ |
| 1 | 121 | 280.04 | 263.11 | 260.24 |
| 2 | 44 | 371.82 | 367.48 | 362.85 |
| 3 | 40 | 344.30 | 344.24 | 240.30 |

sample was extremely low and therefore the intensities of the lines were 100 cps or less, the temperature can only be estimated to within ±40°K or to about 15% of the true temperature. The theoretical matrix elements yeild a temperature about 3°K lower than first order perturbation theory, or a reduction by ~1%. However the best temperature in all cases converges to ~299±1°K which, in light of the rotational temperature determinations, is 3 to 5°K too high. This indicates that there is an additional correction which has not been determined. Tables XXIII-XXVIII are from a sample Bob Sherman bought back from Switzerland. The composition of the gas as

Table XXIV: TEMPERATURE FROM HD Q-BRANCH INTENSITIES

Background=16

| J | INTENSITY | T | T(FOPT) | T(AIC) |
|---|---|---|---|---|
| 0 | 1490 | ------ | ------ | ------ |
| 1 | 3067 | 344.87 | 311.61 | 307.79 |
| 2 | 2121 | 303.40 | 299.17 | 296.10 |
| 3 | 835 | 299.13 | 298.66 | 295.66 |
| 4 | --- | ------ | ------ | ------ |
| 5 | 42 | 292.41 | 293.26 | 290.39 |

determined by Raman analysis was $H_2$=0.012%, HD=2.50%, HT=1.67%, $D_2$=46.20%, DT=40.24%, and $T_2$=9.37%. In Table XXIV J=4 is obscured by a $D_2$ $S_1(4)$ line. The same trends seen in the $H_2$ data are apparant in the data for the rest of the isotopomers. In $D_2$ and DT the J=0 and J=1 lines overlap while

Table XXV: TEMPERATURE FROM HT Q-BRANCH INTENSITIES

Background=16

| J | INTENSITY | T | T(FOPT) | T(AIC) |
|---|---|---|---|---|
| 0 | 566 | ------ | ------ | ------ |
| 1 | 1137 | 295.22 | 267.63 | 264.89 |
| 2 | 851 | 286.05 | 281.70 | 278.98 |
| 3 | 406 | 296.85 | 296.18 | 293.23 |
| 4 | 127 | 298.34 | 298.78 | 295.79 |

Table XXVI: TEMPERATURE FROM $D_2$ Q-BRANCH INTENSITIES

Background=16

| J | INTENSITY | T | T(FOPT) | T(AIC) |
|---|---|---|---|---|
| 0 | ------ | ------ | ------ | ------ |
| 1 | ------ | ------ | ------ | ------ |
| 2 | 82578 | ------ | ------ | ------ |
| 3 | 25096 | 306.93 | 308.92 | 305.69 |
| 4 | 20543 | 300.87 | 302.49 | 299.39 |
| 5 | 3090 | 300.13 | 301.61 | 298.52 |
| 6 | 1433 | 302.02 | 303.44 | 300.32 |
| 7 | 134 | 301.92 | 303.30 | 300.17 |
| 8 | 38 | 294.36 | 295.65 | 292.68 |

in $T_2$ J=0,1 and 2 overlap with the slit widths used in these determinations. In $T_2$ there is a strange alternation in intensity with even J yielding higher temperatures than odd J. The nuclear spin degeneracy has been properly taken account of and the source for the alternation is unknown. As with $H_2$

Table XXVII: TEMPERATURE FROM DT Q-BRANCH INTENSITIES

Background=16

| J | INTENSITY | T | T(FOPT) | T(AIC) |
|---|---|---|---|---|
| 0 | ------ | ------ | ------ | ------ |
| 1 | ------ | ------ | ------ | ------ |
| 2 | 53631 | ------ | ------ | ------ |
| 3 | 36816 | 300.60 | 302.65 | 299.50 |
| 4 | 17993 | 296.60 | 298.25 | 295.20 |
| 5 | 6895 | 299.40 | 300.91 | 297.80 |
| 6 | 2062 | 301.50 | 302.93 | 299.79 |
| 7 | 472 | 300.83 | 302.21 | 299.08 |
| 8 | 86 | 296.12 | 297.43 | 294.40 |

Table XXVIII: TEMPERATURE FROM $T_2$ Q-BRANCH INTENSITIES

Background=16

| J | INTENSITY | T | T(FOPT) | T(AIC) |
|---|---|---|---|---|
| 0 | ------ | ------ | ------ | ------ |
| 1 | ------ | ------ | ------ | ------ |
| 2 | ------ | ------ | ------ | ------ |
| 3 | 13476 | ------ | ------ | ------ |
| 4 | 2747 | 305.80 | 307.35 | 304.07 |
| 5 | 3901 | 302.76 | 304.19 | 300.97 |
| 6 | 526 | 304.87 | 306.26 | 303.00 |
| 7 | 477 | 301.90 | 303.24 | 300.04 |
| 8 | 59 | 304.63 | 305.98 | 302.73 |
| 9 | 50 | 311.27 | 312.66 | 309.27 |

the convergent temperatures cluster around 299-300°K. The data for HD and HT is significantly less intense with final temperatures being less precise and converging to 295°K.

The results for temperature determinations from Q-branch line intensities yield the following conclusions. First of all the sudden turn-on of the polarizability anisotropy as a component of the overall cross-section at J=1 as predicted by Placezk's theory is amply demonstrated. Secondly the J

dependence of the first order perturbation theory cross-section has the wrong sign. Thirdly the J dependence of the theoretical transition matrix elements has the correct sign but not enough magnitude.

## Vg. Results: First Overtone

Finally, in terms of temperature measurements as a way to judge the adequacy of cross-sections, I have made measurements of the first overtone. The spectra is shown in Fig. XXIII, from which intensities were deduced using a ruler. The exact expression for the cross-section of the overtone can be taken from James and Klemperer as:

$$\langle\psi|\alpha|\psi\rangle^2 = \langle K(J)\rangle^2 + \left(\frac{7}{45}\right) \langle\beta(J)\rangle^2 \left[\frac{J(J+1)}{(2J+3)(2J-1)}\right] . \qquad (37)$$

since their expressions are general in v. The theoretical transition matrix elements $\langle K(J)\rangle$ and $\langle\beta(J)\rangle$ are available from Schwartz and LeRoy for the first overtone. The intensities were analysed in three ways, first making the usual corrections of $\nu^3$ $R(\nu)$ $\sigma$ $(2J+1)$ with no cross-section correction, secondly using $\langle K(J)\rangle$ and $\langle\beta(J)\rangle$ for the first overtone from Schwartz and LeRoy and thirdly using the values of $\langle K(J)\rangle$ and $\langle\beta(J)\rangle$ for the fundmental from Schwartz and LeRoy. The results are given in Table XXIX.

Table XXIX: TEMPERATURES FROM $H_2$ FIRST OVERTONE INTENSITIES

| J | I | T1 | $\langle K(J)\rangle$ | $\langle\beta(J)\rangle$ | $T_2$ | $T_3$ |
|---|---|---|---|---|---|---|
| 0 | 18.4 | ----- | -0.06828 | -0.002921 | ----- | ----- |
| 1 | 101.4 | 343.7 | -0.06866 | -0.003260 | 336.2 | 314.2 |
| 2 | 18.2 | 310.2 | -0.06941 | -0.003944 | 303.3 | 304.2 |
| 3 | 16.3 | 316.9 | -0.07055 | -0.004982 | 310.4 | 313.7 |

Using $\langle\psi|\alpha|\psi\rangle^2=1$, the temperature for J=0,1 is high suggesting the onset of the polarizability anisotropy. However, as opposed to the case for $\Delta v=1$, the ratio of $\langle K(J)\rangle/\langle\beta(J)\rangle=23$ instead of 1.2, and the effect of the onset is minimized. Using the cross-section for $\Delta v=1$ the temperatures are more reasonable indicating that the theoretical transition matrix element $\langle\beta(J)\rangle$ for $\Delta v=2$ is much too small with respect to $\langle K(J)\rangle$. Also note that $\langle\beta(J)\rangle$ increases by 70% in going from J=0 to J=3, which is a remarkably large J dependence.

The relative magnitude of pure rotational Stokes scattering, $\Delta v=1$ Q-branch scattering and $\Delta v=2$ Q-branch scattering can be compared using experimental intensities and theoretical transition cross-sections. The equations from James and Klemperer, substituting in the theoretical transition matrix elements are:

$$I(\text{Stokes}) = \frac{64\pi^4\ \nu^3\ I_o\ N_{v,J}\ 7\ (J+1)\ (J+2)}{h\ c\ 30\ (2J+3)\ (2J+1)}\ \langle\psi|\alpha|\psi\rangle^2 \tag{38}$$

$$I(\text{Q-branch},\Delta v=1) = \frac{64\pi^4\ \nu^3\ I_o\ N_{v,J}}{h\ c}\ [\langle K1(J)\rangle^2 + \langle\beta1(J)\rangle^2\ \frac{7}{45}\ \frac{J(J+1)}{(2J+3)(2J-1)}]. \tag{39}$$

$$I(\text{Q-branch},\Delta v=2) = \frac{64\pi^4\ \nu^3\ I_o\ N_{v,J}}{h\ c}\ [\langle K2(J)\rangle^2 + \langle\beta2(J)\rangle^2\ \frac{7}{45}\ \frac{J(J+1)}{(2J+3)(2J-1)}]. \tag{40}$$

Looking at J=1, assuming that $\langle\beta(J)\rangle$ makes an insignificant contribution compared to the experimental error, the respective intensities are given by:

$$I(S):I(Q1):I(Q2) = \nu^3\ \frac{7}{30}\ \frac{(J+1)\ (J+2)}{(2J+3)(2J+1)}\ \langle\psi|\alpha|\psi\rangle^2\ R(\nu):\nu^3\ R(\nu)\ \langle K1\rangle^2:\nu^3\ R(\nu)\ \langle K2\rangle^2. \tag{41}$$

The intensity data are taken from $H_2$ spectra recorded over two days with the same slit widths and $H_2$ pressure, and presumably the same laser intensity

and collection efficiency. Because of the experimental uncertainties, the intensities may be off by a factor of 2 to 3 between the three sets. The data are given in Table XXX.

Table XXX: COMPARISON OF PURE ROTATIONAL, FUNDAMENTAL AND OVERTONE INTENSITIES FOR J=1

| | Pure Rotation | Q-branch, dv=1 | Q-branch,dv=2 |
|---|---|---|---|
| I(observed) | $5.4\times10^{5}$ | $6.4\times10^{5}$ | 804 |
| $R(\nu)$[%] | 2.3 | 3.0 | 1.4 |
| $\nu^3$ | $8.0\times10^{12}$ | $4.1\times10^{12}$ | $1.7\times10^{12}$ |
| S(J) | 0.09 | 1 | 1 |
| $\langle\psi\|\alpha\|\psi\rangle^2$ | 4.5 | 0.66 | $4.6\times10^{-3}$ |
| $R(\nu)\ \nu^3\ S(J)\ \langle\psi\|\alpha\|\psi\rangle^2$ | 7.5 | 8.1 | $1.1\times10^{-2}$ |
| I(predicted) normalized to pure rotation | $5.4\times10^{5}$ | $5.8\times10^{5}$ | 790 |

The excellent agreement is fortuitous considering the documentation on the data.

## Vh. Conclusion

In summary, for pure rotational Stokes scattering the cross-sections from first order perturbation theory and accurate transition matrix elements are in remarkable agreement. Temperatures calculated using these cross-sections are highly reproducible, indicative of the quality of the data, but seem to be 2°K lower than the thermometer reading. More experiments need to be completed which measure the temperature of the sample cell accurately in order to determine the source of the 2°K discrepancy. The Q-branch cross-sections appear to yield much poorer results. The abrupt contribution of the polarizability anisotropy at J=1 to the Q-branch cross-section has been amply demonstrated. The Q-branch cross-section J dependence using first order perturbation theory has been shown to be incorrect. The theoretical transtion

matrix elements improve the situation, but there is still an additional correction to the cross-section needed. More experiments are needed to determine the source of the measured temperature discrepancies, additional corrections to the cross-section or more accurate spectrometer calibration. The first overtone Q-branch cross-sections have been shown to have the same functional dependence upon the polarizability anisotropy as the fundamental. The theoretical transition matrix elements for the polarizability anisotropy appear to be too small by at least an order of magnitude. The relative intensities of pure rotational, fundamental, and first overtone scattering agree quite well with the theoretical calculations, as opposed to the J dependence.

## Figure Captions

Fig. 1 Integration of monochromator and collection optics showing the distances between the focusing optical components. The exact distances were selected to maximize the collected light reaching the detector.

Fig. 2 The beam waist ($\omega_o$), Rayleigh length ($Z_r$), and arbitrary beam waist ($\omega_Z$) at distance Z in Gaussian optics. The distance Z represents the location of the laser beam focusing optic.

Fig. 3 The final external cavity/collection-optics design. The focal lengths and diameters of the lenses and mirrors are determined from the physical characteristics of the laser and monochromator.

Fig. 4 Non-linear response of the Spectra-Physics 171 power meter with ND filter. The x-axis is the true laser power and the y-axis is the ratio of the true laser power to response of the power meter shielded with an ND filter. The ND filter exhibits saturation behavior which leads to anomalously high power readings at high laser power.

Fig. 5 Raman spectroscopy cell for use with tritium containing gases. The cell is all metal and glass construction including metal o-rings with a small volume of about 1.5 $cm^3$.

Fig. 6 The effect of discriminator setting on signal and noise. The number on the right is the signal divided by $10^5$ or the noise.

The number on the left is the S/N ratio divided by $10^4$. After a discriminator setting of 1 the noise rises precipitously causing a sudden fall in the S/N ratio.

Fig. 7 Possible orientations of No Dew window with lens. The orientation in (a) is as delivered by manufacturer whereas the (b) orientation results in slightly higher signals.

Fig. 8 Curcuit used for calibration lamp operation. The current/voltage regulator senses the current or voltage at the lamp and automatically regulates the voltage source. The additional voltmeter allows independent monitoring of the current/voltage and manual fine-tuning.

Fig. 9 Etaloning from intensity calibration lamp. The 1% variation in intensity is due to interference at the detector of light from the lamp filament which either passes straight to the detector or is first reflected from the lamps glass envelope. The 1% variation was damped out by increasing the spectrometer bandwidth with wider slits.

Fig. 10 Two methods for determining line intensities. In I the line intensity is determined by summing the total number of counts in the vicinity of a peak and subtracting the total background counts, determined on each side of the peak. In II the line intensity is determined from the peak intensity of the line and the average background intensity. Both methods are easily implemented with digital data.

Fig. 11 Effect of polarization on spectrometer response, calculated and measured. The y-axis is the percent efficiency as calculated or measured. The x-axis is the spectrometer position in absolute wavenumbers.

Fig. 12 Ratio of spectrometer response with perpendicular and parallel polarized light. The y-axis is the ratio of the measured efficiencies and the x-axis is the spectrometer position in wavenumbers. The relative flatness of the curve in the region of interest (15,000 - 17,000 $cm^{-1}$) still represents a change more than 2 orders of magnitude above the required accuracy.

Fig. 13 Spex depolarizer. The wedge shape allows the birefrigence of the quartz to rotate the polarization of the incident light an amount dependent upon the vertical position.

Fig. 14 Effect of Spex depolarizer on polarized light. A telescope expands a He-Ne beam to fill the aperture of the depolarizer. The light is polarized incident upon the depolarized and resolved on a screen after the depolarizer. The device works well when incomplete depolarization can be tolerated.

Fig. 15 Effect of depolarizer on the polarization of a rotation Raman line. A polarizer with $10^{-5}$ extinction ratio was used to analyze the polarization of a rotational Raman line. The y-axis is relative intensity of the Raman line and the x-axis is the angular

position of the analyzing polarizer. Data was taken with and without the Spex depolarizer. The Spex depolzrizer was always before the polarization analyzer.

Fig. 16 $H_2$ 5←3 with Uranium calibration. The y-axis is the intensity in counts per second and the x-axis is the Raman shift in wavenumbers. A shutter rejected the uranium hollow cathode lamp light when the spectrometer scanned over the Raman line of interest. The entrance and exit slits were increased when scanning over the Raman line to insure detectable amounts of light.

Fig. 17 Pure rotational line positions, differences between <u>ab initio</u> calculations and best experimental measurements for $H_2$. the y-axis is the difference between line positions calculated from ab initio energy levels and the best experimental measurements in units of $10^{-3}$ $cm^{-1}$. The x-axis is the rotational quantum number J. The error bars are experimental.

Fig. 18 $H_2$ S-branch line positions for v=1 to v=4, differences between ab initio calculations and best experimental measurements. The x and y-axis are the same as in Fig. 17. The error bars are for the experiment.

Fig. 19 Difference between theory and experimental vibrational levels for HD. The y-axis is the same as in Fig. 17 except that the units are $cm^{-1}$ and the x-axis is the vibrational quantum number, v. The points are determined from J=0, neglecting the rotational dependent error.

Fig. 20 Isotopic dependence of the difference between theory and experimental vibrational levels.

Fig. 21 Differences between measured intensity models. The y-axis is the difference between the experimental ratio of the O and S-branch corrected intensities originating from the same J-level and intensity ratios calculated from various models. The theoretical calculation points are derived from the ratio of the square of the transition matrix elements. Three entries for first-order perturbation theory include $\chi$=0.38, 0.40, 0.42. Second order effects are included in the formulation by Hamaguchi and Buckingham. The x-axis is the rotational quantum number J. The error bars are for the experimental measurements.

Fig. 22 $H_2$ and $T_2$ J-dependent cross-sections from first-order perturbation theory and <u>ab initio</u> calculations. The y-axis is the relative Q-branch Raman cross-section normalized to J=0. The x-axis is the rotational quantum number J.

Fig. 23 $H_2$ first overtone (v=2 ← v=0). The y-axis is the absolute intensity in counts per second and the x-axis is the Raman shift. The low intensity is partially due to a lower cross-section and partially due to the photomultiplier tube red fall-off in quantum efficiency.

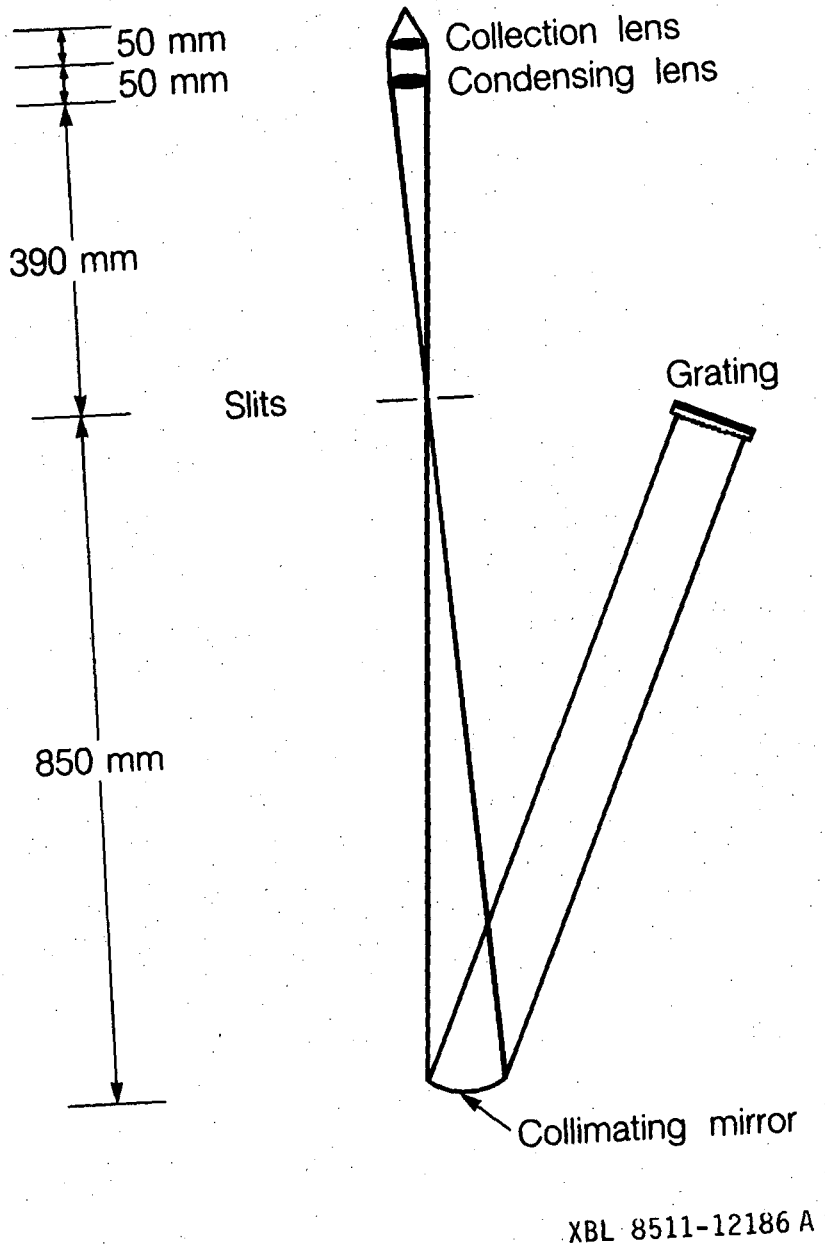
50 mm
50 mm
390 mm
850 mm
Collection lens
Condensing lens
Slits
Grating
Collimating mirror
XBL 8511-12186 A

Fig. 1

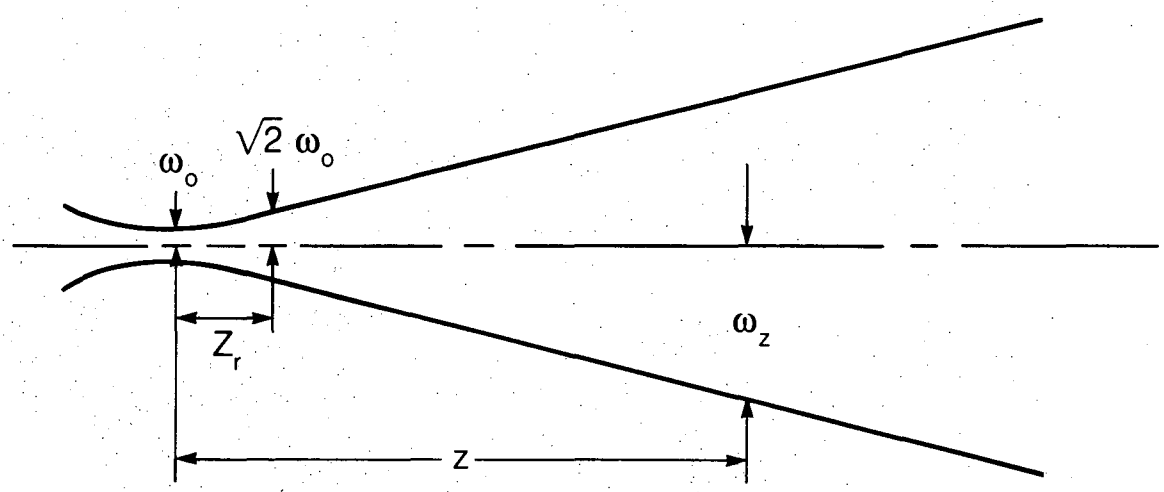


XBL 8511-12187 A

Fig. 2

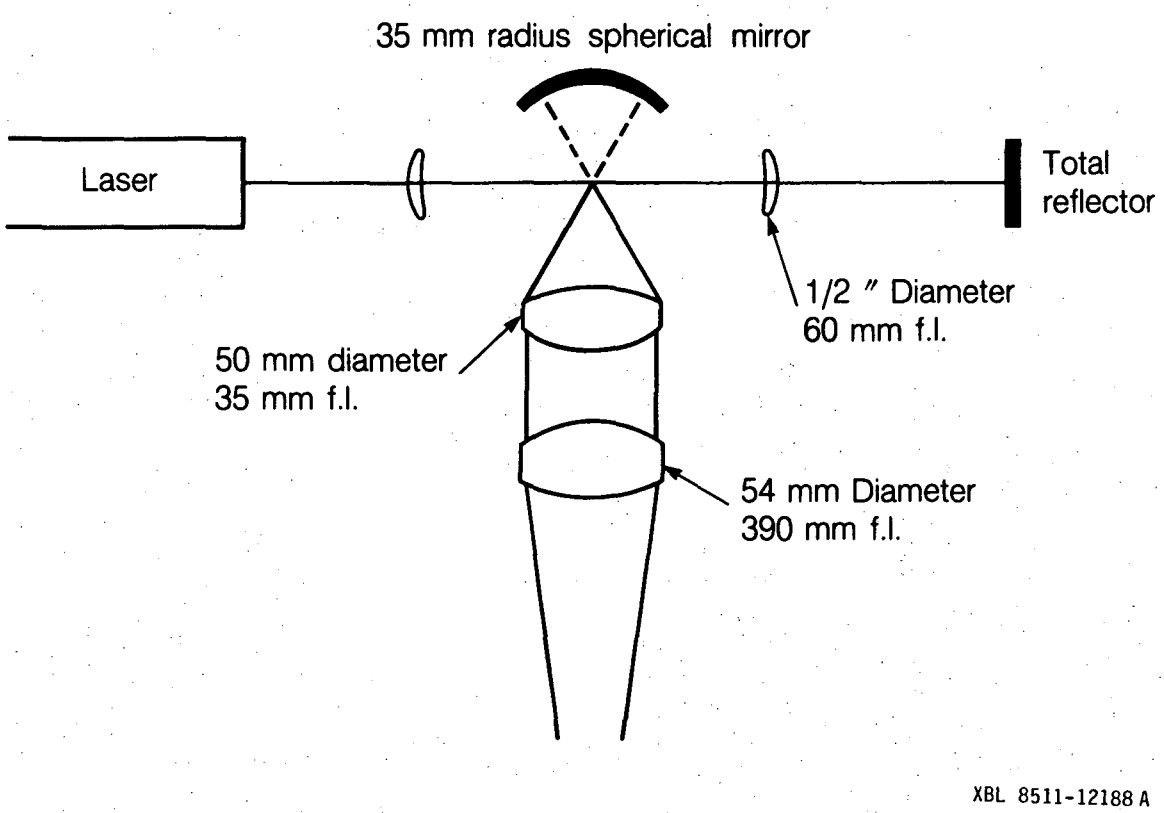
35 mm radius spherical mirror
Laser
Total
reflector
1/2 ″ Diameter
60 mm f.l.
50 mm diameter
35 mm f.l.
54 mm Diameter
390 mm f.l.
XBL 8511-12188 A

Fig. 3

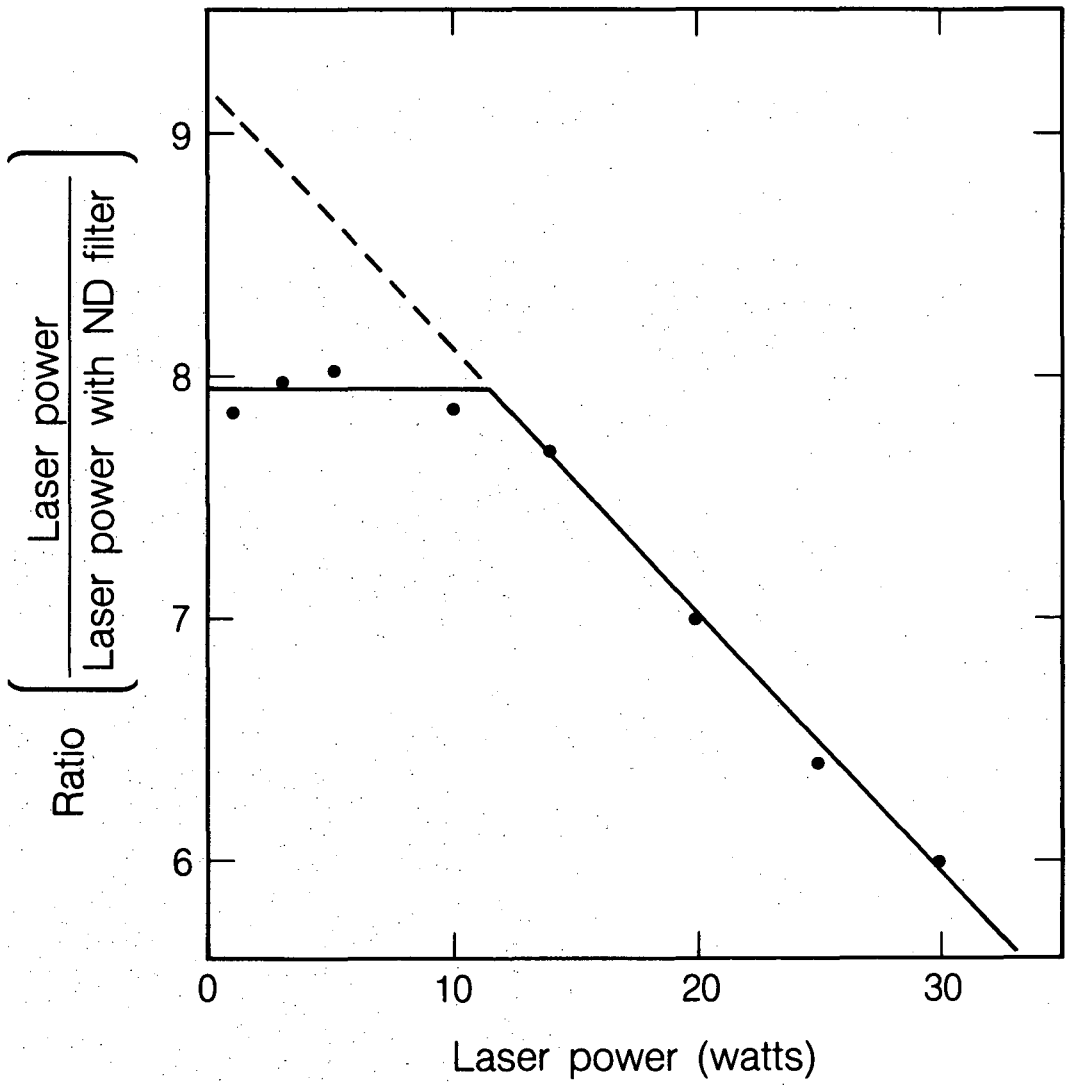


XBL 8511-12189 A

Fig. 4

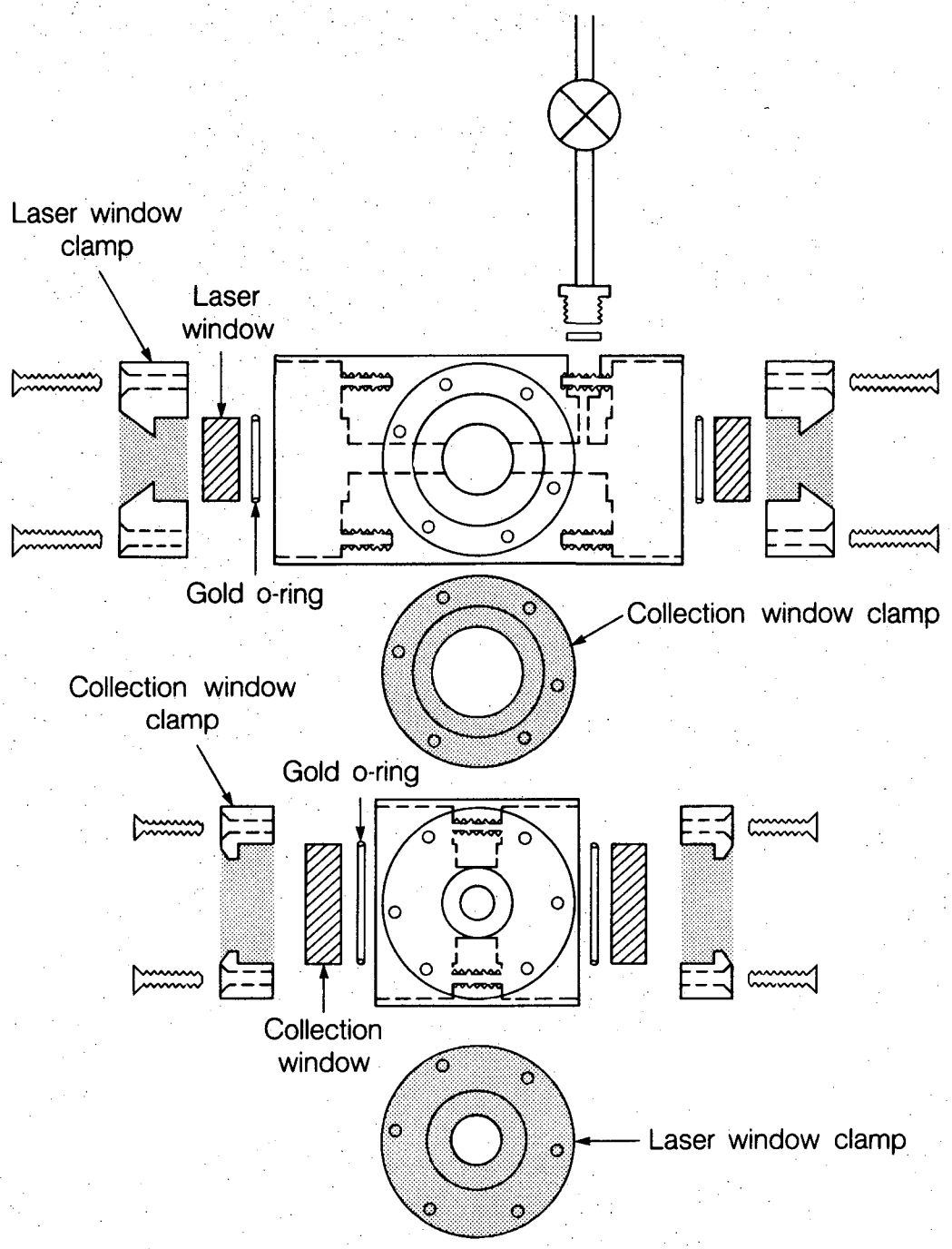


XBL 8511-12190 A

Fig. 5

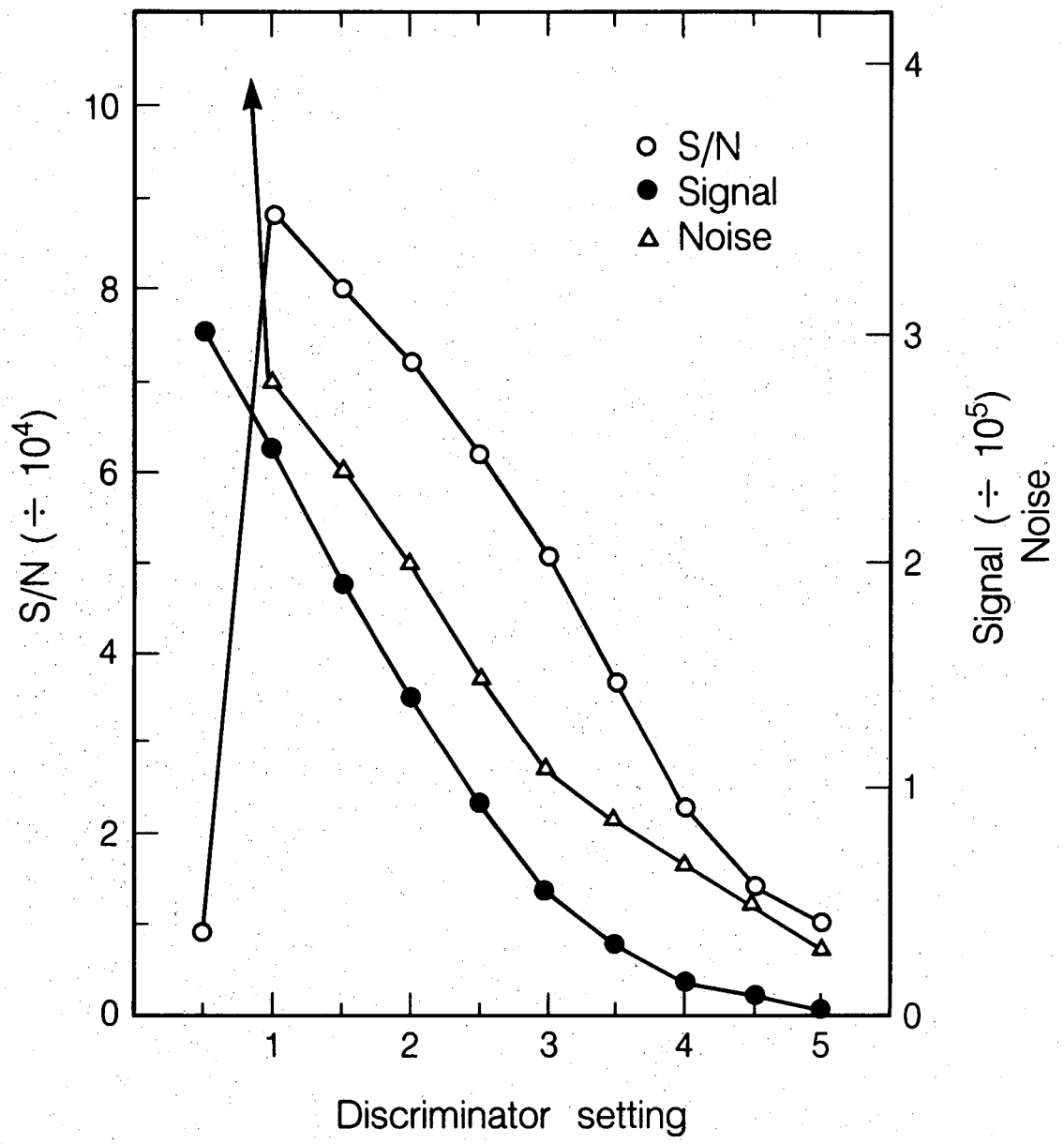


XBL 8511-12191 A

Fig. 6

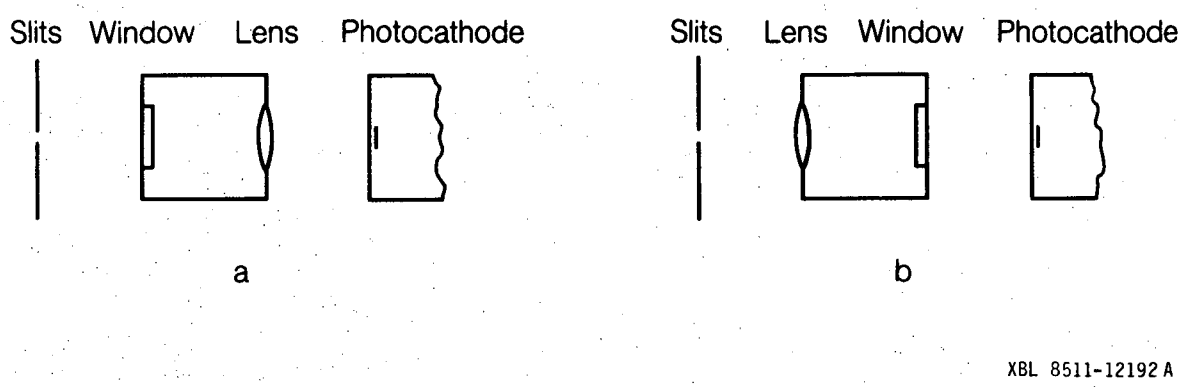
Slits
Window
Lens
Photocathode
a
Slits
Lens
Window
Photocathode
b
XBL 8511-12192 A

Fig. 7

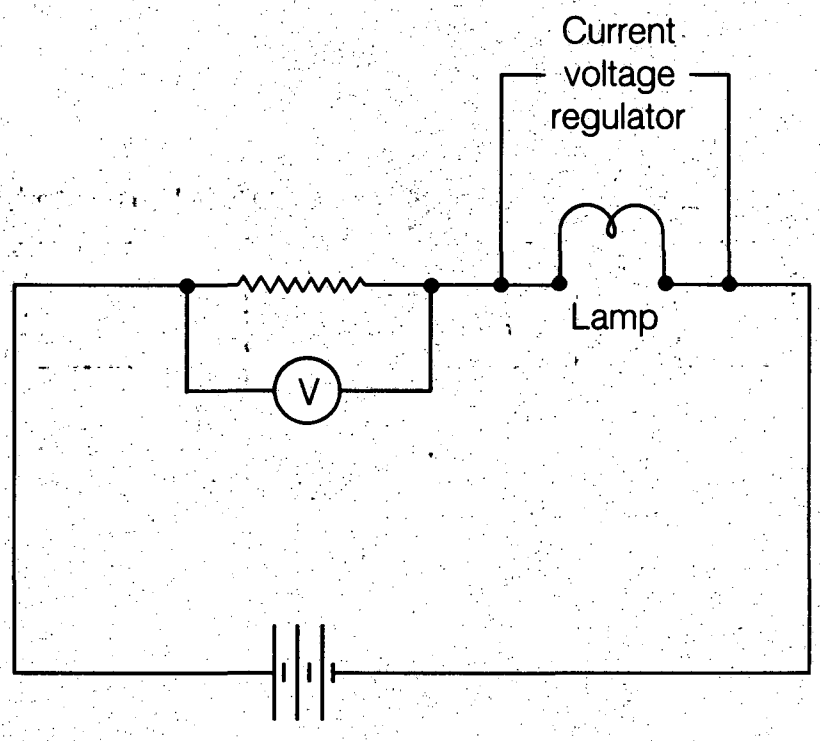


XBL 8511-12193 A

Fig. 8

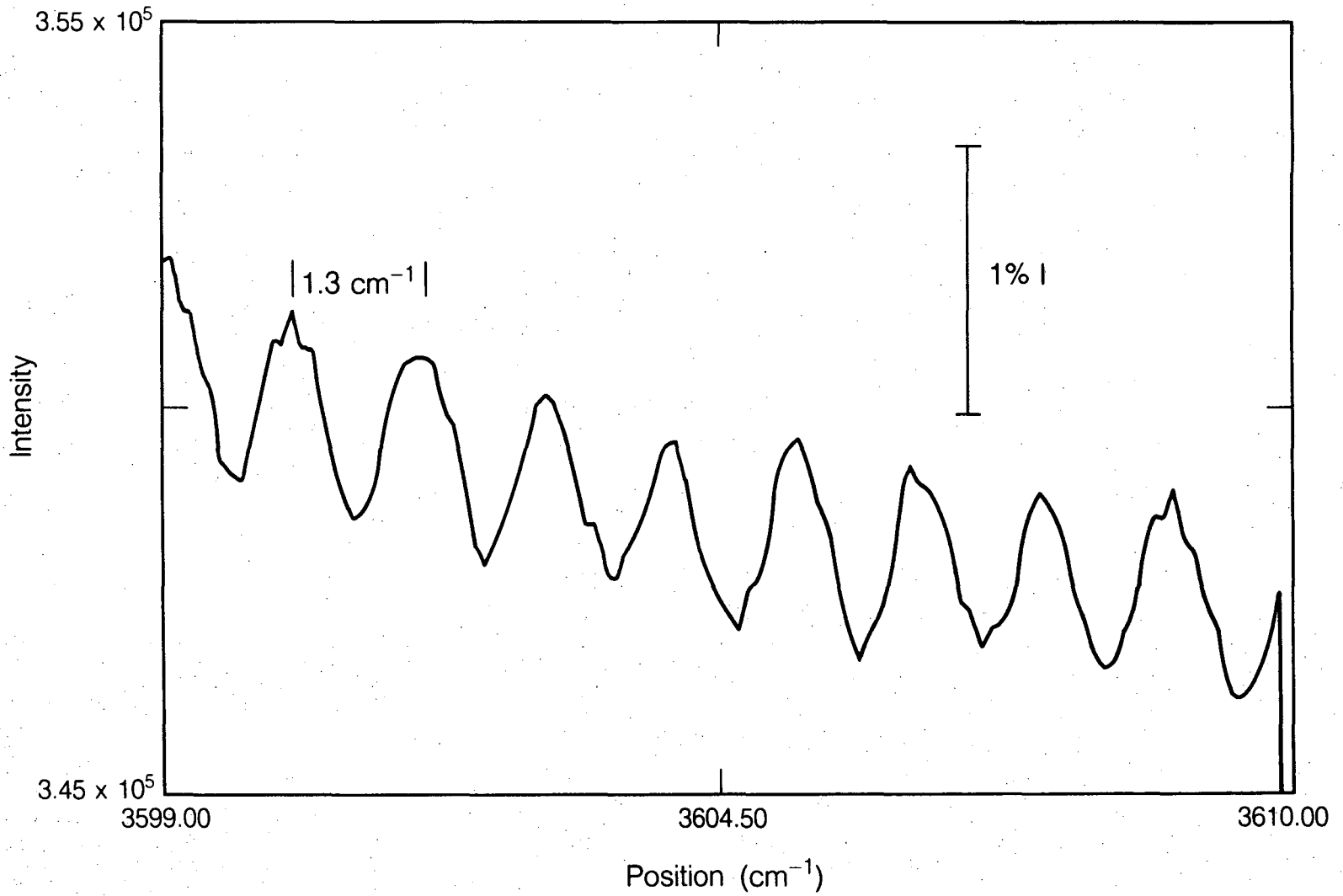


XBL 8511-12210 A

Fig. 9

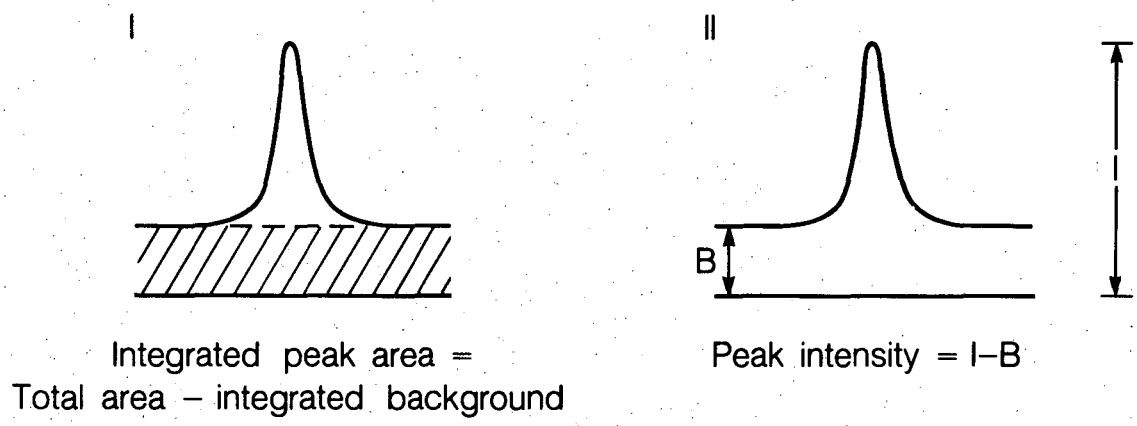


XBL 8511-12194 A

Fig. 10

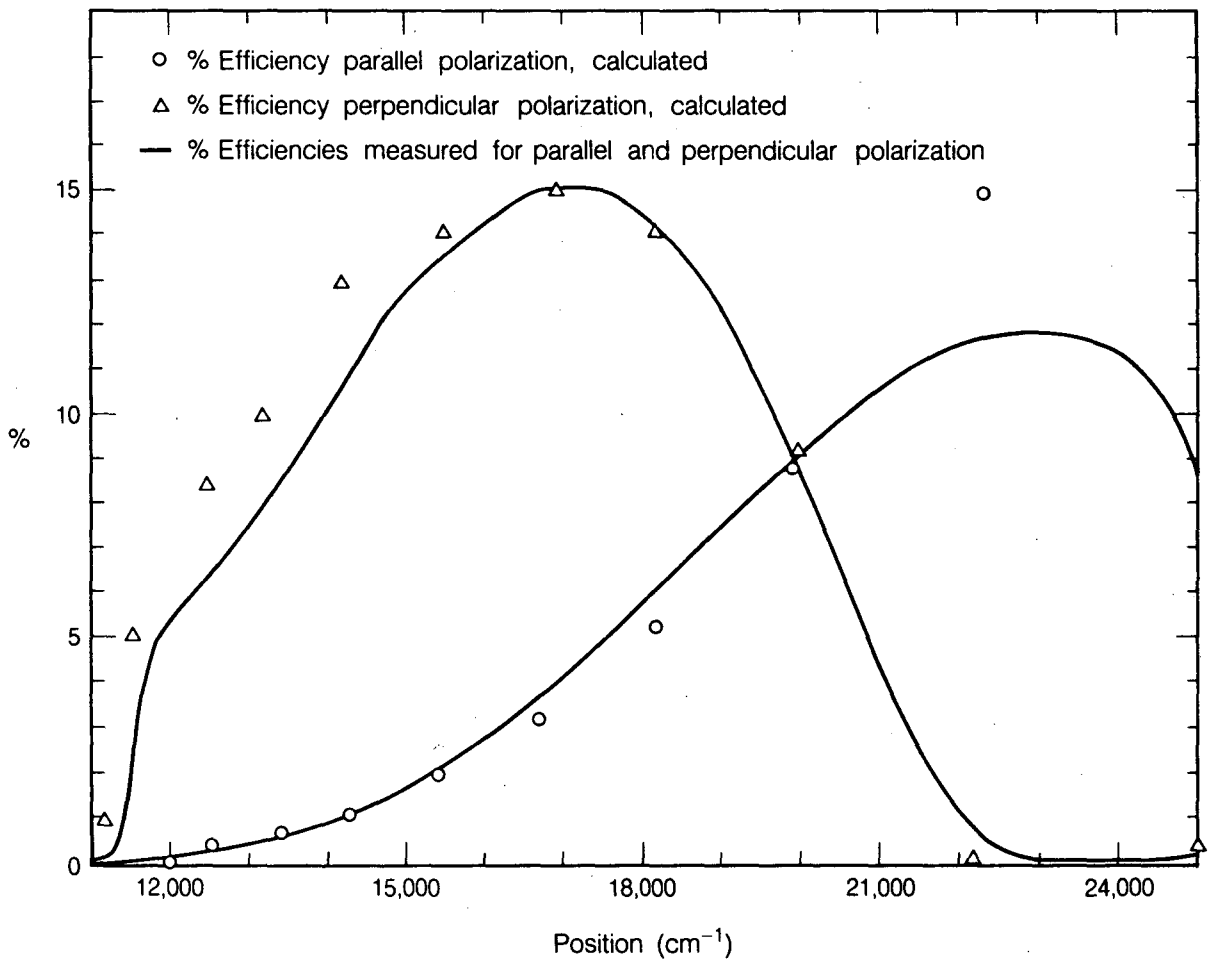


XBL 8511-12195 A

Fig. 11

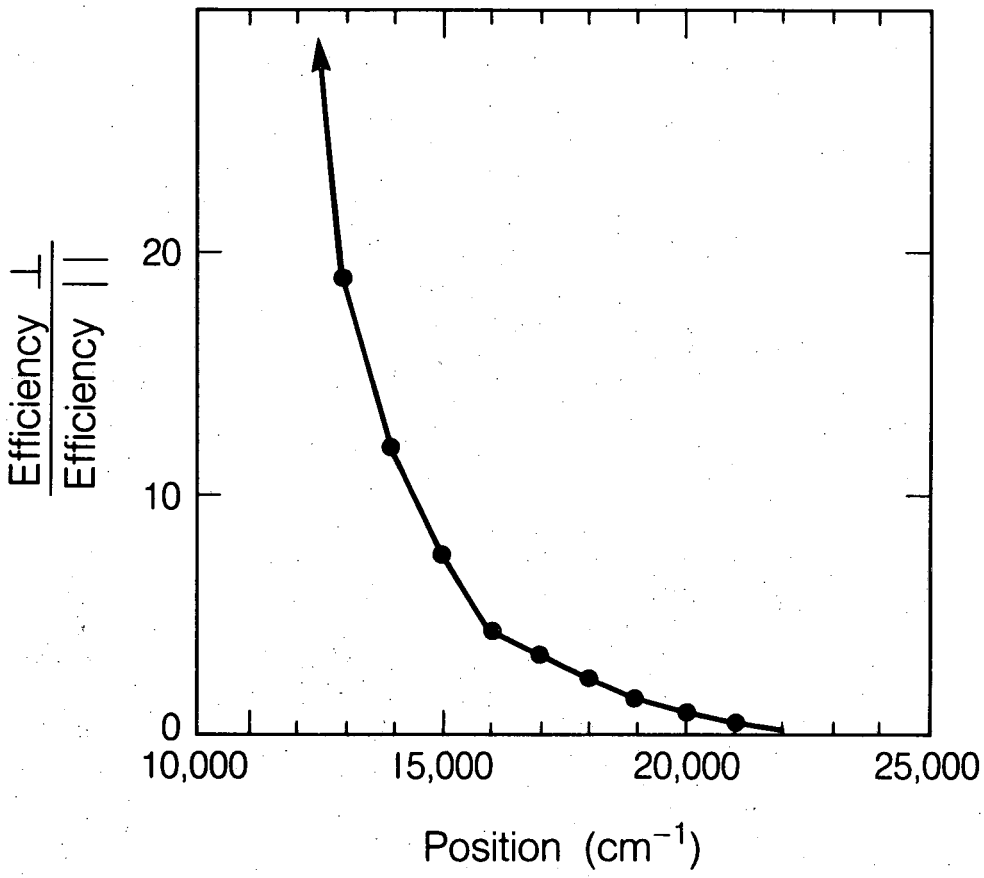


XBL 8511-12196 A

Fig. 12

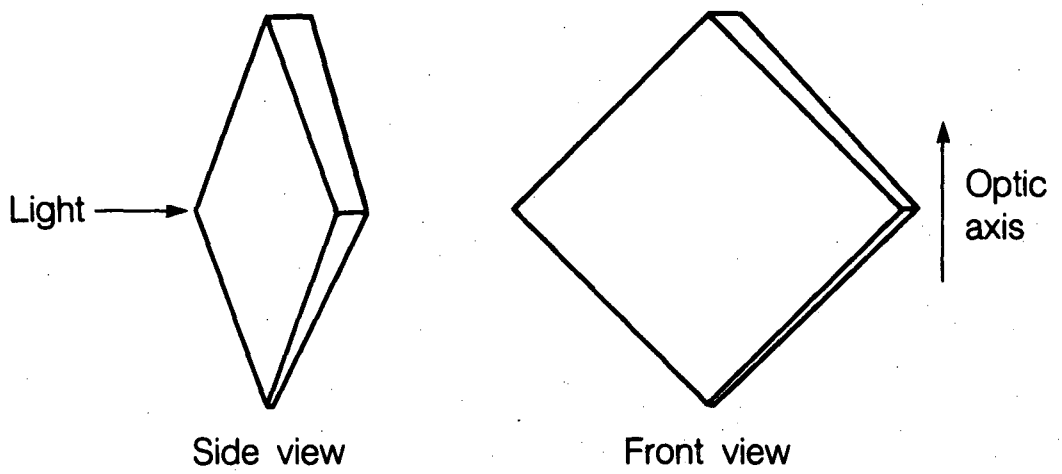


XBL 8511-12197 A

Fig. 13

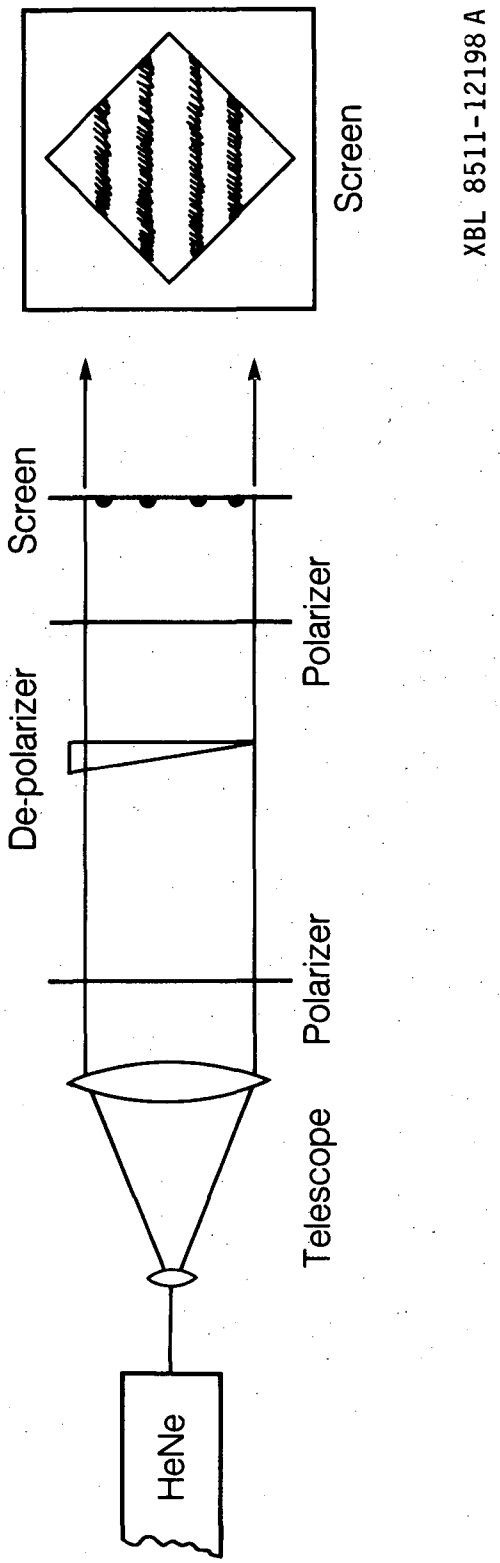


XBL 8511-12198 A

Fig. 14

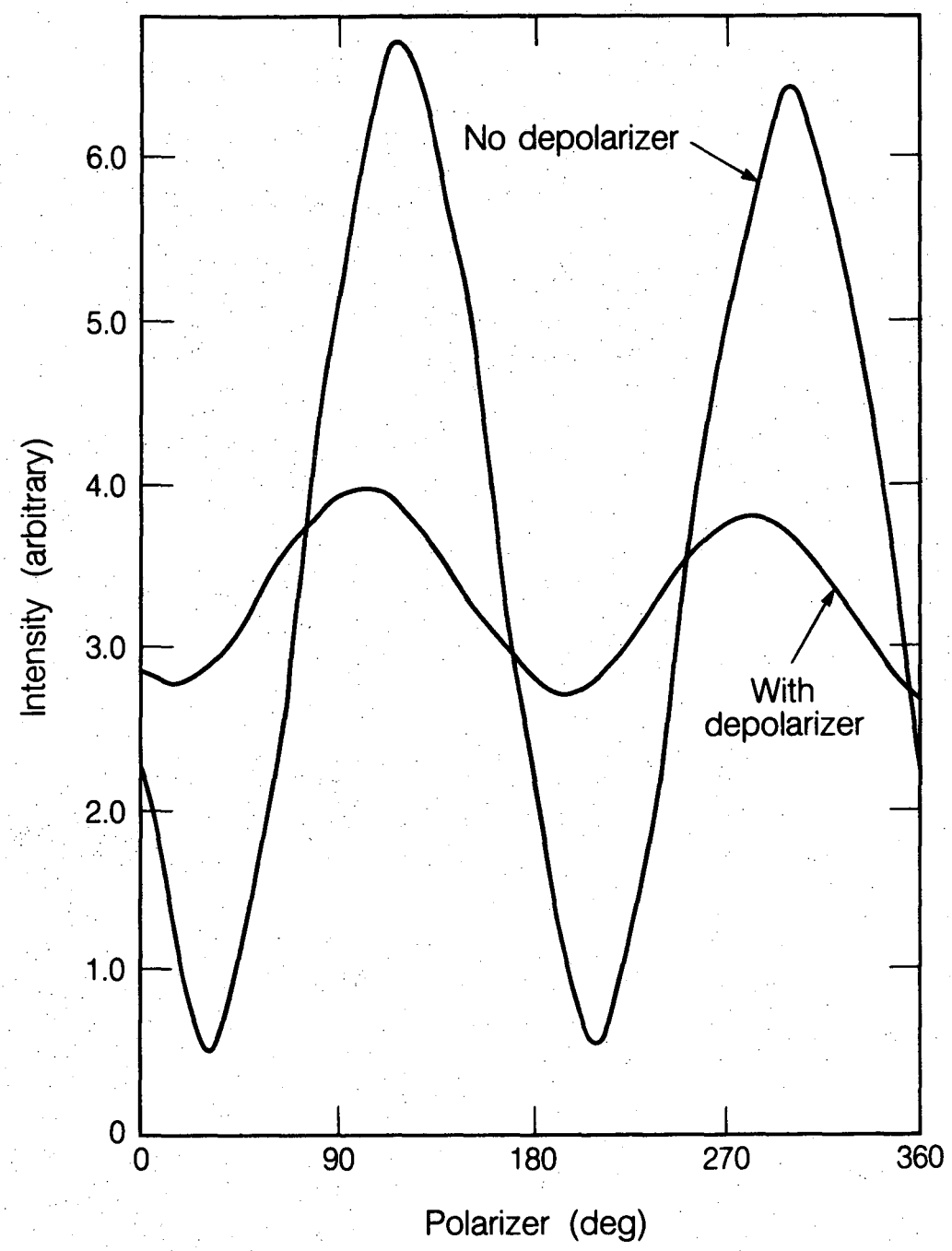


XBL 8511-12199 A

Fig. 15

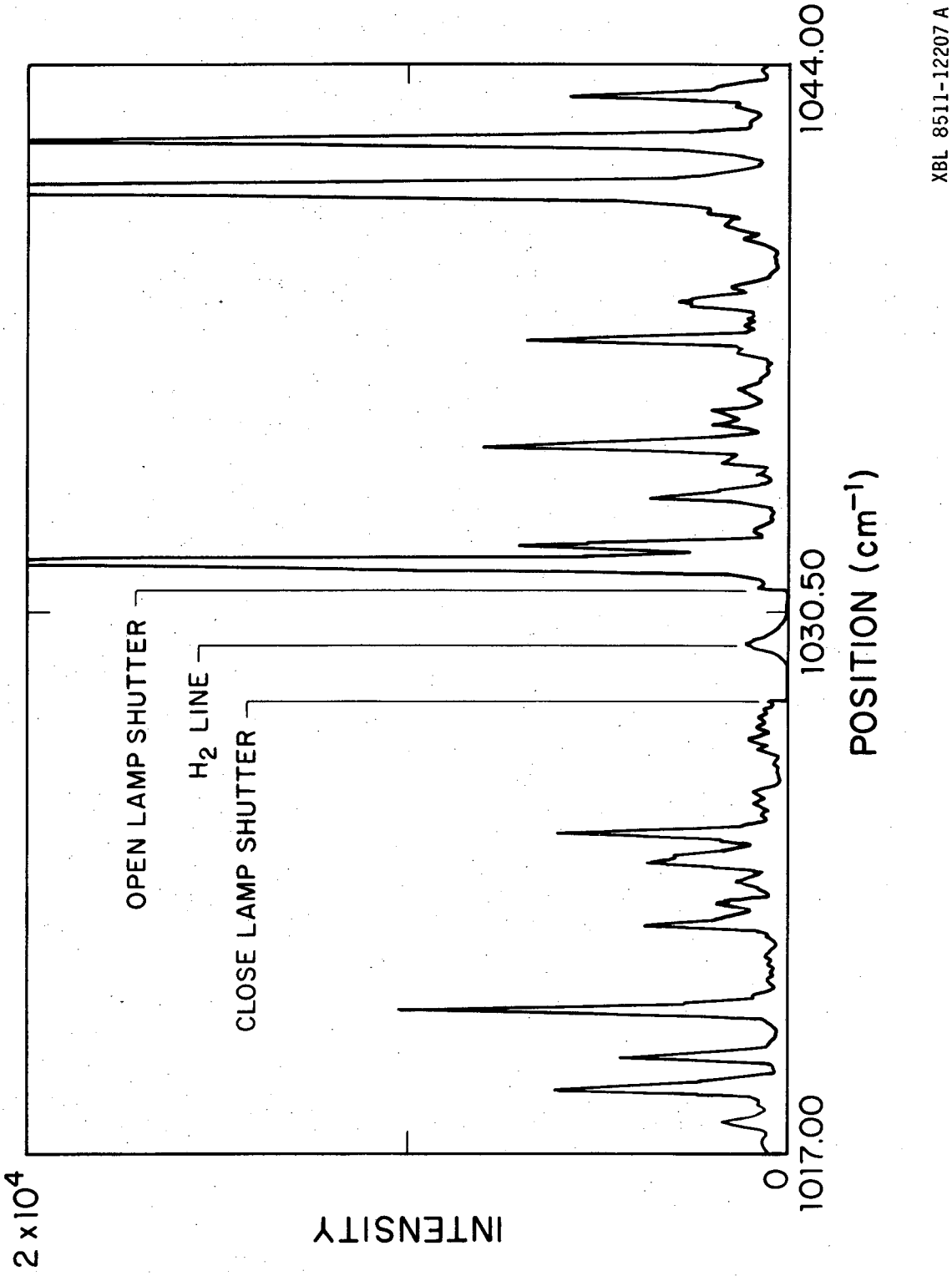


XBL 8511-12207 A

Fig. 16

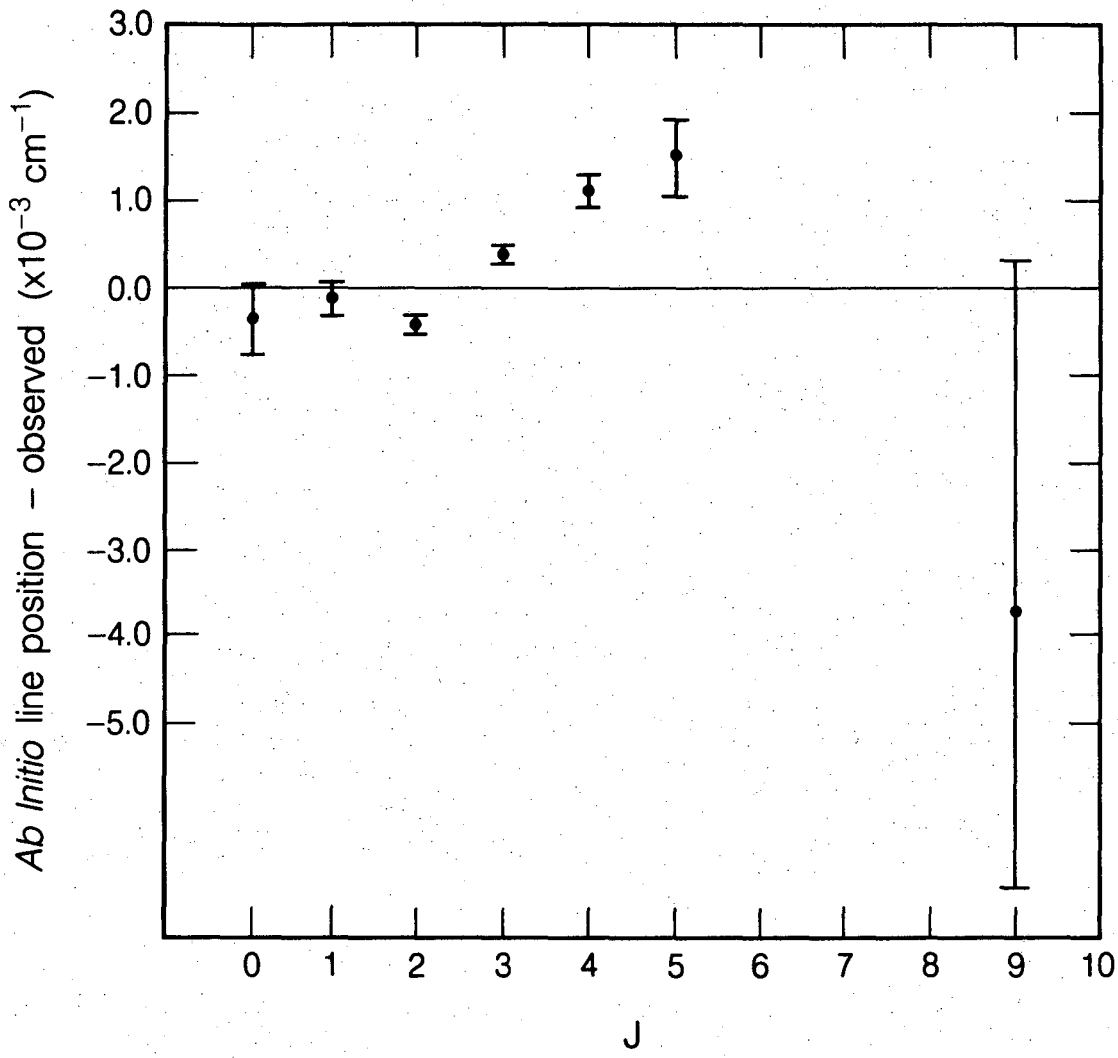


XBL 8511-12200 A

Fig. 17

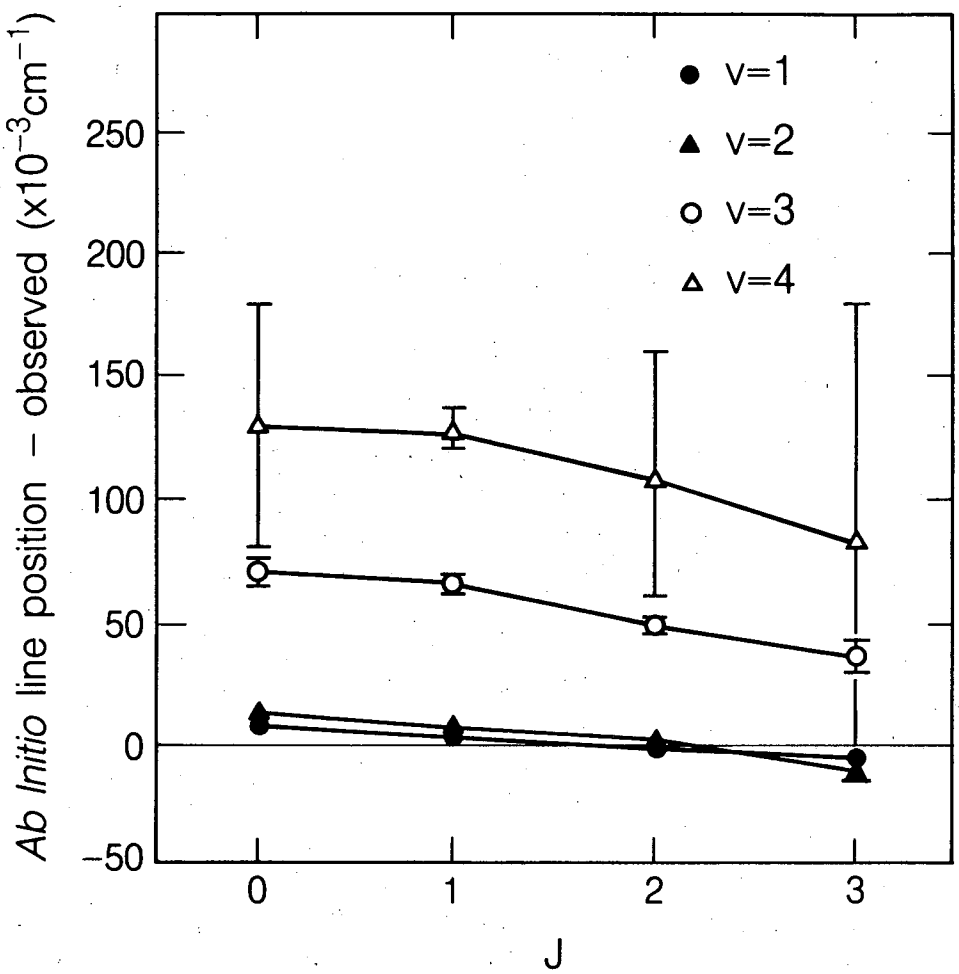


XBL 8511-12202 A

Fig. 18

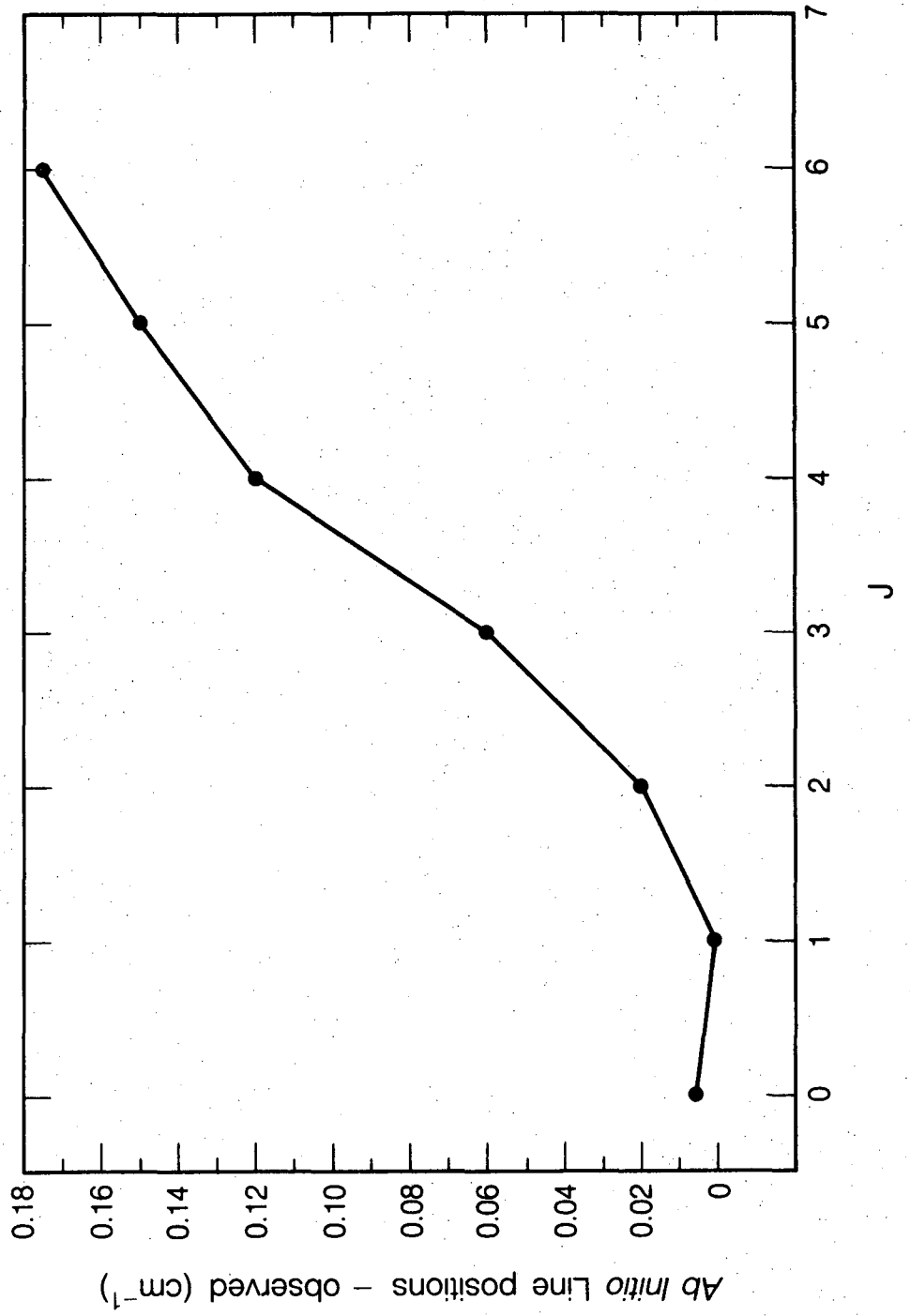


XBL 8511-12201 A

Fig. 19

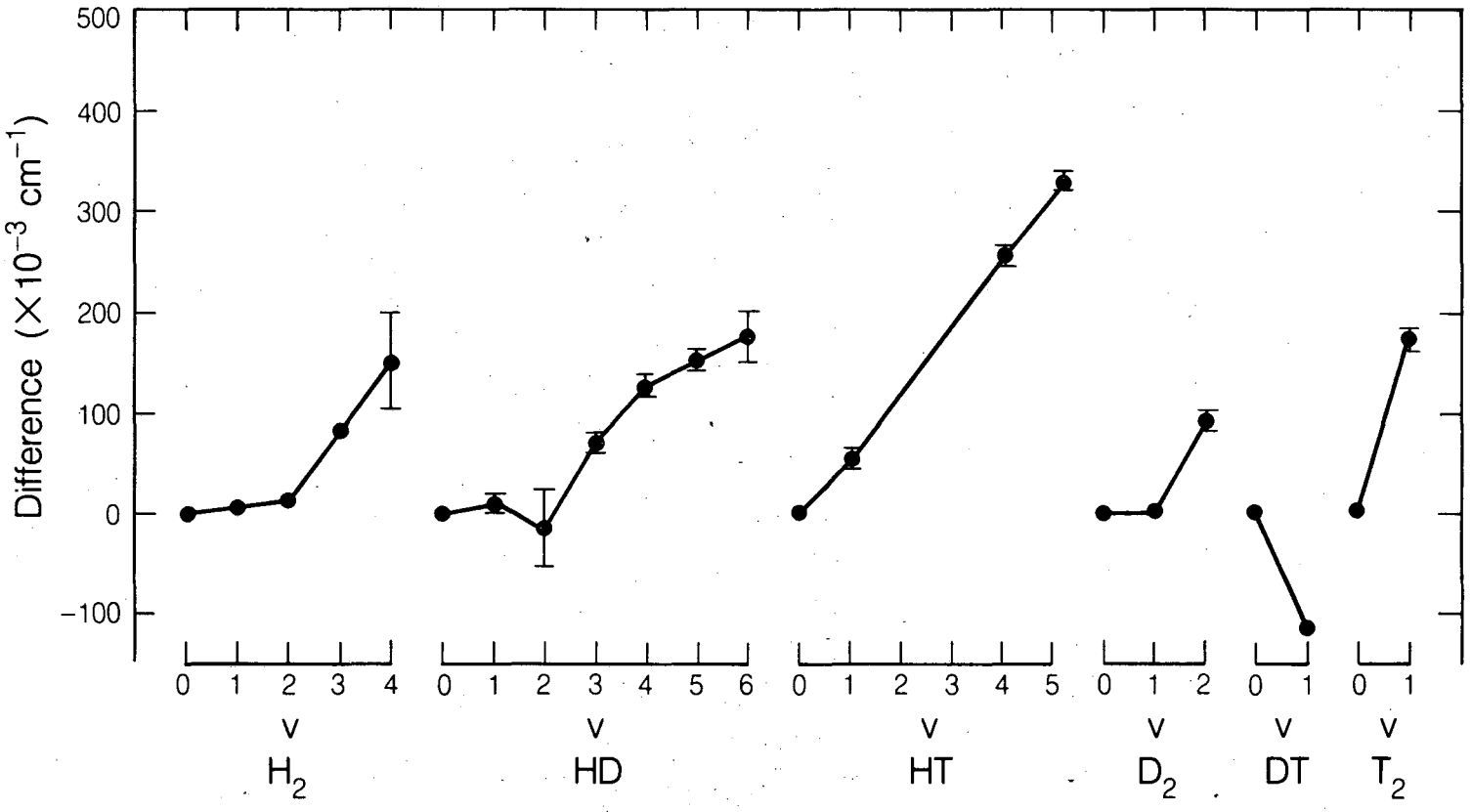


XBL 862-11026

Fig. 20

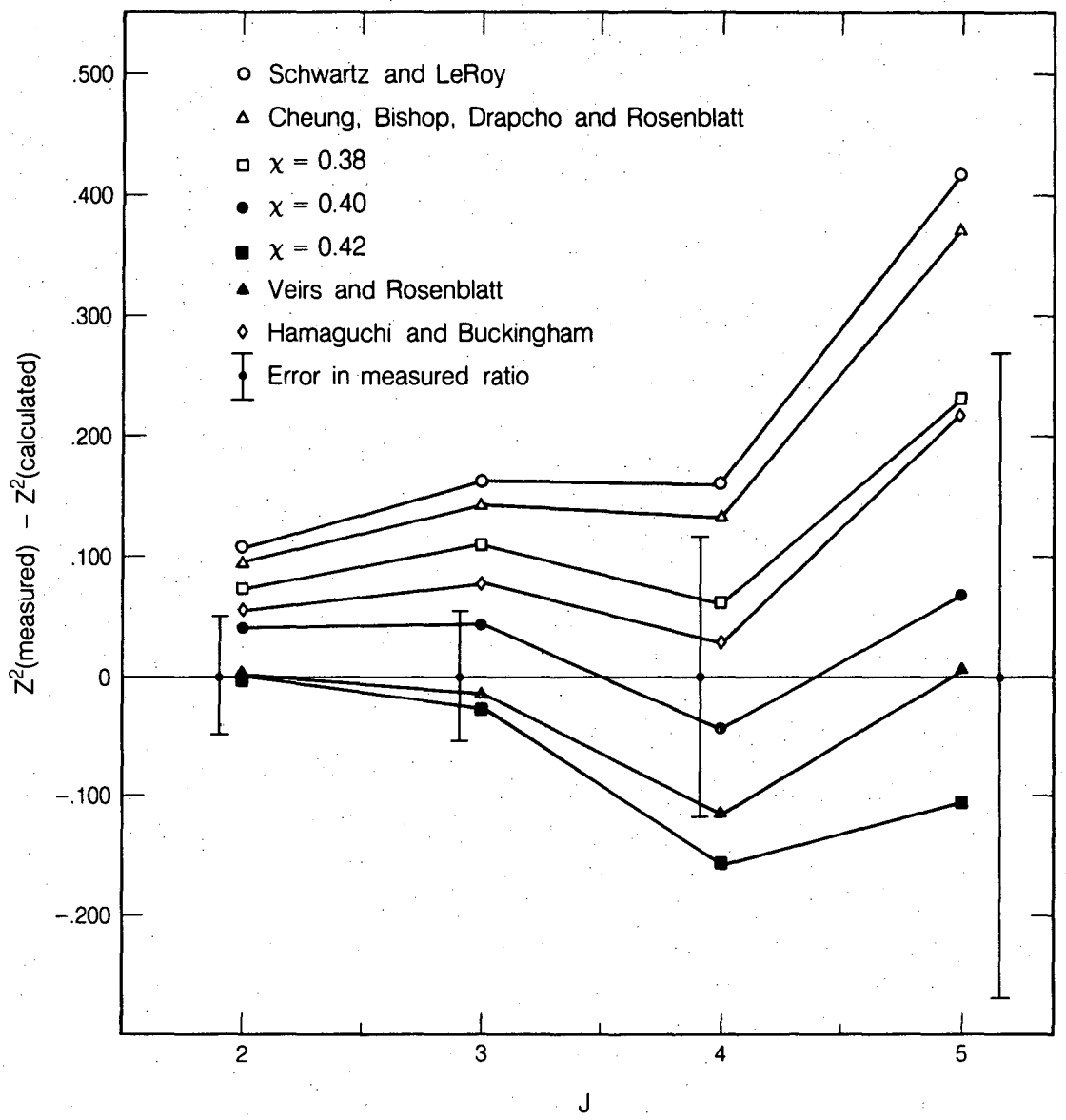


XBL 8511-12206 A

Fig. 21

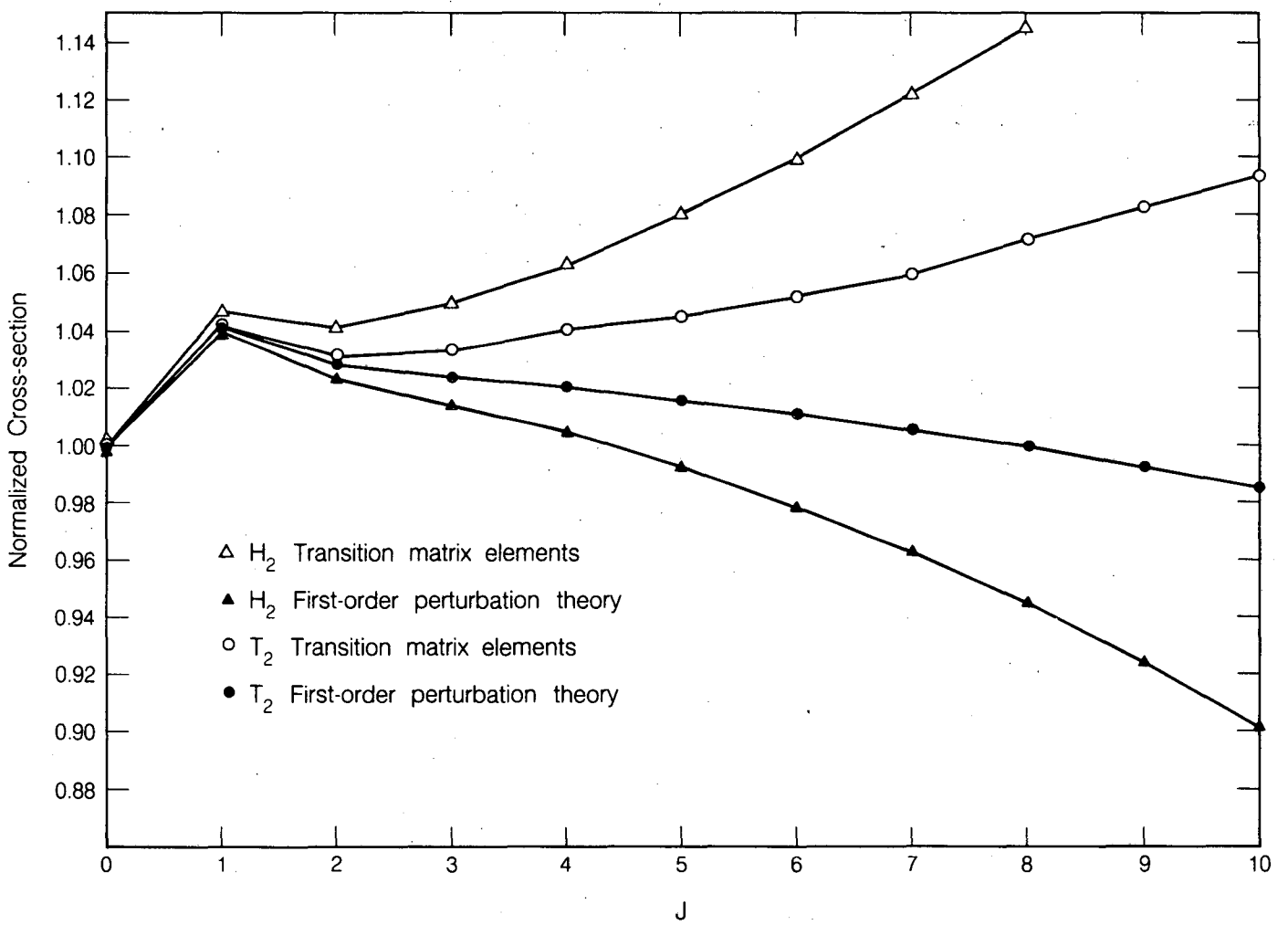


XBL 8511-12203 A

Fig. 22

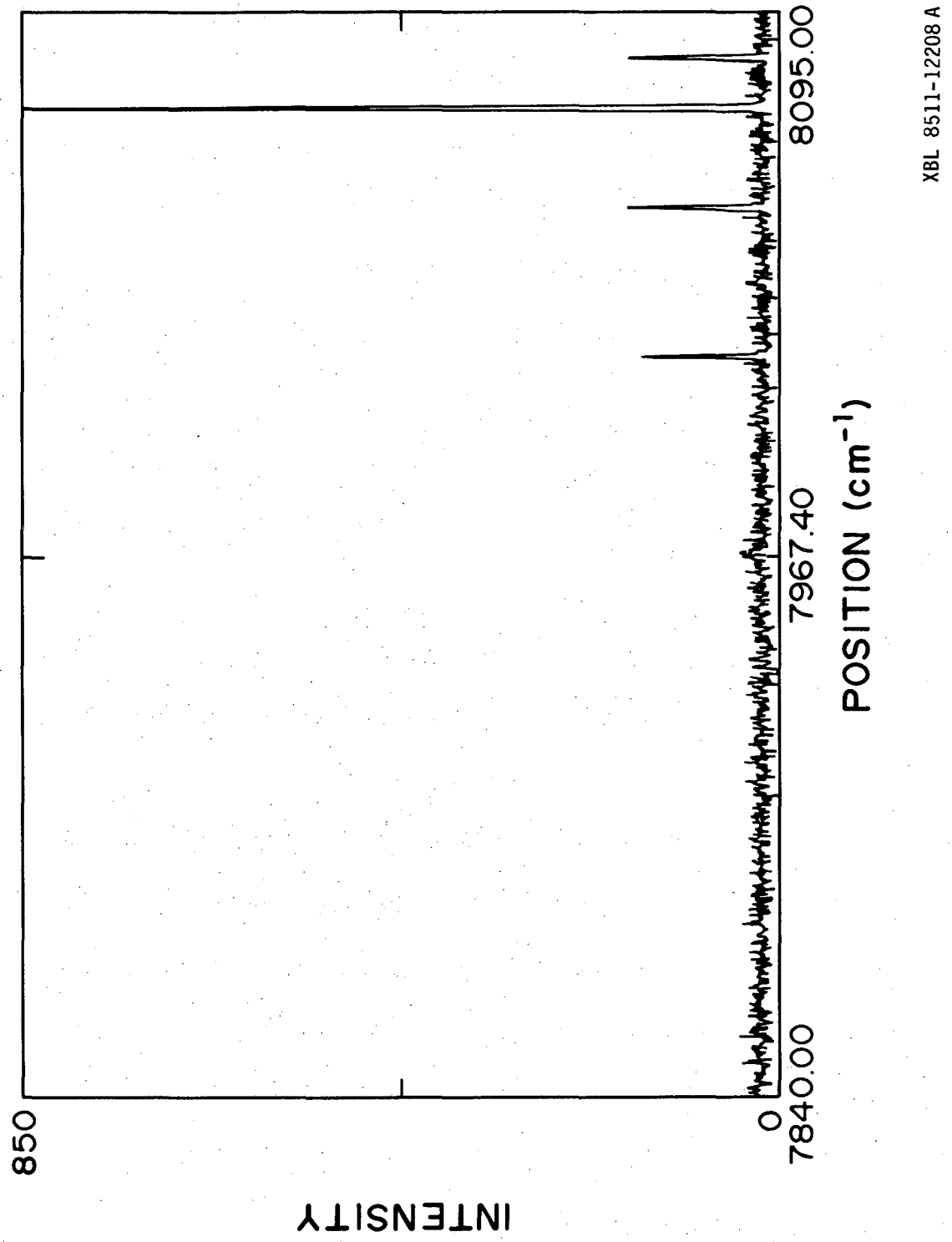
850
0
INTENSITY
7840.00
7967.40
8095.00
POSITION (cm$^{-1}$)
XBL 8511-12208 A

Fig. 23

# BIBLIOGRAPHY


1. C. Schwartz and R.J. LeRoy, private communication.

2. R. Stair, W. E. Schneider, and J. K. Jackson, "A New Standard of Spectral Irradiance", Applied Optics 2, 1151 (1963).

3. J. C. De Vos, "A New Determination of the Emissivity of Tungsten Ribbon", Physica 20, 669 (1954).

4. R. D. Larrabee, "Spectral Emissivity of Tungsten", Journal of the Optical Society of America 49, 619 (1959).

5. K. Schurer, "Discussion of Some Uncertainties in the Spectral Emissivity of Tungsten", Optik 28, 44 (1968).

6. G. A. W. Rutgers, "Standards for Photometry", Applied Optics 10, 2595 (1971).

7. Byron A. Palmer, Richard A. Keller, and Rolf Engleman, Jr., "An Atlas of Uranium Emission in a Hollow Cathode Discharge", Los Alamos Scientific Laboratory Report #LA-8251-MS, July 1980.

8. S. C. Hurlock and J. R. Hanratty, "Measuring Line Centers from Digitally Recorded Spectra Using a Minicomputer", Applied Spectroscopy 28, 362 (1974).

9. B. P. Stoicheff, "High Resolution Raman Spectroscopy of Gases IX. Spectra of $H_2$, HD, and $D_2$", Canadian Journal of Physics 35, 730 (1957).

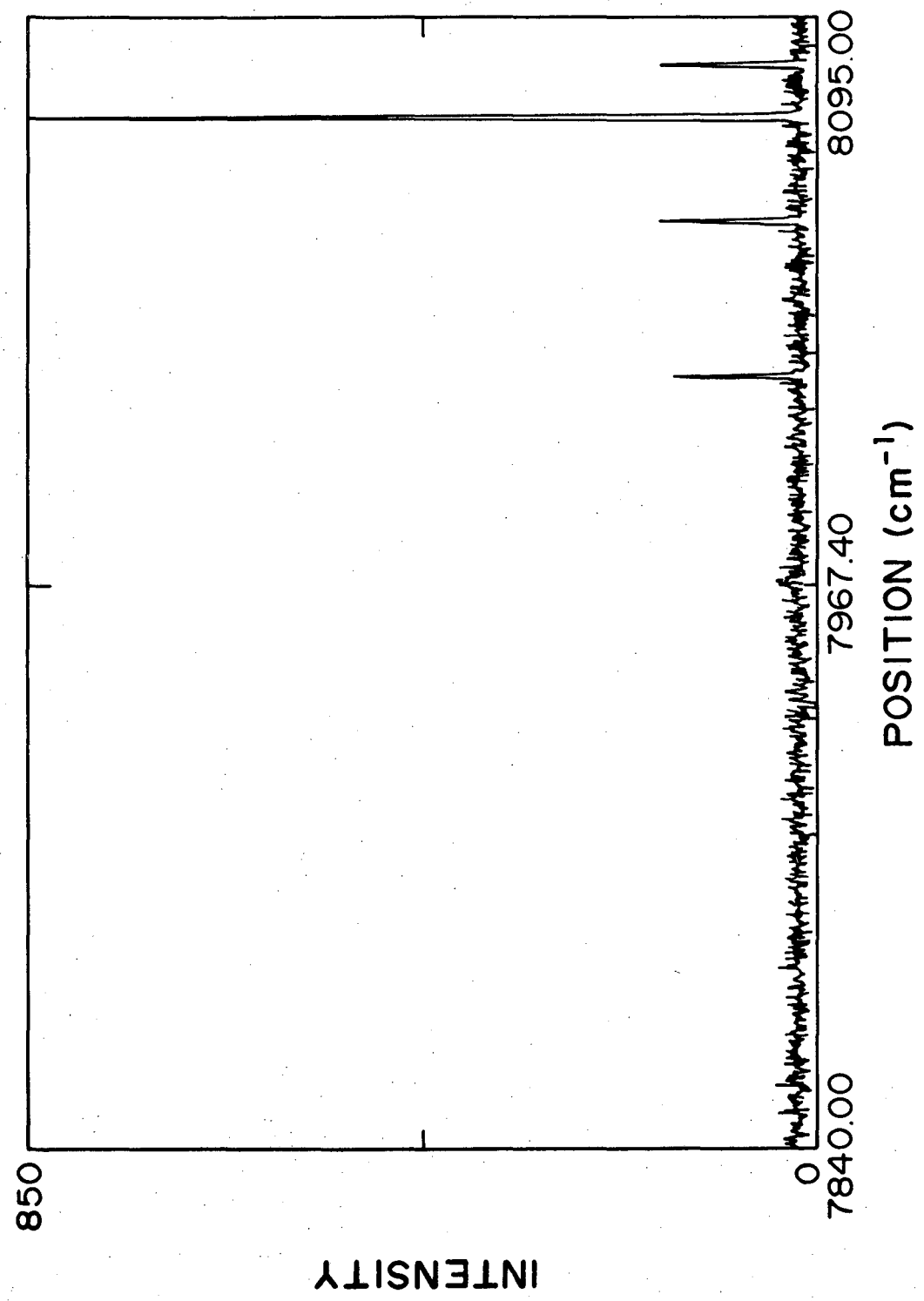


XBL 8511-12208 A

Fig. 23

# BIBLIOGRAPHY


1. C. Schwartz and R.J. LeRoy, private communication.

2. R. Stair, W. E. Schneider, and J. K. Jackson, "A New Standard of Spectral Irradiance", Applied Optics 2, 1151 (1963).

3. J. C. De Vos, "A New Determination of the Emissivity of Tungsten Ribbon", Physica 20, 669 (1954).

4. R. D. Larrabee, "Spectral Emissivity of Tungsten", Journal of the Optical Society of America 49, 619 (1959).

5. K. Schurer, "Discussion of Some Uncertainties in the Spectral Emissivity of Tungsten", Optik 28, 44 (1968).

6. G. A. W. Rutgers, "Standards for Photometry", Applied Optics 10, 2595 (1971).

7. Byron A. Palmer, Richard A. Keller, and Rolf Engleman, Jr., "An Atlas of Uranium Emission in a Hollow Cathode Discharge", Los Alamos Scientific Laboratory Report #LA-8251-MS, July 1980.

8. S. C. Hurlock and J. R. Hanratty, "Measuring Line Centers from Digitally Recorded Spectra Using a Minicomputer", Applied Spectroscopy 28, 362 (1974).

9. B. P. Stoicheff, "High Resolution Raman Spectroscopy of Gases IX. Spectra of $H_2$, HD, and $D_2$", Canadian Journal of Physics 35, 730 (1957).

10. U. Fink, T. A. Wiggins, and D. H. Rank, "Frequency and Intensity Measurements on the Quadrupole Spectrum of Molecular Hydrogen", Journal of Molecular Spectroscopy 18, 384 (1965).

11. P. Lallemand, P. Simova, and G. Bret, "Pressure-Induced Line Shift and Collisional Narrowing in Hydrogen Gas Determined by Stimulated Raman Emission", Physical Review Letters 17, 1239 (1966).

12. V. G. Cooper, A. D. May, and B. K. Gupta, "Interferometric Measurement of Line Widths and Frequencies of the S0(0) and S0(1) Rotational Raman Lines of $H_2$", Canadian Journal of Physics 48, 725 (1970).

13. E. C. Looi, J. C. Stryland, and H. L. Welsh, "Pressure Shifts in the Vibrational Raman Spectra of Hydrogen and Deuterium, 315-85K", Canadian Journal of Physics 56, 1102 (1978).

14. P. J. Brannon, C. H. Church, and C. W. Peters, "Electric Field Induced Spectra of Molecular Hydrogen, Deuterium and Deuterium Hydride", Journal of Molecular Spectroscopy 27, 44 (1968).

15. S. C. Beck, J. H. Lacy, T. R. Geballe, "Detection of the 12.28 Micron Rotational Line of Molecular Hydrogen in the Orion Molecular Cloud", The Astrophysical Journal 234, L213 (1979).

16. R. F. Knacke and E. T. Young, "Detection of the S(9), v=0→0 Rotation Line of the Hydrogen Molecule in Orion", The Astrophysical Journal 242, L183 (1980).

17. R. F. Knacke and E. T. Young, "Detection of the S(8), S(12), S(13), S(14), and S(15), v=0→0 Rotation Lines of Molecular Hydrogen in Orion", The Astrophysical Journal 249, L65 (1981).

18. D. E. Jennings and J. W. Brault, "Laboratory Measurements of the Pure Rotation S(2) and S(3) Transitions in $H_2$", The Astrophysical Journal 256, L29 (1982).

19. S. L. Bragg, J. W. Brault, and W. H. Smith, "Line Positions and Strengths in the $H_2$ Quadrupole Spectrum", The Astrophysical Journal 263, 999 (1982).

20. D. E. Jennings and J. W. Brault, "The Ground State of Molecular Hydrogen", Journal of Molecular Spectroscopy 102, 265 (1983).

21. D. E. Jennings, S. L. Bragg, and J. W. Brault, "The v=0→0 Spectrum of $H_2$", The Astrophysical Journal 282, L85 (1984).

22. D. E. Jennings, L. A. Rahn, and A. Owyoung, "Laboratory Measurement of the S(9) Pure Rotation Frequency in $H_2$", The Astrophysical Journal 291, L15 (1985).

23. V. De Cosmo, H. P. Gush, and M. Halpern, "The S0(1) Quadrupole Line of $H_2$", Canadian Journal of Physics 62, 1713 (1984).

24. J. Reid and A. R. W. McKellar, "Observation of the S0(3) Pure Rotational Quadrupole Transition of $H_2$ With A Tunable Diode Laser", Physical Review A 18, 224 (1978).

25. W. Kolos and L. Wolniewicz, "Accurate Adiabatic Treatment of the Ground State of the Hydrogen Molecule", Journal of Chemical Physics 41, 3663 (1964).

26. W. Kolos and L. Wolniewicz, "Accurate Computation of Vibronic Energies and of Some Expectation Values for $H_2$, $D_2$, and $T_2$", Journal of Chemical Physics 41, 3674 (1964).

27. W. Kolos and L. Wolniewicz, "Potential-Energy Curves for the $X^1\Sigma_g^+$, $b^3\Sigma_u^-$, and $C^1\Pi_u$ States of the Hydrogen Molecule", Journal of Chemical Physics 43, 2429 (1965).

28. L. Wolniewicz, "Vibrational-Rotational Study of the Electronic Ground State of the Hydrogen Molecule", Journal of Chemical Physics 45, 515 (1966).

29. W. Kolos and L. Wolniewicz, "Improved Theoretical Ground-State Energy of the Hydrogen Molecule", Journal of Chemical Physics 49, 404 (1968).

30. Robert J. LeRoy, "Eigenvalues and Certain Expectation Values for All Bound and Quasibound Levels of Ground-State $(X^1\Sigma_g^+)H_2$, HD, and $D_2$", Journal of Chemical Physics 54, 5433 (1971).

31. David M. Bishop and Shing-kuo Shih, "An Effective Schrodinger Equation for the Rovibronic Energies of $H_2$ and $D_2$", Journal of Chemical Physics 64, 162 (1976).

32. L. Wolniewicz, "The $X^1\Sigma_g^+$ State Vibrational-Rotational Energies of the $H_2$, HD, and $D_2$ Molecules", Journal of Chemical Physics 78, 6173 (1983).

33. J. L. Hunt, J. D. Poll, and L. Wolniewicz, "Ab Initio Calculation of Properties of the Neutral Diatomic Hydrogen Molecules $H_2$, HD, $D_2$, HT, DT, and $T_2$", Canadian Journal of Physics 62, 1719 (1984).

34. A. R. W. McKellar, "The Significance of Pressure Shifts for the Interpretation of $H_2$ Quadrupole Lines in Planetary Spectra", Icarus 22, 212 (1974).

35. R. A. Durie and G. Herzberg, "Forbidden Transitions in Diatomic Molecules V. The Rotation-Vibration Spectrum of the Hydrogen-Deuteride (HD) Molecule", Canadian Journal of Physics 38, 806 (1960).

36. N. H. Rich, J. W. C. Johns, and A. R. W. McKellar, "Frequency and Intensity Measurements in the Fundamental Infrared Band of HD", Journal of Molecular Spectroscopy 95, 432 (1982).

37. A. R. W. McKellar, W. Goetz, and D. A. Ramsay, "The Rotation-Vibration Spectrum of HD: Wavelength and Intensity Measurements of the 3-0, 4-0, 5-0, and 6-0 Electric Dipole Bands", The Astrophysical Journal 207, 663 (1976).

38. F. W. Dalby and J. Vigue, "Observations on the v=0→v=5 Rotational-Vibrational Band of HD", Physical Review Letters 43, 1310 (1979).

39. P. Essenwanger and H. P. Gush, "Rotational Spectrum of HD at Low Pressures", Canadian Journal of Physics 62, 1680 (1984).

40. H. G. M. Edwards, D. A. Long, H. R. Mansour, and K. A. B. Najm, "The Pure Rotational and Vibration-Rotational Raman Spectra of HT and DT", Journal of Raman Spectroscopy 8, 251 (1979).

41. M. Chuang and R.N. Zare, private communication.

42 M. A. Henesian, M. D. Duncan, R. L. Byer, and A. D. May, "Absolute Raman Frequency Measurement of the Q(2) Line in $D_2$ Using cw CARS", Optics Letters 1, 149 (1977).

43. A. R. W. McKellar and T. Oka, "A Study of the Electric Quadrupole Fundamental Band of $D_2$ Using An Infrared Difference Frequency Laser System", Canadian Journal of Physics 56, 1315 (1978).

44. J. E. Barefield, L. H. Jones, and R. Liepens, "Vibration-Rotation Analysis of Deuterium Tritide", Journal of Molecular Spectroscopy 80, 233 (1980).

45. H. G. M. Edwards, D. A. Long, and H. R. Mansour, "Pure Rotational and Vibration-Rotational Raman Spectra of Tritium, $^3H_2$", Journal of the Chemical Society Faraday Transactions II 74, 1208 (1978).

46. T. C. James and W. Klemperer, "Line Intensities in the Raman Effect of Diatomic Molecules", Journal of Chemical Physics 31, 130 (1959).

47. A. D. Buckingham and A. Szabo, "Determination of Derivatives of the Polarizability Anisotropy in a Diatomic Molecule from Relative Raman Intensities", Journal of Raman Spectroscopy 7, 46 (1978).

48. C. Asawaroengchai and G. M. Rosenblatt, "Rotational Raman Intensities and the Measured Change with Internuclear Distance of the Polarizability Anisotropy of $H_2$, $D_2$, $N_2$, $O_2$, and CO", Journal of Chemical Physics 72, 2664 (1980).

49. H. Hamaguchi, I. Suzuki, and A. D. Buckingham, "Determination of Derivatives of the Polarizability Anisotropy in Diatomic Molecules I. Theoretical Considerations on Vibration-Rotation Raman Intensities", Molecular Physics 43, 963 (1981).

50. H. Hamaguchi, A. D. Buckingham, and W. J. Jones, "Determination of Derivatives of the Polarizability Anisotropy in Diatomic Molecules II. The Hydrogen and Nitrogen Molecules", Molecular Physics 43, 1311 (1981).

51. L. M. Cheung, D. M. Bishop, D. L. Drapcho and G. M. Rosenblatt, "Relative Raman Line Intensities for $H_2$ and $D_2$. Correction Factors for Molecular Non-Rigidity", Chemical Physics Letters 80, 445 (1981).

52. R. Herman and R. F. Wallis, "Influence of Vibration-Rotation Interaction on Line Intensities in Vibration-Rotation Bands of Diatomic Molecules", Journal of Chemical Physics 23, 637 (1955).

53. R. A. Toth, R. H. Hunt, and E. K. Plyler, "Dipole Moment Matrix Elements for the 1-0, 2-0, and 3-0 Vibration-Rotation Bands of Diatomic Molecules", Journal of Molecular Spectroscopy 23, 74 (1969).

54. M. C. Drake and G. M. Rosenblatt, "Rotational Raman Scattering from Premixed and Diffusion Flames", Combustion and Flame 33, 179 (1978).

55. M. F. Crawford and R. E. MacDonald, "Field-Induced Absorption in Hydrogen", Canadian Journal of Physics 36, 1022 (1958).

56. E. Ishiguro, T. Arai, M. Mizushima, and M. Kotani, "On the Polarizability of the Hydrogen Molecule", Proceedings of the Physical Society (London) A65, 178 (1952).

57. W. Kolos and L. Wolniewicz, "Polarizability of the Hydrogen Molecule", Journal of Chemical Physics 46, 1426 (1967).

58. S. R. Langhoff, C. W. Bauschlicher, Jr. and D. P. Chong, "Theoretical Study of the Effects of Vibrational-Rotational Interactions On the Raman Spectrum of N2", Journal of Chemical Physics 78, 5287 (1983).

59. G. Leyendecker, J. Doppelbauer, D. Böuerle, P. Geittner, and H. Lydtin, "Raman Diagnostics of CVD Systems: Determination of Local Temperatures", Applied Physics A 30, 327 (1983).

60. C. J. Seliskar, P. A. Spangler, M. D. Hale, and C. R. Rudy, "Concerning the Quantitative Analysis of Hydrogen Gas by Rotational Raman Spectroscopy", Applied Spectroscopy 37, 77 (1983).

This report was done with support from the Department of Energy. Any conclusions or opinions expressed in this report represent solely those of the author(s) and not necessarily those of The Regents of the University of California, the Lawrence Berkeley Laboratory or the Department of Energy.

Reference to a company or product name does not imply approval or recommendation of the product by the University of California or the U.S. Department of Energy to the exclusion of others that may be suitable.

*LAWRENCE BERKELEY LABORATORY*
*TECHNICAL INFORMATION DEPARTMENT*
*UNIVERSITY OF CALIFORNIA*
*BERKELEY, CALIFORNIA 94720*